MASTERARBEIT

SAXS and WAXS investigations on cellulose of *Picea abies* - The influence of thermal treatment on the microfibril angle

verfasst von

Ursula Ludacka BSc

angestrebter akademischer Grad

Master of Science (MSc)

Wien, 2014

Studienkennzahl lt. Studienblatt:	A 066 876
Studienrichtung lt. Studienblatt:	Masterstudium Physik
Betreut von:	Univ.-Prof. Mag. Dr. Herwig Peterlik

Abstract

Thermal treatment of timber is a common method of preservation, but has several effects on the structural integrity. The cellulose microfibril angle, which plays a major role in the mechanical strength of wood, is likely to be affected by high temperature treatment. A common method to investigate changes in the microfibril angle of cellulose in the secondary (S2) layer of the wood cell wall is small angle X-ray scattering (SAXS). In the present study SAXS was applied to samples of selected annual rings of a cross section of a trunk of *Picea abies*. This procedure was repeated for four temperatures: 20°C (reference sample), 160°C, 190°C and 220°C. Because of their different cell structure the obtained data was separated into early-and latewood. It was found that a change in the microfibril angle occurs due to thermal treatment, depending on the value of the initial microfibril angle (in the reference samples). Small initial angles decrease, whereas large initial angles increase. Furthermore, the mean microfilbril angle shows a tendency to shrink with increasing treatment temperature.

Zusammenfassung

Thermische Behandlung von Holz ist eine gängige Konservierungsmethode, welche allerdings Auswirkungen auf die strukturelle Integrität hat. Der Mikrofibrillenwinkel von Zellulose, welcher von großer Bedeutung für die mechanische Belastbarkeit von Holz ist, wird durch diese Art der Behandlung beeinflusst. Eine verbreitete Methode, Veränderungen des Mikrofibrillenwinkels von Zellulose der Sekundärschicht (S2) von Holzzellen, zu untersuchen ist Röntgenkleinwinkelstreuung (SAXS). In der vorliegenden Arbeit wurden Proben ausgewählter Jahresringe eines Stammes der Spezies *Picea abies* mittels SAXS untersucht. Dies wurde für vier verschiedenen Behandlungstemperaturen durchgeführt: 20°C (Referenzproben), 160°C, 190°C und 220°C. Aufgrund des unterschiedlichen Aufbaus der Zellwände, wurden die Proben von Früh- und Spätholz getrennt betrachtet. Es stellte sich heraus, dass eine Änderung des Mikrofibrillenwinkels aufgrund thermischer Behandlung auftritt, allerdings in Abhängigkeit vom ursprünglichen Wert der unbehandelten Proben. Kleine Winkelwerte zeigen eine Tendenz zu schrumpfen, wohingegen große tendenziell größer werden. Weiters zeigt sich, dass der Wert des mittleren Mikrofibrillenwinkels mit steigender Behandlungstemperatur tendenziell abnimmt.

Contents

Acknowledgements

I would like to express my sincere gratitude to my supervisor Univ.-Prof. Mag. Dr. Herwig Peterlik who offered me the opportunity to immerse in the exciting field of biological composite materials.
I want to thank for the guidance, encouragement and friendly advice throughout my master's thesis. He generously shared both his time and his profound knowledge with me.

I would like to thank Daniel Gitschthaler for his support and his great ideas during the sample preparation. His commitment was essential for the success of the project.

Futhermore, I would like to thank Yvonne Simon for her advie and motivation during this time.

Last but not least I would like to express my gratitude to my mother Gisela Ludacka for proofreading this thesis with patience and great enthusiasm.

1. Introduction and motivation

Timber itself, as well as its main component cellulose is of fundamental importance for a wide field of technical applications. Therefore basic research is of high interest to understand the underlying mechanisms and nexus. Living organisms are subdued to metabolic processes to gain growth and reproduction. Strictly speaking of the biota, the fauna and flora, are usually organised in tissues, fulfilling certain tasks. Tissues responsible for mechanical strength, stability and vertical growth are of large interest in the field of constructional engineering, to gain stability with concurrent lightweight construction.

In nature materials are frequently organised in hierarchical structures. Examples for these are wood, bone or tendon. In bone and tendon the modular units are mostly collagen microfibrils with a length of $\sim 300\ nm$. They are arranged in bundles, encapsulated with conjunctive tissue, the fascia. In a larger array they build up the sinews of mammals and non-mammals, their size distribution of diameter goes up to one centimetre like the calcaneal tendon in the human body. The structure of bone is quite similar, but to obtain strength and bending stiffness there is a three dimensional net of crystalline hydroxyapatite. Wood or more exactly timber is also built as composite material. In contradiction to tendon the modular unit is cellulose.

Cellulose itself has a large area of applications beginning of course with the wood industry. In this branch it is used in form of timber as a construction material. It is as well the main component of paper. Further applications can be found in medical cases, for example as artificial blood vessels [33] or moreover the sanitary area.

The focus of this work lied on cellulose in timber and its behaviour due to thermal treatment. This kind of modification of timber is a widely used method to conserve wood without the use of certain chemicals, which are often as well poisonous as lacking in environmental compatibility.

Thermal treatment itself causes chemical changes of different components of timber. The composition of so called additive materials in compound with cellulose influences the mechanical stability. A further factor of influence for mechanical strength in living timber is the so called cellulose microfibril angle. This is the helical angle, under which the fibrils are coiled around the cell axis of the wood cells. Therefore, the main topic of this work is to examine if there occurs a change in the microfibril angle caused by thermal treatment.

Every tree species has its own slightly different composition and specifications of timber in comparison to others. For example the distribution on a percentage basis of cellulose, hemicellulose and other additives. Even the chemical make-up differs between them. Furthermore the distribution of the microfibril angle is depending on the type of timber and additionally on the position in a tree. It adapts to the mechanical load or pressure.

The choice for the type of timber fell on *Picea abies*, a commonly occurring species in Austria and as well used in a large amount for diverse applications. It is quite fast growing and as consequence of a relatively high harvesting rate. Therefore, it is a rather cheap timber but with obvious constraints. *Picea abies* belongs to the category of softwoods.

A conventional method of determining the microfibril angle is the technique of small angle X-ray scattering (SAXS) and as well wide angle x-ray scattering (WAXS).

2. X-ray scattering

2.1. SAXS - theory

This chapter is a short introduction to the theory of small angle X-ray scattering and is based primarily on the work of Glatter et al. [10].

In scattering processes one can distinguish between elastic and inelastic scattering. In the first case there occurs no change in wavelength or energy from incoming to outgoing beam, whereas in inelastic (Compton scattering) processes, a change of both of them is measurable. The latter case is shown in Fig. 2.1. Certainly inelastic scattering is in most cases negligible, especially for stronger bound electrons.

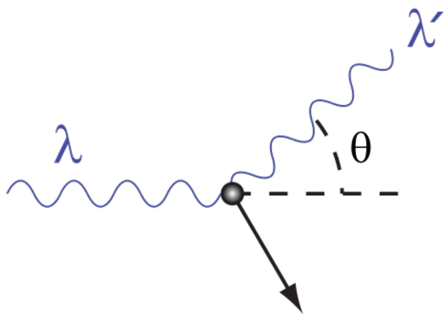

Figure 2.1.: Compton Scattering [6]

X-ray radiation interacts with the atomic electron shell of the target. Thus atoms with higher Z (mass number) scatter stronger.
Beside these two scattering events, elastic- and Compton scattering, fluorescent X-ray radiation is to mention likewise, which has lower energy than the incoming radiation, due to energy loss. Fluorescent X-ray radiation occurs at absorption edges. A schematical overview is shown in 2.2.

Inelastic scattering, as well as fluorescent radiation are part of the background scatter. Both do not interfere with the elastically scattered waves, because of different wavelengths.

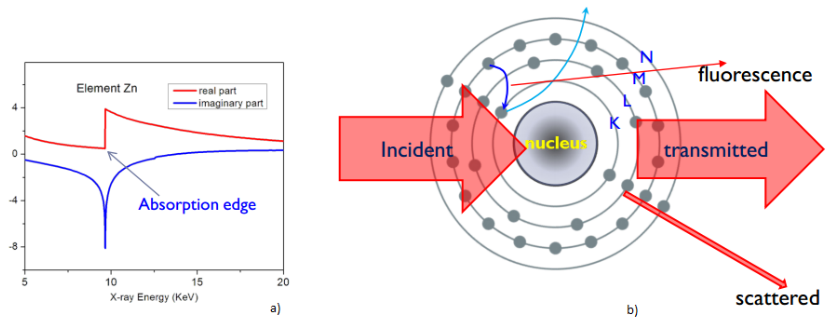

Figure 2.2.: a) Absorption edge of Zn b) schematic representation of fluorescent radiation [40]

Interference only occurs among the elastically scattered waves, which are coherent and therefore have a phase relation. The signal on the detector is a mixture of constructive and de-constructive interference pattern, encoding the difference of the distance of scatterers. Additionally there always occurs a certain amount of background radiation, which can be either ignored or subtracted from the interference pattern.

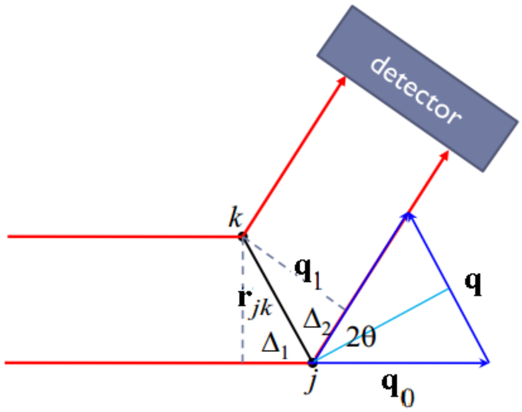

Figure 2.3.: Scattering process with 2 scatterers (Position k, j) in distance $\mathbf{r}_{jk}$; $\mathbf{q}_0$ ... incoming wave vector; $\mathbf{q}_1$ ... scattered Vector; $\mathbf{q} = \mathbf{q}_1 - \mathbf{q}_0$ ... difference vector; $|\mathbf{q}| = q = \frac{4\pi}{\lambda} \cdot sin\,\theta$ [40]

The interference pattern on the detector depends on the path difference of the incoming beams, which are scattered by electrons at different positions. This is illustrated in 2.3. For the two particles k and j the path difference is $\Delta = \Delta_1 + \Delta_2$. Using geometric consderations yields

$$-\mathbf{q}_0 \cdot \mathbf{r}_{jk} + \mathbf{q}_1 \cdot \mathbf{r}_{jk} = \mathbf{q} \cdot \mathbf{r}_{jk}. \tag{2.1}$$

The incoming wave, emitted by an X-ray source can be described as a plane wave of the form

$$E(t) = E_0 \cdot e^{i(2\pi\nu t)\cdot \mathbf{qr}} \tag{2.2}$$

becoming

$$E'(t) = E'_0 \cdot e^{i(2\pi\nu t+\phi_0)} \cdot e^{i\mathbf{qr_j}} \tag{2.3}$$

with the resulting amplitude (in q space)

$$A'(\mathbf{q}) = A_j(\mathbf{q}) = f_e \cdot e^{i\mathbf{qr_j}} \tag{2.4}$$

and f_e being the form factor of one single atom. The total amplitude A_{tot} is a superposition of all scattering events, therefore

$$A_{tot}(\mathbf{q}) = A_j(\mathbf{q}) + A_k(\mathbf{q}) \tag{2.5}$$

$$= f_e\left(e^{i\mathbf{qr_j}} + e^{i\mathbf{qr_k}}\right) \tag{2.6}$$

$$= f_e \cdot e^{i\mathbf{qr_j}} \cdot \{1 + e^{i\mathbf{q}(\mathbf{r}_k - \mathbf{r}_j)}\} \tag{2.7}$$

$$= f_e \cdot e^{i\mathbf{qr_j}} \cdot \{\underbrace{1 + cos\,(\mathbf{q}\,\mathbf{r}_{jk})}_{real\ part} + i \cdot \underbrace{sin\,(\mathbf{q}\,\mathbf{r}_{jk})}_{imaginary\ part}\}. \tag{2.8}$$

On the detector itself, there is only intensity $I(\mathbf{q})$ to measure, which means a loss of phase information. The phase problem emerges in all kinds of scattering processes and signal processing.

$$I(\mathbf{q}) = |A_{tot}(\mathbf{q})|^2 = A_{tot}(\mathbf{q}) \cdot A^*_{tot}(\mathbf{q}) \tag{2.9}$$

$$= f_e^2 \left|e^{i\mathbf{qr_j}}\right|^2 \times \left|1 + cos\,(\mathbf{qr_{jk}}) + i \cdot sin\,(\mathbf{qr_{jk}})\right|^2 \tag{2.10}$$

$$= f_e^2 \times 1 \times [\underbrace{1+1}_{contribution\ of\ single\ scattering\ events} + \underbrace{2 \cdot cos\,(\mathbf{q}\,\mathbf{r}_{jk})}_{interference\ term}] \tag{2.11}$$

The scattered intensity $I(\mathbf{q})$ is a superposition of two parts. The term for single scattering, where the scattering event of each electron is considered and the interference term, where the distance $\mathbf{r}_{jk}$ between the scatterers is crucial.

Because of the former mentioned loss of phase information it is not possible to calculate the original structure directly from an inverse Fourier transformation. There are various methods of "phase guessing" in X-ray crystallography, including brute force approaches.

A further method is to affiliate obtained pattern to known, simpler structures, like spheres or rods for example. The resulting diffraction pattern will be discussed in more detail below.

In Fig. 2.3 the scattering process with two scatterers was introduced. Atoms or molecules themselves are ensembles of N electrons, therefore the detected intensity becomes

$$I(\mathbf{q}) = \left| \sum_{j=1}^{N} A_j(\mathbf{q}) \right|^2 = \left| \sum_{j=1}^{N} f_e \cdot e^{i\mathbf{q}\mathbf{r}_j} \right|^2 . \tag{2.12}$$

Hence the atomic scattering factor $F(\mathbf{q})$ can be introduced

$$F(\mathbf{q}) := \sum_{j=1}^{N} f_e \cdot e^{i\mathbf{q}\mathbf{r}_\mathbf{j}}. \tag{2.13}$$

In macroscopic objects atoms or molecules can be arranged as well in more or less ordered structures. Therfore an electron density function $\rho(\mathbf{r})$ is introduced in the continuum limit for a large number of scatterers:

$$F(\mathbf{q}) \propto \int \rho(\mathbf{r}) \cdot e^{i\mathbf{q}\mathbf{r}} d\mathbf{r}. \tag{2.14}$$

The basis of macroscopic crystal lattices can be occupied by single elctrons or larger elctron density distributions like atoms or molecules. Here a continuous density function gets supplemented by the information about the lattice site. Hence the intensity becomes

$$I(\mathbf{q}) \propto \left| F(\mathbf{q}) \underbrace{\int \sum_{j=1}^{N} \delta(\mathbf{r} - \mathbf{r_j}) e^{i\mathbf{q}\mathbf{r}} d\mathbf{r}}_{S(\mathbf{q})} \right|^2 , \tag{2.15}$$

where $S(\mathbf{q})$ is the structure factor, giving information about the lattice structure. This relation is sketched in Fig. 2.4.

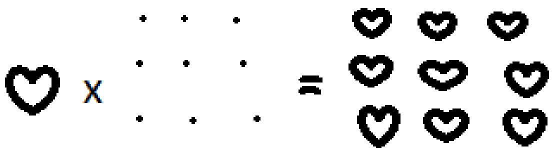

Figure 2.4.: Atomic form factor x structure factor of the lattice

The calculation of the form factor $F(\mathbf{q})$ in a Cartesian coordinate system yields

$$F(\mathbf{q}) = \iiint_V \Delta\rho(\mathbf{r}) \cdot e^{i\mathbf{qr}} dx\, dy\, dz \tag{2.16}$$

with $\Delta\rho(\mathbf{r}) = \rho_{in} - \rho_{out}$ and ρ_{in} being the electron density of the object and ρ_{out} the electron density of the surrounding environment. The form factor depends on the electron density distribution difference.

2.1.1. Form factor of a sphere

First the form factor $F(q)$ of a sphere will be calculated. A radial uniform density distribution $\rho(r)$ leads to

$$F(q) = 4\pi \int dr\, \rho(r)\, r^2 \,\frac{sin\,(qr)}{qr} \tag{2.17}$$

$$= \rho_0 \frac{3(sin\,(qR) - qR \cdot cos\,(qR)}{(qR)^3}. \tag{2.18}$$

Therefore the intensity becomes:

$$I(q) = F(q) \cdot F*(q) = \rho_0^2 \left(\frac{3\,(sin\,(qR) - qR \cdot cos\,(qR))}{(qR)^3} \right)^2. \tag{2.19}$$

The model of a scattering sphere is a commonly used model and shown in Fig. 2.5, representing a spherical Bessel-function (Eqn.2.19) .

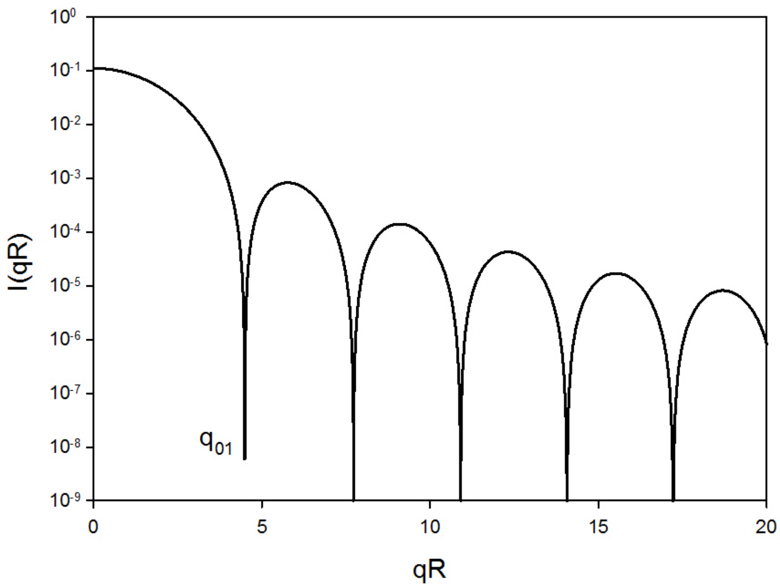

Figure 2.5.: Scattering from a single solid spherical particle of radius R

One can calculate the radius out of this plot, using the q coordinate of the first minimum q_{01}. This can be approximated as

$$R \approx \frac{4,5}{q_{01}} \tag{2.20}$$

2.1.2. Form factor of a cylinder

In this case the form factor $F(\mathbf{q})$ will be obtained by use of cylindrical coordinates. To separate the volume integration into two parts, the coordinates and shown in Fig. 2.6. For symmetry reasons cylindrical coordinates ($x = \varrho \cdot sin\ \alpha;\ y = \varrho \cdot sin\ \alpha;\ z = z$) are used.

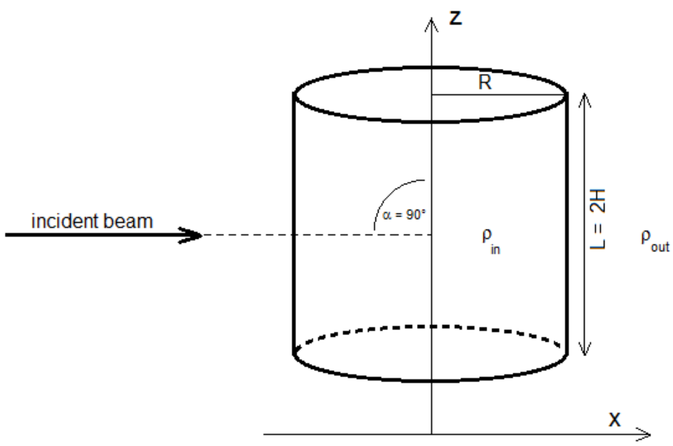

Figure 2.6.: Cylindrical electron density distribution (ρ_{in}) with radius R and length $L = 2H$ in solution ρ_{out}

For a cylinder with $L >> H$ one can separate the contributions of the length (in z-direction) and the cross-sectional (perpendicular to z-direction) parts to the form factor:

$$F(\mathbf{q}) = \iiint_V \Delta\rho(\mathbf{r}) \cdot e^{-i\mathbf{qr}} dx\, dy\, dz \;=\; F_1(q_z) \cdot F_2(q_\perp). \tag{2.21}$$

According to Glatter et al. [10], the first part (F_1) gives, averaged for different angles of incidence α:

$$F_1(q_z) \;=\; \int_{-H}^{H} dz\, e^{-i\, q_z\, z} = 2H \left(\frac{sin\ (q_z H)}{q_z H} \right) \tag{2.22}$$

Therefore the intensity $I_1(qz)$ becomes:

$$I_1(q_z) \quad = < F^2(q_z) > = \;(2H)^2 \cdot \int_0^\infty d\ cos\ \alpha \left(\frac{sin\ (qH)\ cos\ \alpha}{q\ H\ cos\ \alpha} \right)^2 \tag{2.23}$$

$$= 2H \cdot \frac{\pi}{q} = L \cdot \frac{\pi}{q} \tag{2.24}$$

The second part (F_2) is the cross-sectional contribution. Without loss of generality the incident wave vector takes the form

$$\mathbf{q} = \begin{pmatrix} cos\ \alpha \\ 0 \end{pmatrix} \tag{2.25}$$

which leads to

$$F_2(q_\perp) = \Delta\varrho \iint d\varrho \, d\alpha \, \varrho \, e^{-i\, q\, r\, cos\, \alpha} \tag{2.26}$$

$$= \Delta\varrho \, 2\pi \, R^2 \, \tfrac{J_1(qR)}{qR} \tag{2.27}$$

and

$$I_2(q_\perp) = F_2(q_\perp) \cdot F_2 * (q_\perp) = (\Delta\varrho)^2 \, (\pi R^2)^2 \cdot \left(\frac{2J_1(q_\perp R)}{q \perp R}\right)^2 . \tag{2.28}$$

In equation Eq. 2.27 the Bessel function of the first kind and first order $J_1(qR)$ was used, which is illustrated in Fig. 2.7. The scattering intensity distribution of cylindrical shaped scatterers is then (for an arbitrary scattering vector q)

$$I(q) = I_1(q) \cdot I_2(q) = (\Delta\varrho)^2 V^2 \, \frac{\pi}{L} \cdot \frac{1}{q} \cdot \left(\frac{2J_1(qR)}{qR}\right)^2 \tag{2.29}$$

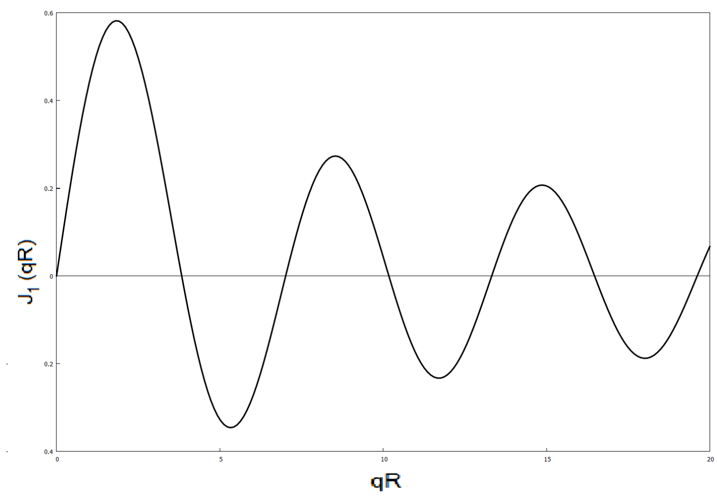

Figure 2.7.: Bessel function of the first kind and first order

Hence the form factor becomes

$$F(q_\perp, \, q_z) = \Delta\rho \, J_0(q_z \, H) \quad \underbrace{\int_0^R d\varrho \, J_0(q_\perp \, \varrho)}_{q_\perp \varrho \cdot J_1(q_\perp \varrho) \, = \, \int d\varrho \; J_0(q_\perp \varrho) \, \cdot \, q_\perp \varrho} \tag{2.30}$$

$$F(q_\perp, \, q_z) = \Delta\rho J_0 \, (q_z \, H) \cdot \frac{J_1(q_\perp \, \varrho)}{q_\perp \, \varrho}. \tag{2.31}$$

In Eq. 2.31 $q_{\perp}$ and q_z can be written as $q_z = q \cdot cos\ \alpha$ and $q_{perp} = q \cdot sin\ \alpha$ with respect to the incoming beam. Where α is the angle between the incoming beam and the long axis of the cylinder. In Fig. 2.6 the case of $\alpha = 90°$ and $q \rightarrow \infty$ is shown which leads to the simplified form factor

$$F(q) = \Delta\rho \frac{1}{q^2 R} \left(2J_1(qR)\right)^2 . \tag{2.32}$$

The form factor of cylindrical scatterers is shown in Fig. 2.8, by use of equation Eq. 2.32.

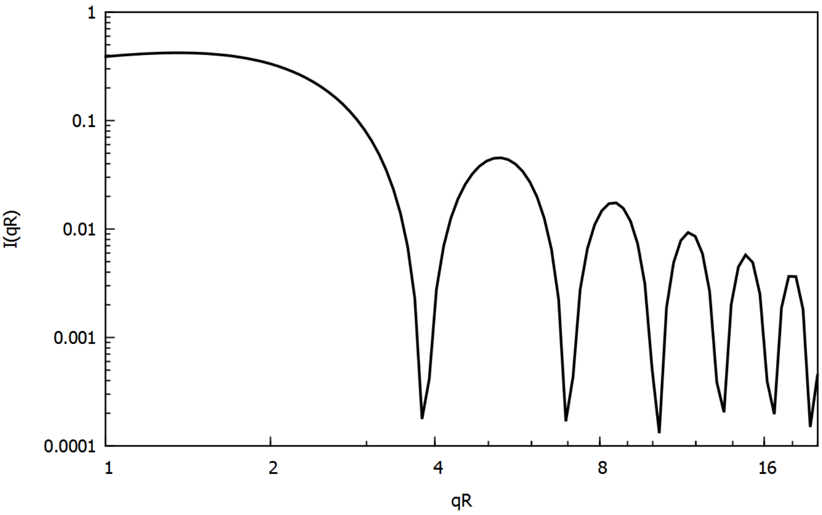

Figure 2.8.: Scattering from a single solid cylindrical particle of radius R and length L = 2H

2.2. Evaluation of SAXS and WAXS data

As mentioned before there exist several methods to calculate back the full form factor. One of them is to compare the gained scattering pattern with those of known forms. This is useful for scatterers of simple geometric shapes, like spheres or cylinders. In the case of materials consisting of these types of building blocks, it is possible to learn about their internal structures and the systematic mutual alignment. Bone, skin, tendon and cellulose based materials can serve as examples. It is possible to gain information about the spatial extension of single units and their position relative to each other.

For instance, in the case of tendon, the structural unit is collagen. Using SAXS its length (300 nm) can be determined as well as its orientation. It is worthwhile to mention, that this information can be used in the medical field, particularly in cancer diagnosis. In the work of

James and Kirby [13] the changes in the fibre diffraction patterns of skin that indicated the presence of a melanoma have been shown.

In this study the orientation of cellulose is the object of research. Therefore a typical SAXS pattern is shown in Fig. 2.9 (a) and (b). The pictures show possible paths of integration, either in **q**- or in χ- direction.
Now its is depending on the scope which intensity distribution should be taken into account. Either the axial (**q**) or the radial (χ) can be considered or both of them. To evaluate the microfibril angle it is necessary to perform an integration along the χ axis, within a circle of certain thickness in **q**- direction. This leads to the curve displayed in Fig. 2.9 (c).
For further investigations it can be useful to consider the integration along the $q(\AA)$, however this path of integration was not required.
The mean microfibril angle can be seen as half the angle between the two side maxima.

In Fig. 2.10 (a) a typical wide angle scattering pattern is shown. As for the intensity distributions gained by SAXS two types of integrations are possible. Again the integration along the azimuthal angle χ, within a circle of certain thickness, was chosen. The ring of the integration was chosen to include the inner circular intensity distribution of Fig. 2.10 (a). The resulting intensity distribution, in dependence of the azimuthal angle χ is illustrated in Fig. 2.10 (b).

More detailed information concerning the single data records evaluation are given in Sect. 4.2.

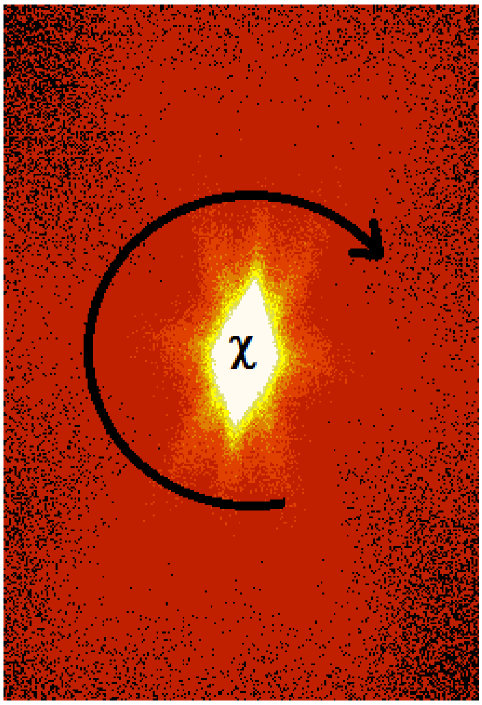

(a)

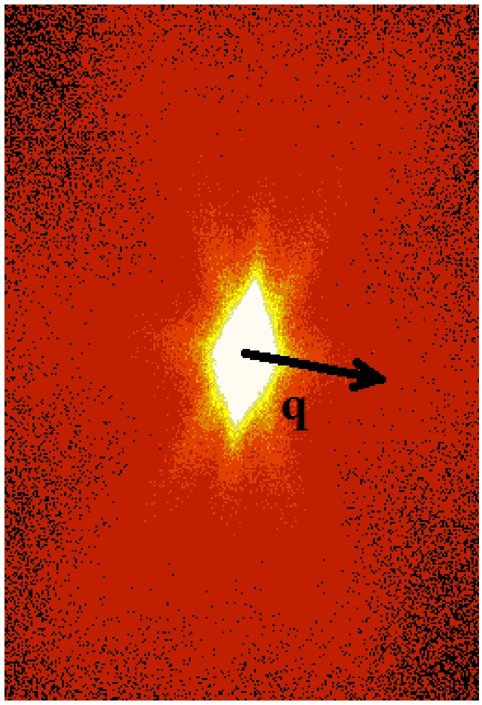

(b)

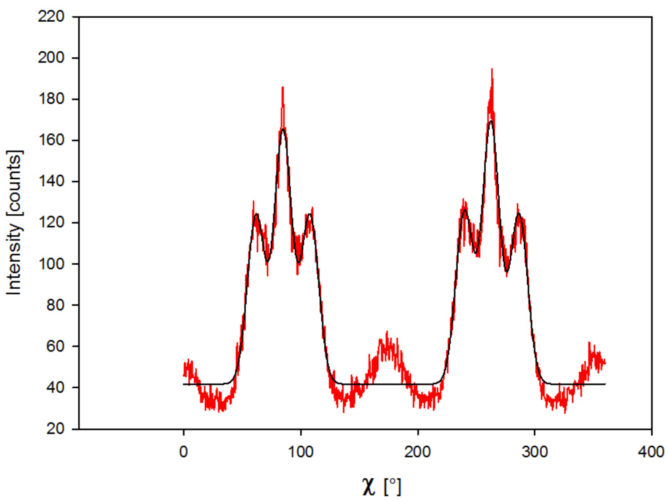

(c)

Figure 2.9.: (a) Intensity distribution in the SAXS regime of a wood sample; the illustrated path of integration in azimuthal direction (χ) and in (b) radial direction ($\mathbf{q}$). (c) Intensity distribution in dependence on the azimuthal angle after integration.

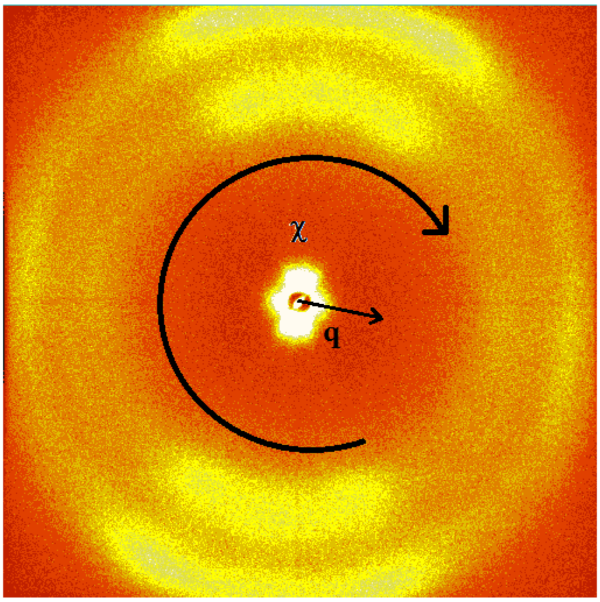

(a)

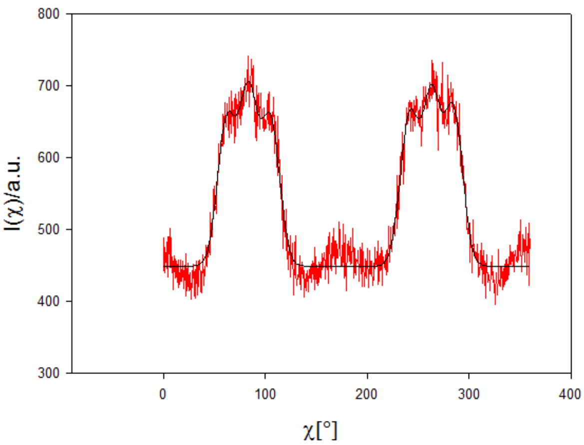

(b)

Figure 2.10.: (a) Intensity distribution in the SAXS regime of a wood sample; the illustrated path of integration in azimuthal direction (χ) and in radial direction (**q**). (b) Intensity distribution pattern after integration along the azimuthal angle, within a circular ring.

3. Material

3.1. Wood

3.1.1. Structure and function of wood

The following section relates primarily to *"Botany: An introduction to plant biology"* (J. Mauseth) [19].

Wood is an example for a biological composite material which has a hierarchical structure. In this case the basic units are arrangements of different types of cells, in different stages of development. After the end of their life cycle, the remaining cell walls of the dead cells still are able to sustain a mechanical load.

The main functions of living cells are the conduction of water from the roots to the crown to each single leave, giving mechanical strength, to withstand gravity and other types of external influences, such as windstorms. Furthermore it serves as storage of nutrients. The cells are the main venues for synthesis of biochemicals and regeneration of damaged structures (e.g. damage caused by game). Different types of wood have evolved over millions of years. One roughly distinguishes between softwood and hardwood. For example conifers, which belong to the large group of softwoods. Whereas most of deciduous trees like beech, teak and mahogany reassemble to hardwoods.

In evolutionary context groves of softwoods pertain to the older species. They are of a slightly more primitive composition, in contrast to groves of hardwood. They own a more complex and differentiated structure on the cellular level.

To show the setup of a timber, it is suggestive to start from the larger scale to the micro- and further to the nano-structure. A tree itself can be subdivided into the subterranean part, the roots and the parts above the surface, stem and crown. The most widely used part of a tree, for technical applications is its stem. Its alignment is of importance, the tube cane has to be straight without holes, splitting and knots. As well the xylem has to be numerously and even. The other components of a tree are often wrinkled and too small a diameter but are of use for paper industry or as combustible material.

The trunk itself is subdivided into a number of distinguishable parts. Therefore it is appropriate to have a closer look on the typical structure of the stem composition.
A cross section is shown in Fig. 3.1.

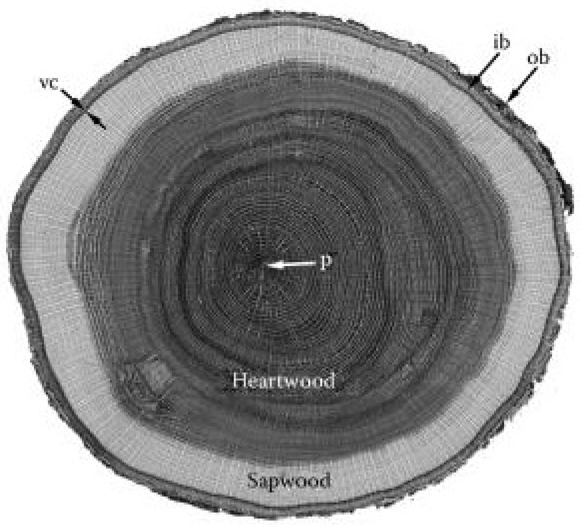

Figure 3.1.: Cross section of a softwood stem; Parts of the stem: P...pit; Heartwood, Sapwood; VC...vascular cambium; ib...inner bark; ob...outer bark [30]

The outermost part is the outer bark (ob), providing a protective barrier function and for functional reasons containing mostly dead cells. The inner bark (ib) or secondary phloem is formed in a thin cylindrical layer around the circumference of the stem. The inner and outer bark belong to epidermal tissues. Cells of such tissues are layered with *adcrustations* which are water repellent. Important *adcrustations* are *suberin* (cork-substances) and *cutin* [17]. In contrast to the *adcrustations* are the *incrustations*, being incorporated into the cell wall.
Further the vascular cambium (vc) is a rather thin layer consisting of unspecialised living meristematic cells, which are responsible for producing secondary vascular tissue.

The secondary phloem or secondary xylem consists of a radial and axial system. The latter providing the function of conducting liquids between the highest and lowest parts of a tree.

One has to differentiate between the secondary phloem in angiosperms (companion cells) and gymnosperms (sieve cells). Fibres and non-conducting parenchyma are found in both (angiosperms and gymnosperms) in the axial system, which can be discriminated into early - and latewood. [19]

The vascular cambium (vc) is a meristem that produces secondary the plant body [1] [19, p.172]. So if there is a secondary plant body, there has to exist a primary one [2]. The latter is also named primary tissue, which is the tissue from which non - woody plants such as herbaceous vegetation are built of.

In woody species additionally tissues are developed in the vascular cambium. It should further be noted that only if a region of a grove is old enough, a vascular cambium can be formed. Therefore, roots and shoots need to be several weeks old, before they are able to produce this tissue. Before that certain age, there can only be primary growth [19, p.172].

[1]The **secondary plant body** summarizes lignified plant tissues. They are built up in a later stage of growth. [19]

[2]The **primary plant body** is the first occurring tissue of a new (tree) shoot. It is a non-lignified plant tissue. Herbaceous tissues and plants consist of a primary plant body [19]

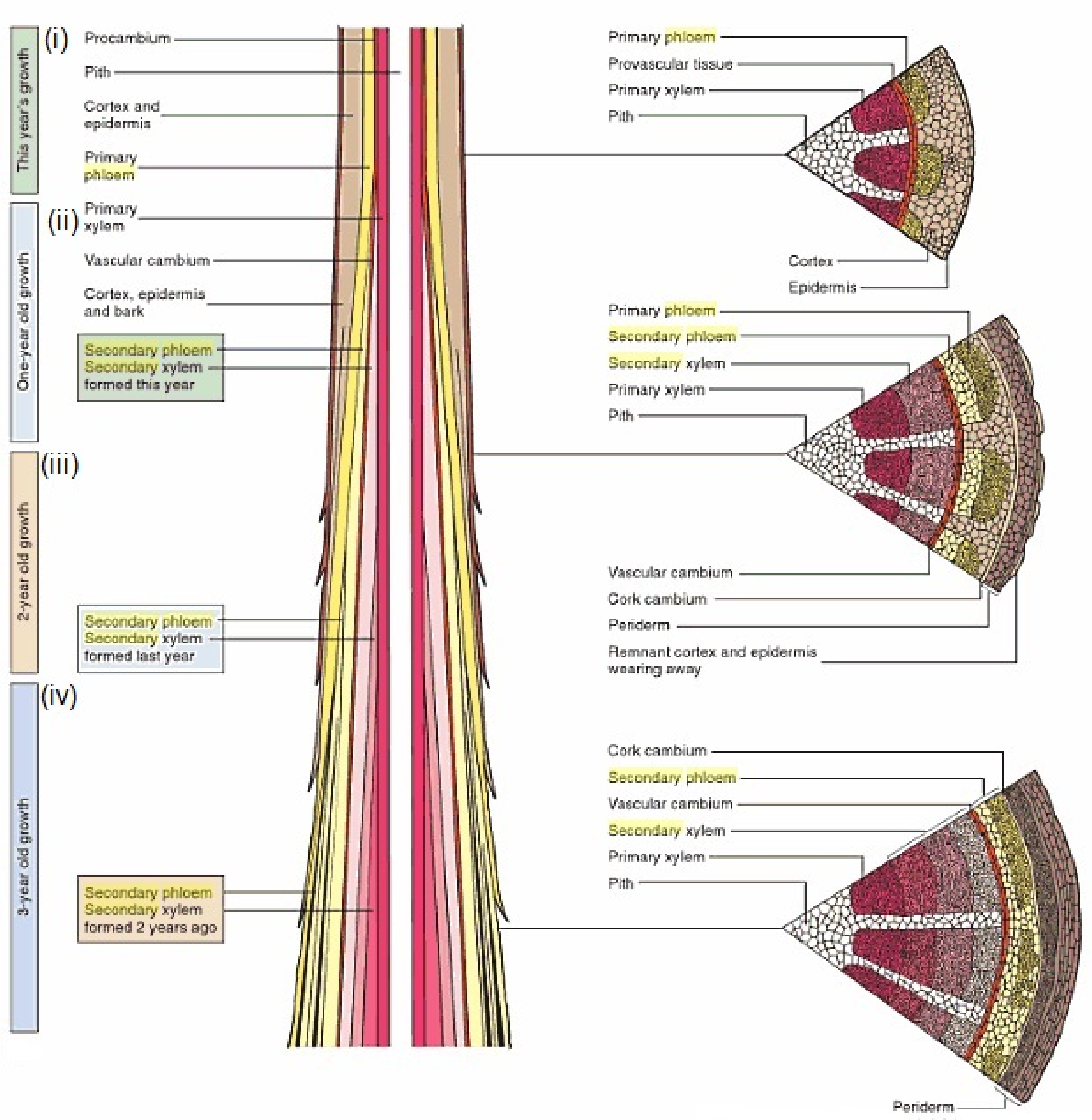

Figure 3.2.: Stages of development and degree of lignification of a stem: (i) lignification and tissues of a new shoot (ii) lignification and tissues after one year of growth; after one year of growth the *vascular cambium* and secondary xylem emerges (iii) lignification and tissues after the second year of growth;a new secondary phloem and xylem emerges, the bark becomes thicker and forms cork (iv) lignification and tissues after the third year of growth [19]

Fig. 3.2 indicates the point of time at which different tissue forms. Furthermore wood is always built in the interior of the vascular cambium, bark always on the outside [19, p.174]. In regions of seasonal climatic variations, the vascular cambium is quiescent during a certain period, namely in winter or in dry periods. This causes the annual rings. Early woods, which is also called spring wood, needs a high capacity for conduction to sustain the emergent leaves. Therefore wide vessels, that have a large amount of conductance of liquids, are a necessity. At these early periods in the growth season, this is of higher importance than mechanical strength and stability. This relation changes during the growing period and wood, produced at later times, has a thickened cuticle.

Latewood or summer wood provides more mechanical stability, which is of importance because of the increasing amount of leaves and larger branches and the concomitant growing wind- and water load. After the growing period, in the end of the season, the vascular cambium again becomes quiescent [19, p.234].

Sapwood is the layer further inside than vascular cambium and much thicker than the latter. Sapwood is optically easy to distinguish from the darker heartwood. There is a risk of confusion with the term "hardwood".
The difference between sap- and heartwood occurs, since with increasing age of the tree, in the older (innermost) parts of the stem, vessels lose their ability of conduction. These vessels are wide enough to allow fungi to grow. So there exist a bunch of mechanisms which seal the dried-out canal. The surrounding parenchyma of the vessel form bubbles of protoplasm into the canal, building a plug which locks the vessel.

This process is called a *tylosis* and is built in the whole length of the vessel. Additionally the parenchyma cells in heartwood undergo numerous metabolic changes and produce large amounts of phenolic compounds, some of them build up toxic levels (suggested by i.a. Rudman [31] & Stewart [35]), lignin, and other dark coloured, aromatic substances. These inhibit growth of bacteria and fungi so it gains more resistance to decay.
The process of turning sapwood to heartwood is the death of the parenchyma cells. Accompanying with the latter is the loss of active defence. In the case of wounded timber it is the development of *necrophylactic periderm* [22].

In living sapwood there are two kinds of defence mechanisms, active (induced by attack or wound) and passive (produced prior to infection) [36]. The during *tylosis* produced aromatic chemicals are usually of dark color and as they accumulate, wood becomes darker and more fragrant. Wood from conifers, like cedar wood [19, p. 184], can serve as an example. But on the other hand it is also possible that one cannot really distinct between sap- and heartwood on the gross level (e.g. abies spp.).

The vascular cambium builds every year new layers of sapwood, replacing the dried up, older vessels. According to this it has about the same thickness, whereas the heartwood is constantly growing and gaining more thickness. This relation is only valid up to a certain trunk diameter. It would be too specific to go into detail when this transition to a mature tree takes place.
The process of turning sapwood to heartwood is a spontaneous process, a distinction must be made between species forming heart wood (some at an early stage, some at a later, e.g. *alnus spp.*) and those who are not, since trees appear to grow quite well without heartwood, its frequent occurrence suggests that it's beneficial for trees to produce it (its advantage is a higher mechanical stability of the stem). Much evidence suggests that it forms in the dormant season [3]. In the very middle of the stem is the pith often composed of spongy parenchyma cells. In trees this part usually turns into xylem, sometimes if the tree hollows, it simply disappears.

3.1.2. Cell structure of wood

Living plant cells consist for the most part of cell wall enclosing void space, the lumen. Depending on the different functions, the thickness of the cell wall is varying.

For wood cells it is convenient to find a cell without a protoplast. The cell walls prior task is, to provide mechanical functions. A mature tree (height app. 8 m) can weight around 4 -5 tons. Consequently the compound of all wood cells carry the weight of the whole tree and give stability against gravitational and other forces. These are particularly wind or further mechanical influences, caused by creatures, feeding damage for example.

In the lumen of the sapwood transport of liquids takes place. The water transport from the roots to the new shoots forced by transpiration in the leaves through the xylem and the water pressure from the roots. The water column does not break, caused by cohesion forces between the water molecules. The transport is effected by the outer humidity and temperature.

On the other hand the transport of sugar and minerals in the other direction from the leaves down the phloem to the roots takes place. These sieve tubes are tiny cylinders with around 40 micrometres in diameter and length of approximately and 1,200 micrometres. The peak rates of this solute transport in the phloem amounts to 2 metres per hour comprises around 20 litres of sugar sap. The sap transport in the phloem as well is effected by temperature but further by light and the nutritional status of the tree.

Wood cell walls consist mainly of three components: cellulose, hemicellulose and lignin. The first is an organic compound with the chemical formula $(C_6\ H_{10}\ O_5)_n$, a polysaccharide, building a linear chain of $\beta\,(1 \rightarrow 4)$ linked D-glucose units. It will be described in detail in the following chapter "Cellulose". It is the proportionally greatest part of the wood constituents.

The second is a heteropolymer – or more specifically a matrix polysaccharid of a more complex structure than cellulose. In contrast to the latter it is not only a linear chain, but has several branches. These are characterising the types of hemicellulose. Unlike cellulose, it appears only in random, amorphous structures. In the chapter about hemicellulose (chapt. 3.1.6) it will be discussed in a narrower view. The entirety of cellulose and hemicellulose is often referred to as *holocellulose*.

The last of the three components, the lignin, which is also the most complex structure of these, is a polymer consisting of aromatic alcohols, known as monolignols. The composition of lignin is varying between the single species. For example, the composition from an aspen sample is 63.4 % carbon 5.9 % hydrogen, 0.7 % ash, and 30 % oxygen (by difference) corresponding approximately to the formula $(C_{31}\ H_{34}\ O_{11})_n$. [7]

Apart from these three main components one will find extractives ranging from around 0.5 % to 20 % by weight, for different species. Some are water soluble, toluene ethanol soluble or ether soluble. In sum there are a few hundreds of them identified. In some cases their specific role in the tree is understood, whereas there are a few, where there is no real clarity about their function.

The cell wall itself is a composition of mainly three layers:
The primary wall, middle lamella and secondary wall. The first is the middle lamella (ML), which is the layer between two adjacent cells. The cell itself is enclosed by the primary layer (P) but in most cases it is hard to distinguish between this and the middle lammella, especially in those plants, building a secondary cell wall. For sake of completeness, both of them are shown in Fig. 3.3. Although they are mostly summarized in the term middle lamella, being a pectin containing layer cementing two cells together. It is able to form *plasmodesmata*, microscopic channels linking plant cells together, enabling its cell-to-cell transport and

communication between them. Further it's containing magnesium and magnesium pectates. Fig. 3.4 shows the percentage distribution of cellulose, hemicellulose and lignin in the middle lamella. In this part the cellulose is in an amorphous state, the microfibrils are not orientated. The highest part has lignin, with 8.4 %, which is enclosed between the pectin.

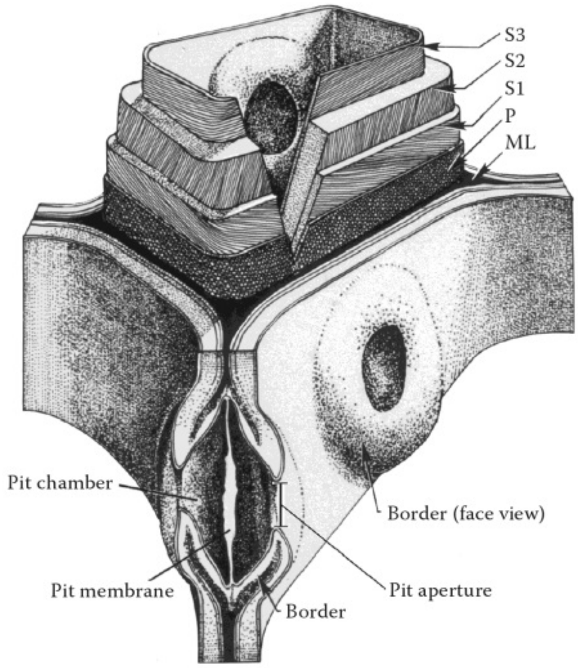

Figure 3.3.: A cut across the the cell wall is shown. The cell wall is composed of three layers: the middle lamella (ML), the primary wall (P) and the secondary wall. Each of them is consisting of three predominant components: cellulose microfibrils (CM), hemicellulose and a matrix (consisting typically of pectin in primary walls and lignin in secondary walls) [30, p. 18].

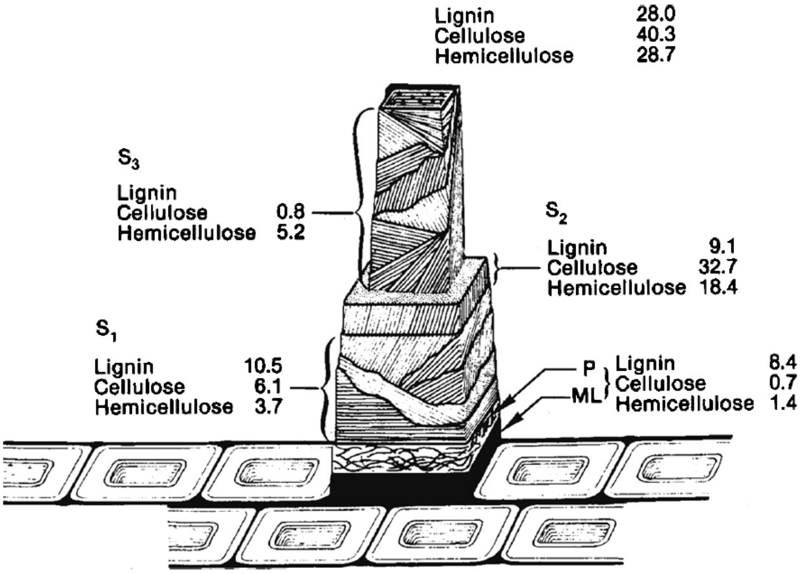

Figure 3.4.: Chemical composition of the cell wall of scots pine [30, p. 59]

The secondary cell wall itself is subdivided into three, easy to distinguishable, layers, namely the S1, S2 and S3 layer. In the three parts of the secondary cell wall cellulose has a higher degree of crystallinity.

The first one, the S1 layer is directly adjacent to the compound middle lamella (in the case of indistinguishable primary cell wall and middle lamella, the term compound middle lamella is used) or the primary wall. As is shown in Fig. 3.4, it consists of 10.5 % lignin, 6.1 % Cellulose and 3.7 % hemicellulose. From the three layers of the secondary wall it is the one with the highest lignification and slightly thicker than the the primary cell wall. It consists of alternating right and left orientated helices, resulting in some kind of a checked pattern. This allows expansion during the cell growth. The slope of the helices is progressively becoming steeper in one direction, resulting in the next S2 layer, arranged in a right handed helix.

The latter is the thickest of the three, occupying the largest amount of cell volume, with the highest amount of cellulose, namely 32.7 %, 9.1 % lignin and 18.4 % hemicellulose, determining the properties of the cell. It comprises approximately 78 % of the cell wall. The helices of this layer are wound in steep helices of defined cellulose microfibrils. The microfibril angle in this layer is a parameter for mechanical stability of wood. In juvenile wood it is larger than in mature wood, allowing the new sprout to be flexible and not breaking because of exposure to wind. As the tree matures, these high flexibilities yield to higher mechanical strength and the microfibril angle of the S2 layer is shrinking, the cellulose gets more orientated into vertical direction. There are several other external influences, affecting the orientation of this layer, namely humidity, nutrient supply and weather. There is also a change in the microfibril angle between early- and latewood. Another not assessable factor is the species of wood. As well there are variations in the microfibril angle, depending on the position in the tree. To this thematic exist several studies, for example the paper of Lichtenegger et al. [15]. Here the microfibril angles of softwoods (*Pinus sylvestris* and *Picea abies*) and hardwoods (*Quercus robur* and *F. sylvatica*) were compared.

There were several attempts to find dependencies of the orientation of the S2 layer. For example Preston, in 1934, [26] was the first to remark on a relationship between the orientation of cellulose micelles in the wall and the length of the conifer tracheid. He formulated a precise mathematical relationship:

$$L = a + b \cdot \Theta \tag{3.1}$$

where L is the length of the cell, Θ the microfibril angle and a and b are constants. Afterwards it could be shown that this relationship (Eq. 3.1) also held for S1 and S2 layer, when considered separately (Preston, 1948 [27]; Preston & Wardrop, 1949 [29]). Preston (1974) [28] backtracked this assertion, showing that the relationship was only statistical, so the statement "any shorter tracheid shows a flatter S2 helix than any longer tracheid" (Preston, 1974 [28]) is not valid. [4]

The third layer S3 again is a very thin one, even thinner than the S1 layer but with a similar structure. It is remarkable that this one has the lowest amount of lignin. To be consistent with Fig. 3.4, this layer is, depending on the observed species, not lignified. The lack of lignification is supposed to support the conductance of the tree sap. To move water in the canals there has to be a certain amount of adhesion between the conducted water molecules and the conductor, the cell wall and the hydrophobic lignin plays a crucial part. Contrary to latter the cell walls are highly hydrophilic, therefore permeable for water.

As well as the S1 layer, it has a rather low rate of cellulose 0.8 % and hemicellulose 5.2 %.

3.1.3. Cellulose

The main constituent of higher plant cell walls is cellulose, which can be produced as well by some bacteria, fungi and also by a few animals like tunicates. It is first discovered by in 1838 by Anselm Payen [37] . For a long time its molecular structure was undiscovered but concomitant with unravelling it, a wide range of further applications opened. The cellulose molecule itself is a linear macromolecule composed of D-anhydrglucopyranose units linked together by β-1,4-glucosidic bonds, a β-1,4 glucan (polyglucose). The pyranose rings assemble in a $^4C_1$ chair formation, which is energetically preferred configuration.[3]

The molecular structure of the polymer is sketched in Fig. 3.5 where the middle (blue) pyranose ring is repeated, which gives the length of a cellulose chain. On the first enumerated carbon atom C1 are two attached oxygen atoms, on the second and third, C2 and C3 are each hydroxyl substituents (OH), on the fourth (C4) is one attached oxygen atom, which is also the linkage between two pyranose units, the same is C1 and on C5 one finds a hydroxymethyl group.

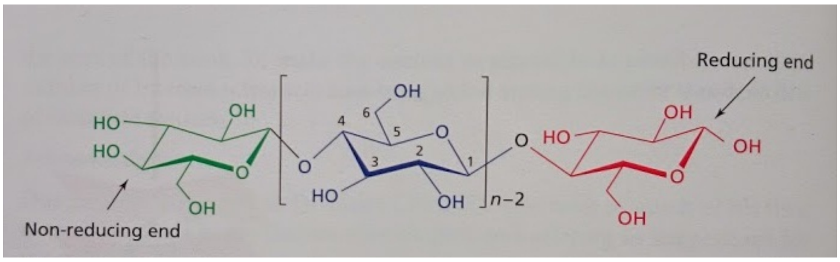

Figure 3.5.: Molecular structure of cellulose; the numbers in the red part each represent a carbon atom,using the conventional numbering; the left, green part: the nono-reducing end with a free hydroxyl a C4; right, the red part: reducing end with a hemiacetal [37]

The structure of a a cellulose chain is a twofold helix conformation, which means two monomers per turn. The linear repeating distance is about 10.3 $\AA$.

There are four known main polymorphs of cellulose I, II, III, IV, where Cellulose I is actual a composite of the two allomorphs Iα and Iβ. Cellulose II is thermodynamically the more stable form and is a transformed form of Cellulose I. Cellulose III obtained from Cellulose I or II due to swelling with liquid ammonia or amines at low temperatures. It has two subclasses III_I or III_{II} depending on Cellulose source. Cellulose III_{II} is supposed to be a hypothetical material, there is no evidence of its existence [37, p. 89].

For Cellulose IV, Cellulose III is annealed in glycerol. As The latter one it has two subclasses IV_I and IV_{II} for the same reason as Cellulose III. Of all these forms, cellulose II is

[3]The used method of method of representation Haworth projection (see also Fig.3.5) which is common for representing monosaccharides. It is based on the Fischer projection. On the edges of the heterocyclic ring carbon atoms are located. [23]

supposed to be the most stable form. In Fig. 3.6 a schematic representation of the transformation of the existing cellulose allomorphs is shown.

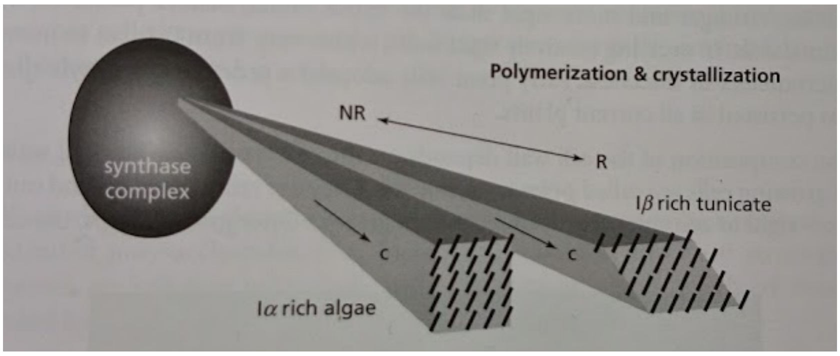

Figure 3.6.: Scheme of cellulose allomorph transformation [37]

The most frequent allotrope is Cellulose I_α, which appears commonly in algae and bacteria and Cellulose I_β, occurring in superior plants.

In 1995, a hypothetical model for plant cell biosynthesis was proposed by Delmer and Amor [37, p. 70] which is shown in Fig. 3.7.

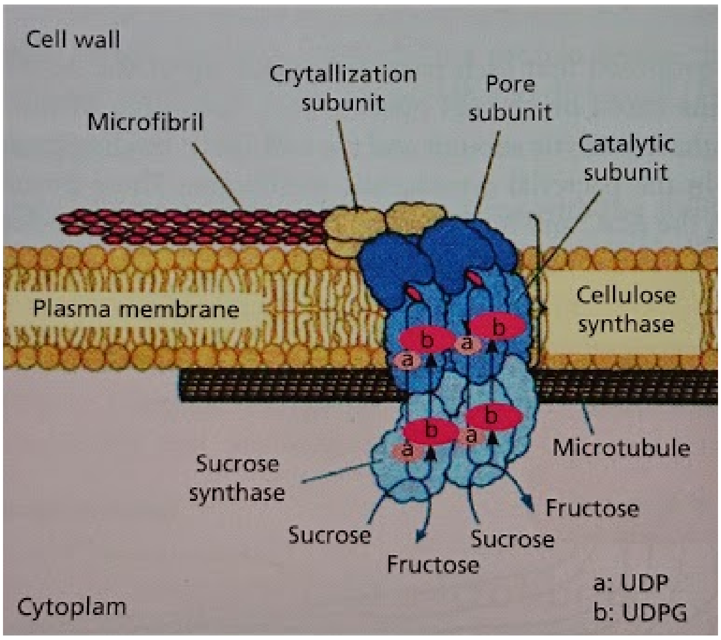

Figure 3.7.: Hypothetical model for biosynthesis of cellulose in plant cells. A microfibril is synthesized via a multisubunit complex [37]

Cellulose in plant cells is synthesized by a syntheses complex on the plasma membrane. A single β -glucan chain is produced by only one single crystallization subunit. These subunits itself are organized in rosettes building again rosette-shaped assembles. Altogether they spin a cellulose microfibril.

Cellulose in a plant cell

Cellulose is the main component of plant cells with several manifestations. It emerges as well in crystalline form as in amorphous form, commonly in alternating areas in single plant cells. For scientific investigations on the cellulose itself, pure cellulose (meaning hemicellulose or lignin has to be removed) with a high degree of crystallinity is desired. Also long fibre lengths are advantageous. The bacterium *Acetobacter xylinum* conduces as a model organism which produces the latter. This, in nature ubiquitous bacterium metabolises ethanol to acetic acids during fermentation its biosythesis of cellulose, is studied well. The ratio between cellulose I_α and I_β changes depending on the culture conditions, e.g. additives and temperature. Investigation on *Acetobacter xylinum* helped to find out why there exist allomorphs and why they vary in nature. The amount of the cellulose allomorph I_α is decisive for the Young's modulus due to different water capacity [33].
Another model organism is *Valonia ventricosa*, known as *Bubble algae* and is a species of algae with high distribution all over the worlds oceans. Its produced cellulose has a degree of polymerization of $\sim$ 44 000 [37, p. 23]].

It it recognisable that cellulose produced in presence of hemicellulosic polysaccharide, the crystallinities are altered, meaning that there is more cellulose of type I_β. The polysaccharide mannan is therefore believed to lower the crystallinity of cellulose, in contrary xylan and xyloglucan strive after co-crystallisation with cellulose, causing lattice defects [33, p. 5].

The situation of cellulose production in living timber is, with all certainty not as plain as the production of bacterial cellulose. What is here to mention is that the exact molecular formation of wood in the wood cells still isn't understood yet. It is still a case of further investigations, but there are models which can be seen as quite reliable. This process is depending on a large number of factors as well exogenous (for example photo period and temperature), as well as endogenous (here phytohormones play a significant role) and of course the interaction between both of them.

As mentioned before, all wood cells origin from the vascular cambium, as long as it is active it ensures the perennial life of a tree, through producing new phloem and xylem. In the cambial zone one finds phloem and xylem mother cells, called cambial initials. The differentiation of xylem cells can be subdivided into four major steps: cell expansion, afterwards follows the well arranged deposition of the layers of the secondary cell wall, furthermore the lignification and at last the cell death. Throughout the lifespan the production of cellulose takes place. However, up now not a single enzyme involved in cellulose biosythesis was extracted or maybe cultured in cell cultures. Neither those responsible for the application process on to the cell wall.

But there are genes identified, which encode the catalytic subunit of the cellulose synthase (Ces) complex. Additionally, there exists a bunch of more or less related genes, so-called Ces-like (Csl) genes, approximately 20. These are related to the synthesis of polysaccharides [25, p. 1515].
The biosynthesis of lignin is described quite well, also cloning of some structural genes [38]; [5].

The phytohormones play a crucial role in the building of new cells, even though there only can be guessed about the exact interactions. Also differentiation of the tissues are controlled by them, some of them are identified as auxins, which are phytohormons with morphogen-like features. It is a signalling molecule for phloem or xylem differentiation. This auxin is a indole-3-acetic acid (IAA), which is one of the most abandoned native auxins (Fig. 3.8).

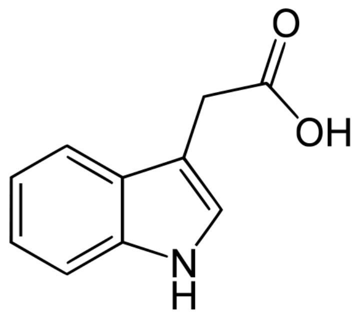

Figure 3.8.: Indole-3-acetic acid (IAA)

There exist three more native endogenous auxins. Mellerowicz et al. ([11], [20]) have described the role of phytohormons during procambium initiation, cambial cell division, primary cell wall expansion and secondary cell wall formation in a more explicit way.

The two cell walls (primary and secondary cell wall) form during different periods of the cell differentiation. Straight after the new cell has accrued, a several day lasting "maturation" process ensues. During this period a distinction between two processes is possible: first the emergent cells are stretched in transverse direction due to the deposition of lignin and cellulose, which is at this stage still in an amorphous phase. Secondly, when the crystallization of cellulose sets in, the microfibrils shrink into longitudinal direction. More precisely, they would shrink:

Because of adjoining cells, the single maturing cells are exposed to tensile stress, which is held up to the date the wood is cut. In Fig. 3.9 this process is viewed schematically.

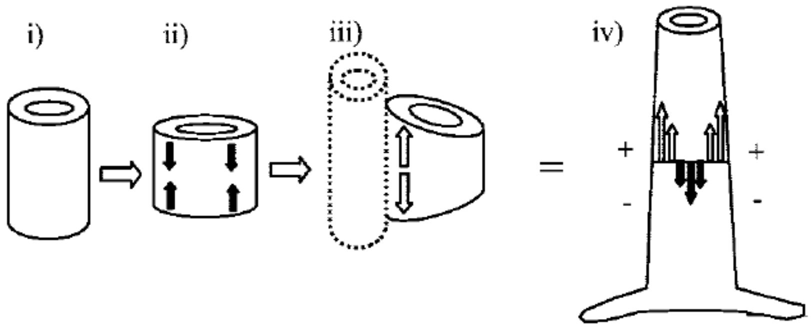

Figure 3.9.: (i) Begin of differentiation (ii) deposition of cellulose and lignin secondary cell wall causes longitudinal shrinkage (black arrows) (iii) due to attached neighbouring cells, it comes to deformation and therfore tensile stress (white arrows) (iv) sketch of a stem with load distribution (+ and white arrows ... tension forces; - and black arrows ... compression forces), each layer, each year exerts tangential forces on the wood [25, p. 1517].

3.1.4. Investigations on cellulose using SAXS

SAXS is a common and successfully used technology for investigating the structure of crystalline cellulose.

Based on the crystalline composition of cellulose in plant cell walls, scattering experiments can be performed. A schematical representation of these investigations is given in Fig. 3.10. In the left column the orientation of microfibrils is sketched, (a) shows a parallel fibril distribution, (b) an angular and (c) a circular distribution. In the middle column of the three cases the related scattering pattern is shown.

In (d) a more realistic case of fibril angle distributions is presented. Therefore the scattering pattern alternate and in (e) is shown one of the obtained scattering intensity distributions via SAXS.

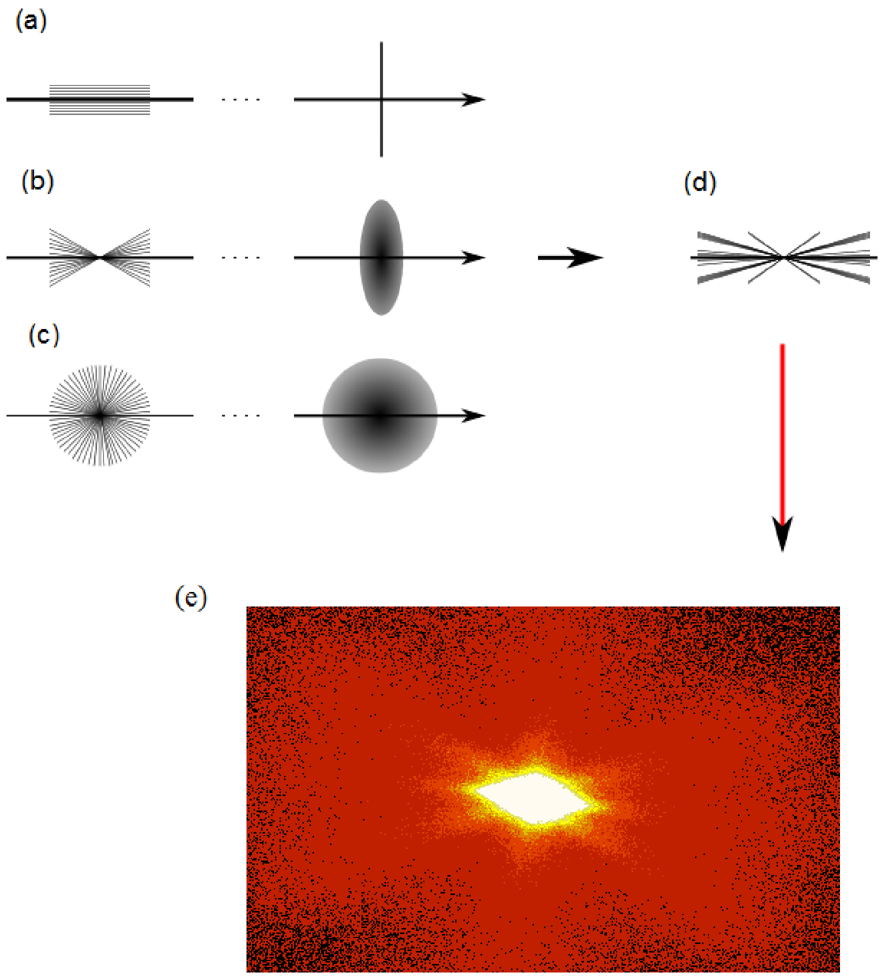

Figure 3.10.: (a) The scattering pattern of parallel arranged fibres is a single thin streak. (b) The scattering pattern of fibres arranged in an angular distribution is an ellipsoidal intensity distribution. (c) The scattering distribution of radial arranged fibres is a circular intensity distribution. (d) The scattering pattern of cellulose fibrils in the the wood cell is a mixture of parrallel fibre bundles arranged in diverse angles. Therefore the scattering pattern of cellulose in the wood cell wall leads to a scattering pattern of smeared out streaks arranged in an angle to each other.

For example Lichtenegger et al. [14] used SAXS to show the change of the microfibril orientation in the different layers of a wood cell. For this purpose they used X-rays from a synchrotron radiation source for non destructive scans with a position resolution of 2 μm applied on a wood sample. The orientation of the latter was the cross section of the cell perpendicular to the incoming beam. An area of 42×52 μm^2 was screened, the size of the single scanned pixel was $2 \times 2 \mu m^2$.

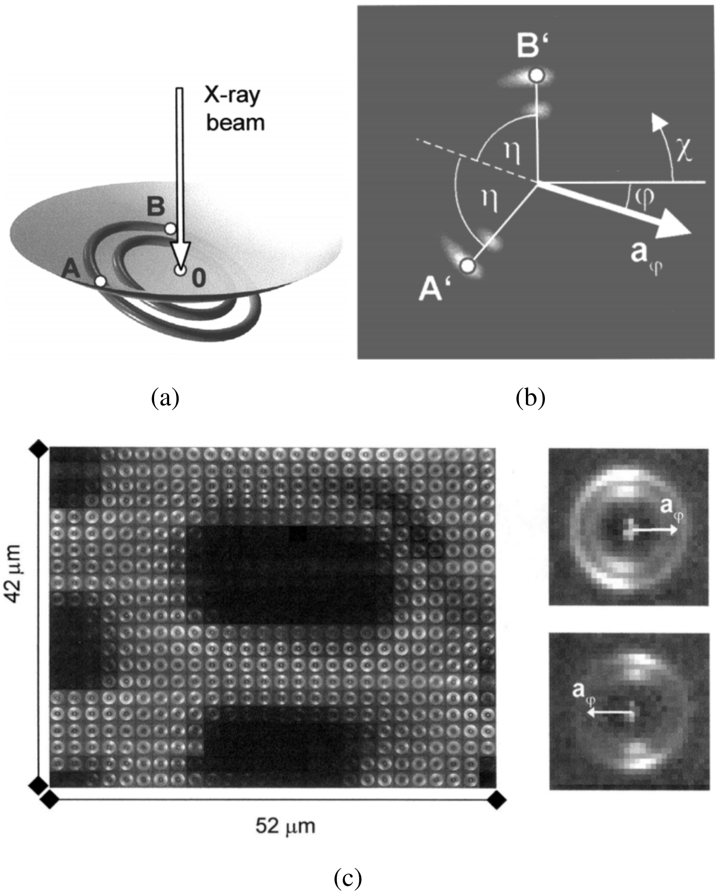

Figure 3.11.: (a) Intersection of Ewald sphere (light grey shaded sphere) with the Debeye-Scherrer rings (dark grey rings) (b) Asymmetric scattering pattern at A' and B'; $\mathbf{a}_\phi$ denotes the orientation of the asymmetry, $\chi = \phi + 180° \pm \eta$ (c) (left) Mesh scan over a complete wood cell in cross section with parts of neighbouring cells, pixel size: 2×2 μm^2. Dark regions correspond to lumina, bright regions showing a scattering signal correspond to cell walls. (right) Two typical diffraction patterns at greater magnification to show the asymmetry in the angular intensity distribution. The direction of asymmetry indicates the local orientation of the cellulose fibrils $\mathbf{a}_\phi$ [14]

Reflections are intersections of the Debye-Scherrer rings with the Ewald sphere (Fig. 3.11 (a)). Due to the connection between real- and reciprocal space an asymmetry in the sample causes an asymmetry in the reciprocal space. Therefore different diffraction spots are viewed shifted about a certain angle on the detector (Fig. 3.11 (b)). Fig. 3.11 (c) shows the local orientation of the microfibrils. The scattering intensity distribution shows a typical difference of about 180°, which allows the determination of the local orientation of the cellulose fibrils with

$$\chi = \phi \; + \; 180^\circ \; \pm \; \eta. \tag{3.2}$$

The two possible orientation of the winding of the cellulose microfibrils is either a left handed (S) helix or a right handed (Z) helix. Lichtenegger et al. were able to show in this experimental setup, that the S2 layer is winded in a right handed (Z) helix (Fig. 3.11 (c) (right) top picture). [14]

Abe et al. [1] observed a change of the diffraction peaks (200) and (004) from cellulose crystals during water desorption and related it to a mechanical interaction between the cell wall and the matrix substance. The key is the moisture content of the wood cell. Whereas the moisture content has a negligible influence on the crystalline cellulose of the microfibrils because their OH groups are satisfied by formation of hydrogen bonds between adjoining fibrils. The cell matrix substance consists of non-crystalline cellulose and hemicelluloses. With increasing moisture content an isotropically shrinkage or swelling takes place. This swelling would in turn effect the microfibrils. Further research on this area is necessary.

A a paper of Jakob, Tschegg and P. Fratzl [12] deals with a similar theme. In this research the distribution of pores and cell wall depending on the moisture content was the aim of the investigation.

As well as wood there is research concerning bacterial cellulose realised via X-ray diffraction methods, e.g. Keshk [33]. For example, the index of crystallinity could be shown with X-ray diffraction methods. Different celluloses, synthesized by different bacteria led to different results. Investigations on bacterial celluloses are quite promising for gaining pure cellulose, additionally in a cheap way. An area of application would be in the medical department due to its high purity, hydropholicity, structure forming potential, chirality and biocompatibility. Especially in skin therapy it could be usable as artificial skin or for covering wounds, as burns or ulcers. [33]

3.1.5. Lignin

Lignin is one of the main constituents of woody plants. It is a filling substance in the interfibrillar space responsible for the mechanical stability of a wood. The remaining space between the microfibrils is 10 nm in spatial extension [17].
Without this constituent it would not be possible to reach the height of trees and the vascular tissues simply collapse due to their own weight. Therefore lignin is one of the most important encrusts in wood. Due to the encrustation of the cell wall, flexibility and plasticity gets lost for the benefit of stability [17]. This process is also known as *lignification*. The percentage of lignin is variable, depending on the cell wall layer (Fig. 3.12).

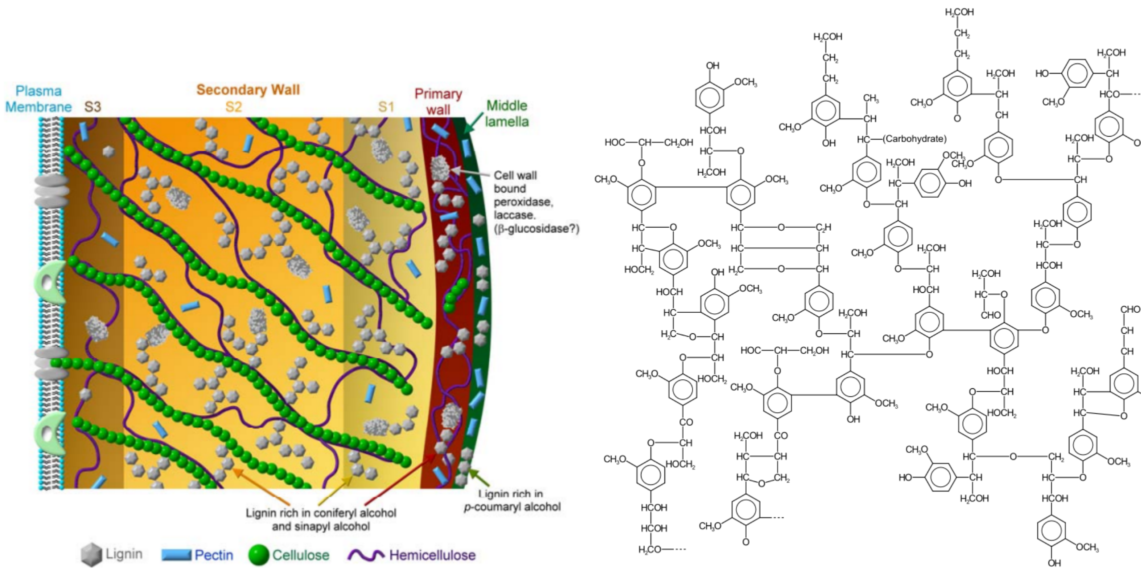

(a) Supramolecular lignin [37]

(b) molecular structure of lignin [7]

Figure 3.12.: (a) Schematic illustration of the distribution of the chemical substances (lignin, pectin, cellulose and hemicellulose) within the individual layers of the cell wall. (b) Example of a structural formula of lignin. The individual polymers can be linked in various ways.

It is especially abundant in compression wood, where mechanical support is necessary. Accept its weight supporting function, lignin is providing the liquor transport in the tree. Due to its hydrophilic properties it partially seals the conducting vessels and tracheids in axial direction. Therefore it supports vertical moisture transportation.
In the cell wall lignin has covalent links to the hemicellulose. The molecule itself is a three-dimensional network of amorphous structure (Fig. 3.12 (b)).

3.1.6. Hemicellulose

Hemicelluloses are heterogeneous, branched polysaccharides occurring in the cell wall of plants. They are characterized by $\beta - (1 \rightarrow 4)-$ linked chains of of sugars. As shown in Fig. 3.13, numbers $\beta - (1 \rightarrow 4)-$ indicate the C atom. Just as with cellulose in Fig. 3.5, the chair conformation was chosen as the most accurate representation.
Usually the chemical composition of hemicellulose is one type of sugar (xylose, glucose or mannose) in equatorial arrangement comparable with cellulose. From the backbone protrude short side branches of sugars. The commonly occurring sugars in the chains are xyloglucans, which is the principal hemicellulose in higher plants, xylans, mannans and glucomannans and $\beta - (1 \rightarrow 3, 1 \rightarrow 4)-$ glucans. In Fig. 3.13 the frequently occurring monosaccharids are shown.

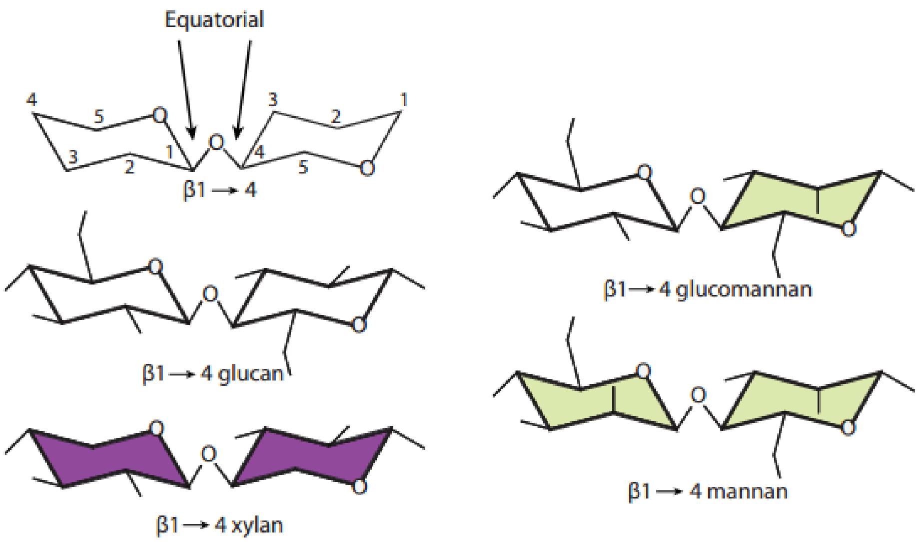

Figure 3.13.: Hemicelluloses are characterized by a $\beta - (1 \rightarrow 4)-$linked backbone with an equatorial configuration at C1 and C4. [32]

The hemicelluloses bind tightly to the cellulose microfibrils and crosslink them into a network. The composition of the hemicelluloses depends on the different kind of species and on the types of cell walls. Those of dicots and conifers are to a high extend by xyluglucans, in contrast to monocots where (glucurono)arabinoxylans are predominant. In cooperation with lignin it is responsible for the strength of the cell wall by tethering the hemicelluloses to the cellulose microfibrils [32].

The microfibrillar structure of cellulose was first proposed by Frey-Wyssling [9] in the year 1937. In the same year a microfibrillar structure of lignin and hemicellulose was further complemented by Bailey [2] using polarization microscopy.

3.1.7. Thermal treatment of timber

There are multiple possibilities for thermal treatment of wood, for example in air, vacuum or under an atmosphere of inert gas such as nitrogen or steamed water. In particular the two latter methods are quite common in industrial usage. Furthermore heat treatment performed in oil is common. For a large range of applications, the exclusion of oxygen is necessary to avoid oxidation processes.

Furthermore one has to distinguish between open or closed systems. As a consequence of the treatment, in closed systems there is an increase in pressure because of decomposition products. Moreover, if the latter cannot be carried away, chemical reactions occur. Stamm postulated in 1956 that the presence of acids produced from acetyl groups on hemicelluloses result in accelerated degradation of the polysaccharide components of the cell wall [34]. An advantage of an open system is apparently the removal of those disintegration products.

In addition there are also effects of species, having different results, mostly between hardwoods and softwoods. Thermal, hydrothermal or hygrothermal treatment of various woods results in weight losses that are generally found to be higher for hardwood compared to softwood species. Research in this area was performed by MacLean [18] already in 1951. In this work different heat treating methods and their effects on wood where compared.
More recent research has been carried out by Zaman [39] (2000). Heated steam treatments where used in order to analyse the effects on the carbohydrates (cellulose and hemicelluloses), especially their degradation reactions. It emerged that the carbohydrates were more amenable to various than lignin in intact wood. [39]

In 2002 Militz [21] provided an overview of the heat treatment technologies in Europe and scientific background and the technological state–of–art.
Different thermal-based wood treatments were presented. As well as their country of origin, the used temperature range, the shielding gas and single steps of the treatments are shown. As a result, the chemical transformation processes between the single methods were considered.

4. Experiment

4.1. Preparation of timber

As mentioned in the introduction (Sect. 1), the aim was the investigation of the influence of a thermal treatment on the nano-structure of wood, in particular the microfibril angle of cellulose. The chosen timber was a stem cross section of a freshly harvested *Picea abies*. At the date of felling, the age of the tree was approximately 80 years. Subsequently the stem cross section was sun dried for 7 days. After the drying process a small rod with rectangular cross section and dimensions $1 \times 4 \times 17\ cm^3$ was cut out and this in turn quartered lengthways. As a result 4 rods of these dimensions came out and are displayed in Fig. 4.1.

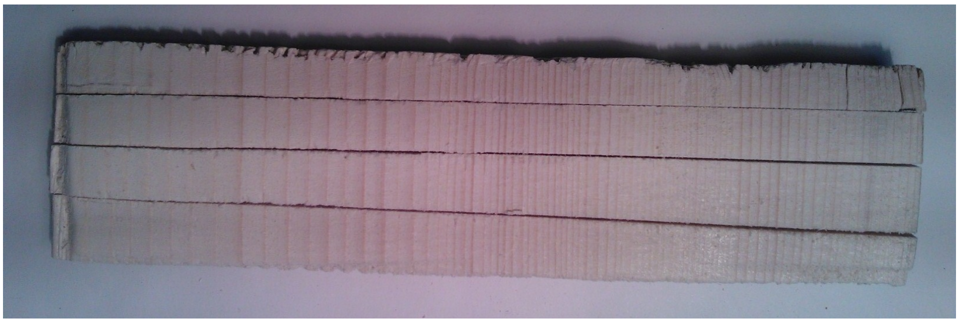

Figure 4.1.: Untreated samples

For the thermal treatment it was necessary to construct a furnace. The challenges where to heat up the timber up to a certain temperature, above 150°C. This is the temperature of the denaturation of hemicellulose and lignin. To avoid oxidation this has to happen in a protective gas atmosphere. In our case nitrogen was chosen. This was the chosen option because it is both easy to handle and easily available. Furthermore it is a common used method and recommended in literature (for example: [21]).

Another challenge was the removal of the decomposition products which occur during this process (as described in chapter: thermal treatment of timber). To solve this, a constant flow of N_2 was maintained, just slow enough to keep the temperature at a constant level. This was

controlled with temperature sensor. The furnace used for thermal treatment is shown in Fig. 4.2.
The grey cylinder displayed in Fig. 4.2 (a) is the heating device. Into this device a glass cylinder was placed, which serves as sample holder during the heating process. The edges where closed with two valves (Fig. 4.2 (b) displays a magnified view on the right valve). The right one served as gas inlet of the protective gas and holder for the temperature sensor, the left one as gas outlet.
To control the nitrogen flow, the outflowing gas was conducted through a glass of water. Its through-flow was controlled with the aid of a needle valve.

Before the thermal treatment, temperature curves where collected. To provide a constant temperature during the thermal treatment, it was necessary to monitor the temperature curve over a certain time.
Afterwards the first rod was heated up to 160°C, the second to 190°C and the third to 220°C each for 1.5 h. The fourth rod was taken as the reference sample, stored at room temperature.

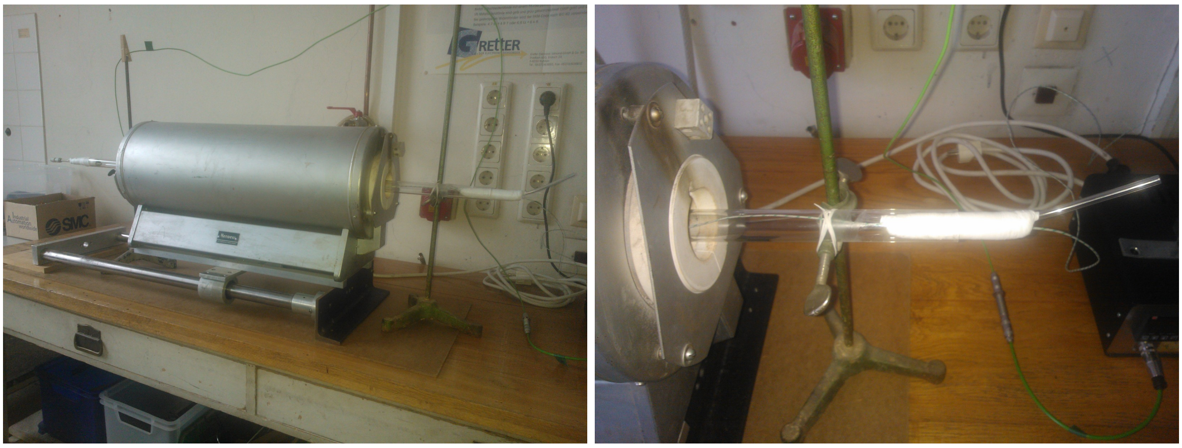

(a) Photograph of the furnace with inserted glass bulb for thermal treatment.

(b) The tube on the right edge is the protective gas inlet; the wire directly below the the tube belongs to the K thermocouple

Figure 4.2.: The used furnace, adapted for the thermal treatment of timber

For the SAXS sample preparation from each rod the best visible annual rings along the cross section were chosen before annealing, for all four rods the same rings. Every annual ring was subdivided in early- and latewood and from both 200μm thick pieces where cut out with a chisel.

The age range of the samples spanned from 3 years up to 75 years. A total of 24 annual rings were chosen, because af their good distinguishability. During extremely dry and humid years years the emerging secondary xylem is quite weak for both, early-, and latewood. For these years it is hard to distinguish or even separate early- and latewood.
Additionally, the distinguishability between them was increasingly difficult with increasing temperature treatment. Likewise, the increase of the brittleness of the samples was observed.

Therefore 48 samples could be extracted from each rod (Fig. 4.3). For each annual ring more samples than needed were produced, in case that a replacement should be necessary. Those used for the SAXS measurements were placed on a copper sample holder providing 27 possible slots for samples. Each slot has a diameter of 3 mm.

The prepared, but not used specimen are shown in Fig. 4.3. There is a notable colour gradient between the samples of different thermal treatments. The darkest shade is visible on the samples treated at 220°C.

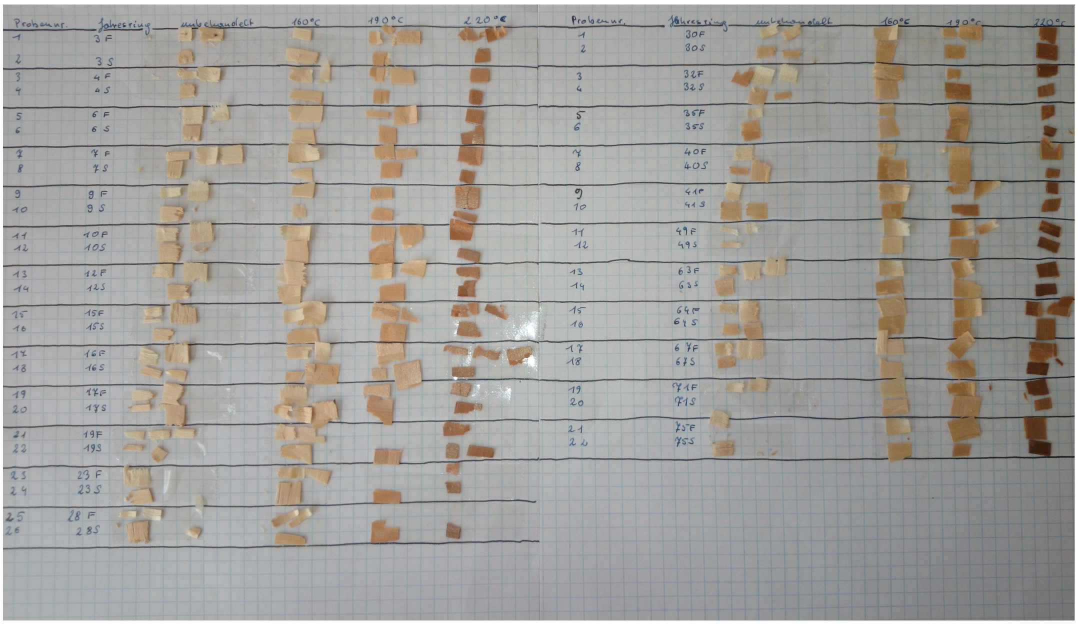

Figure 4.3.: The samples held in reserve

After the SAXS measurements, the used specimens were archived in the in Fig. 4.4 displayed form. The order of the samples was maintained the same way as on the sample holder. Therefore it was traceable, which specimen belongs to the individual scattering pattern.

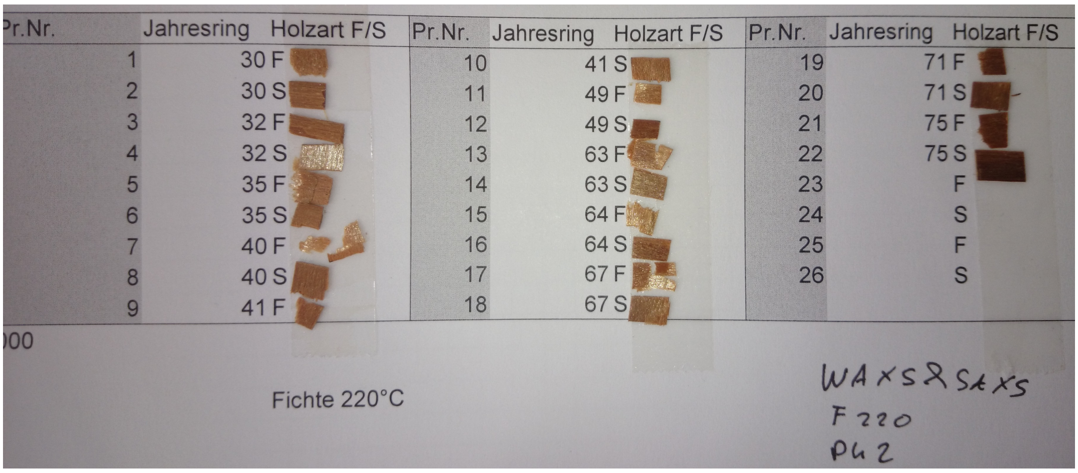

Figure 4.4.: Samples heat treated at 220°C

4.2. SAXS and WAXS data collection

SAXS measurements where carried out with a Bruker SAXS Nanostar equipped with an area detector (Vantec 2000, gas-detector). The beam was obtained by a rotating copper anode. The diameter of the beam is approximately 0.5 mm with a wavelength of 1,542 $\AA$. The total flux of photons is approximately $2 \cdot 10^7$ photons per second on the sample.

For SAXS measurements ,the used configuration was the long configuration, with a distance between sample holder and detector of around 108 mm. This covers up an angular range from 0.1 to 4°. Every sample was exposed to the X-ray beam for 15 minutes.

For WAXS measurements the distance between sample holder and detector has to be shortened to 11 cm (short configuration). The irradiation time was increased to 30 min.

4.2.1. Evaluation of data

The distribution of the scattering intensity of the received data yields information about orientation, size and shape of the object. In the small angle regime the intensity can be written in form of

$$I(\mathbf{q}) = I_0\,(\rho^0_{cellulose} - \rho^0_{matrix})^2 \left| \int_V e^{(i\mathbf{qr})}\, d^3r \right|^2 \tag{4.1}$$

where $\mathbf{q}$ is the scattering vector. The scattering angle 2 Θ enclosed by the incident and the scattered beam, correlated via

$$|\mathbf{q}| = (4\pi/\lambda)\ sin\ \Theta, \tag{4.2}$$

$$\left|\rho^0_{cellulose} - \rho^0_{matrix}\right| = \Delta\,\rho \tag{4.3}$$

ρ refers to the difference in the electron contrast between the cellulose microfibrils and the embedding matrix.
In general, polar coordinates are used. Therefore,

$$I(\mathbf{q}) \ \rightarrow\ I(q,\, \chi) \tag{4.4}$$

whereby $q = |\mathbf{q}|$ and χ is the azimuthal angle in the detector plane. The scattering intensity $H(\chi)$, in dependence on the azimuthal angle is obtained by Formula 4.5.

$$H(\chi) = \int_{q_1}^{q_2} I(q,\, \chi)\ dq. \tag{4.5}$$

From this intensity distribution the microfibril angle is obtained from a fit with a Gaussian function.

Therefore, the gained intensity of the scattered beam by the detector was integrated over q and plotted versus the azimuthal angle χ. This integration was carried out with the Bruker software of the SAXS device. To avoid the influence of pinhole scattering, the lower bound of integration was hence chosen as $q_1 = 0.5\ nm^{-1}$ and the upper as $q_2 = 2.5\ nm^{-1}$. In this q-range, the scattering contrast arises from the electron density difference between the cellulose fibrils and the surrounding matrix.
At very small values of q (($q < 0.3\ nm^{-1}$)) scattering origins from the pores and cavities of the cell wall [12].

For further data treatment, the obtained results of the integration were evaluated with the software Sigma Plot 11.0.

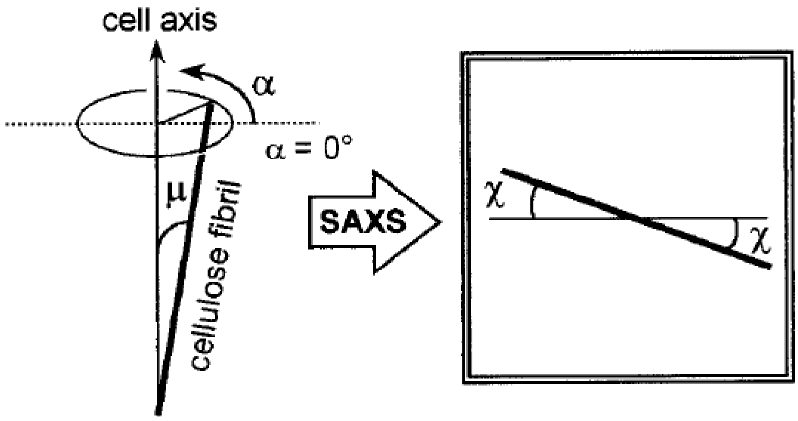

Figure 4.5.: Schematical representation of the small-angle scattering from a cellulose microfibril. On the detector appears an intensity distribution similar to a blurred stripe. Left, its orientation in the real space represented by the microfibril angle μ, is determined from the intensity distribution in reciprocal space via the azimutal angle χ. The rotation angle α, of the fibril around the cell axis, in the plane of observation attains 0°; source: [15].

All samples were measured using as well wide angle X-ray scattering (WAXS). In this configuration the specimen detector distance was changed to 11 cm and the time of X-ray exposure was raised to 30 min. A typical wide angle scattering pattern of cellulose fibrils is given in Fig. 4.6. In this range two main circular reflections appear. Each of them with two maxima, at an interval of 180°. The width of these maxima depends on the orientation of the microfibrils. So it is a second approach to gain information on the microfibril angle. To determine the intensity distribution in the wide angle regime a numerical integration has to be performed, similar to the small angle regime.

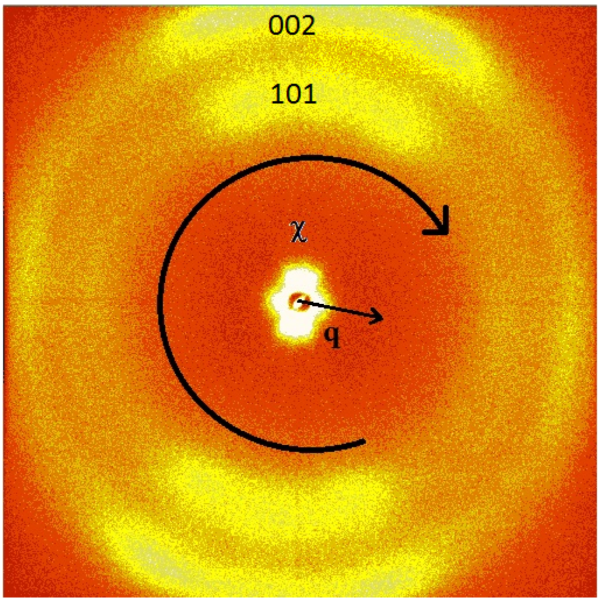

Figure 4.6.: WAXS intensity distribution of wood sample with typical 002 (outer ring) and 101 (inner ring) reflections and alignment of the microfibrils

There the bounds of integration where chosen from $q_1 = 16\ nm^{-1}$ to $q_1 = 19.5\ nm^{-1}$. This q - range includes only the inner ring (101). As the outer one bears the same information, so it is sufficient to chose one of the rings to determine the microfibril angle.

Evaluation was then also performed with the software SigmaPlot 11.0.

As already mentioned before, the microfibril angle depends on the general conditions of growth. One can discriminate between years with a broader distribution and those where the fibrils are more orientated. In the present stem are two salient examples. In the growth ring 17 a large mean microfibril angle is observable, whereas in growth ring 49 it happens to be the opposite case, a very low microfibril angle (high orientation). These two will be viewed in detail, for all treatment temperatures and each growth ring is of course divided into early- and latewood.

Significant differences in the intensity distributions in the SAXS range

This section describes the qualitative differences between the scattering intensity distributions of orientated and unorientated cellulose microfibrils. Likewise, the varieties between the small- and wide angle regime. Therefore, the former mentioned two annual rings will be compared.

In Fig. 4.7 the SAXS scattering pattern of the 17^{th} growth ring is depicted and in fig. 4.8 the one of the 49^{th}. Annual ring 17 was chosen because of the strong splitting between the two outermost Gaussians, especially in latewood. Annual ring 49, on the other side represents the state of strongly orientated microfibrils.

On the left hand side of diagrams are respectively the intensity distributions of earlywood, on the right hand side the one of latewood. The red curves are experimental results from the integration of the measured scattering intensity distributions. The black ones are the corresponding fitting curves.
The latter were achieved by employing a fit with three Gaussian curves for each distribution. The microfibril angle distribution especially for broad ones is a mixture of three Gaussian distributions. There are a central one and two side ones. The peak heights of the side maxima are smaller than that of the central one.

The three peaks resulting from the cellulose fibrils in the front wall and the back wall of the S1 layer of the mainly rectangular shaped wood cells. The scattering intensity distribution of the thin S2 layer (the weaker horizontal streak in Fig. 3.10 (e)) is not taken into account.

In the case of more orientated microfibril angle distributions (Fig. 4.8), the two side peaks almost vanish, whereas only the central one remains clearly visible. Nevertheless the intensity distribution in the peak flanks allows the application of the model with the three Gaussian curves.

In Fig. 4.7 the case of a broad microfibril angle distribution can be observed. The column on the left hand side displays the scattering intensity distributions of earlywood, according to the different thermal treatments. The column on the right hand side shows those of latewood.

There exists a clearly visible difference between the intensity distributions of early- and latewood. Latewood is less orientated than earlywood. The latter has pronounced side peaks on the flanks, particularly at Fig. 4.7 (iii) (right) and (iv) (right). Therefore, the angle of the winding of the cellulose is less steep in latewood than in earlywood.
In earlywood the flanks of the intensity distribution are much smoother, no side peaks are visible.

Generally this effect shows up throughout the thermal treatments. It is observable that the side maxima of the intensity distribution of latewood come out more strongly in Fig. 4.7 (iv) ($220°C$). In case of Fig. 4.7 (iii), this effect can already be seen, but much weaker.

The 49^{th} growth ring, Fig. 4.8 is an example for the opposite case. The microfibril angle distribution is rather small and in both, earlywood as well as latewood. Independent from treatment temperature and type of wood, only one prominent peak is observable. The microfibrils related to such scattering pattern are coiled in a steep helix around the cell axis.

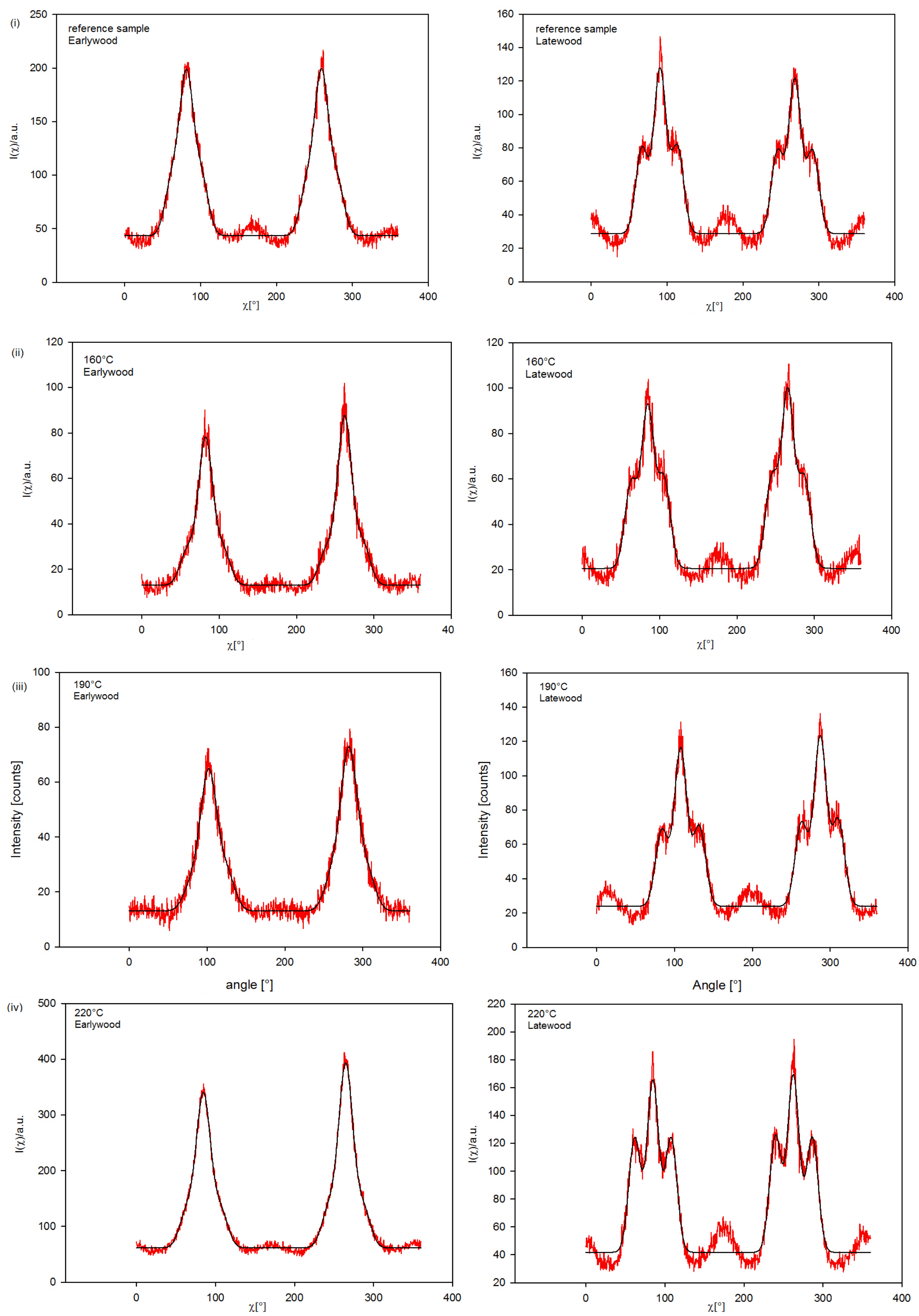

Figure 4.7.: SAXS scattering intensity distribution vs. the azimuthal angle for annual ring 17 and different treatment temperatures: (i) reference sample (ii)160°C (iii) 190°C (iv) 220°C; left column ... earlywood, right column ... latewood

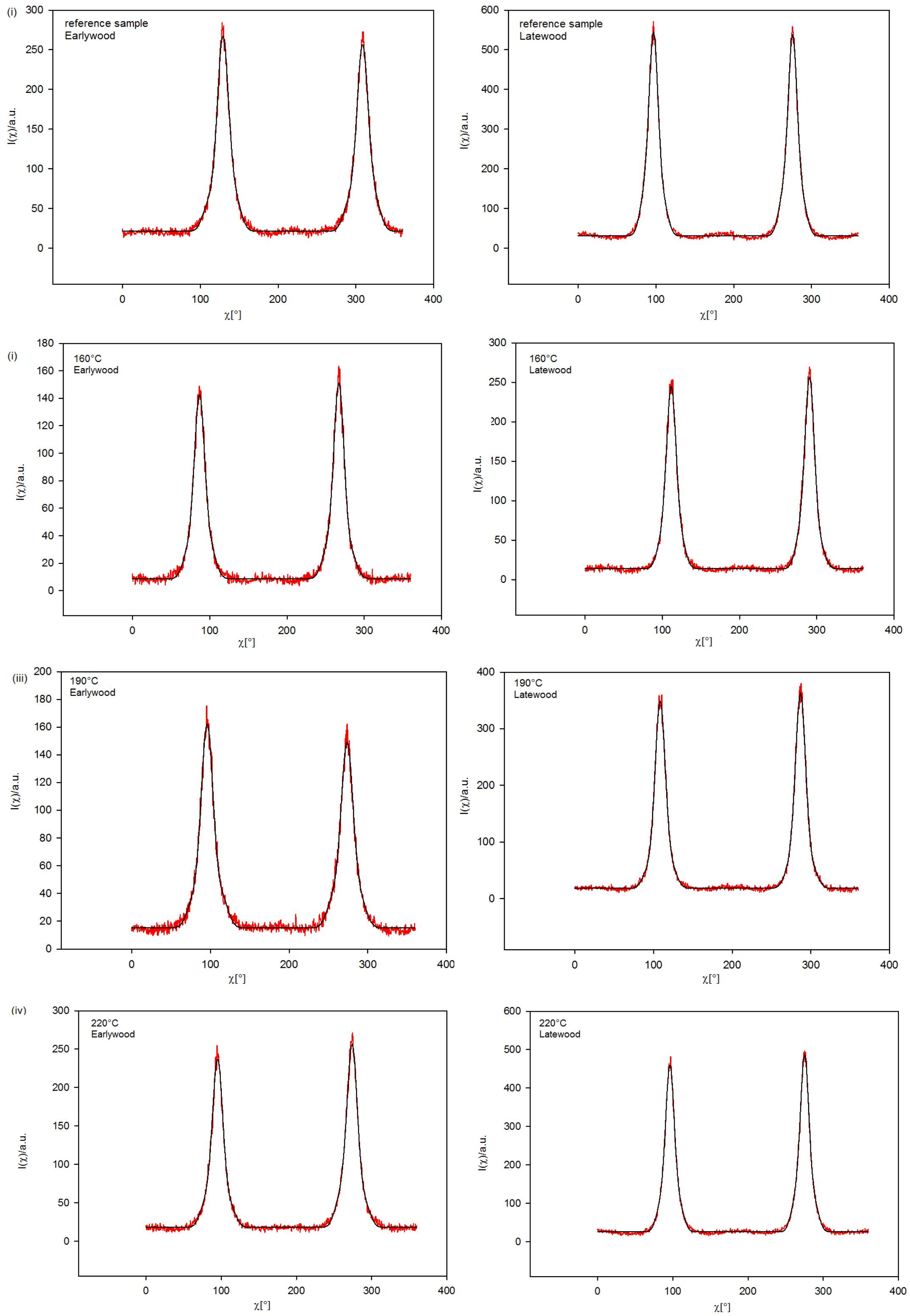

Figure 4.8.: SAXS scattering intensity distribution vs. the azimuthal angle for annual ring 49 and different treatment temperatures: (i) reference sample (ii)160°C (iii) 190°C (iv) 220°C; left column ... earlywood, right column ... latewood

Intensity distributions in WAXS range

In the wide angle regime appear two characteristic rings, the 101 and the 002 reflection (see Fig. 4.6). In this work the inner ring was chosen for the evaluation of the microfibril angle. Figs. 4.9 and 4.10 show the WAXS patterns of the 17^{th} and 49^{th} growth ring. As in the SAXS range, the left columns of diagrams show the scattering intensity distributions of earlywood, the right one the intensity distributions of latewood.There are several differences in the peaks of the two types of scattering patterns and their evaluation.

First of all the intensities are considerably higher in the wide angle regime. Some of the scattering distributions are more smeared out, so there is a higher variance in the WAXS data. Fitting turned out to be more difficult in the WAXS than in the SAXS range. This applies to both, the early- and the latewood data.

It can be said that for strong orientated scattering intensities SAXS and WAXS provide similar results. This is viewed in Fig. 4.10. It illustrates the 49^{th} growth ring. In both scattering regimes and for all treatment temperatures the scattering intensity distributions show a sharp and high peak. This applies as well for early- as for latewood.

In contrast to the latter it appears quite differently for the 17^{th} annual ring, shown in Fig. 4.9. Here the scattering intensity distributions show some irregularities.
The in Fig. 4.9 shown intensity distributions of latewood still have a broader microfibril angle distribution, but the former prominent side-peaks now appear in a slightly different form. The two side maxima have gained a larger peak height. Therefore the flanks are steeper than in the SAXS regime.
The intensity distribution of earlywood is not that much affected, although differences are visible. The curves have lost a certain amount of symmetry, as well on the mirror axis between the two distributions, as on the bisecting line of the single peak.

From these scattering intensity distributions the value of the microfibril angle can be obtained equally. To remain consistent the fitting of the obtained curves was conducted in the same way as in the SAXS regime. Due to a stronger smeared-out distributions, the resulting fit curves lack on symmetry as well.
It is to point out that determining quantitative changes of the mean microfibril angle, due to thermal treatment, it would be advantageous to measure as much samples as possible. In the following chapter all measured scattering pattern will be considered.

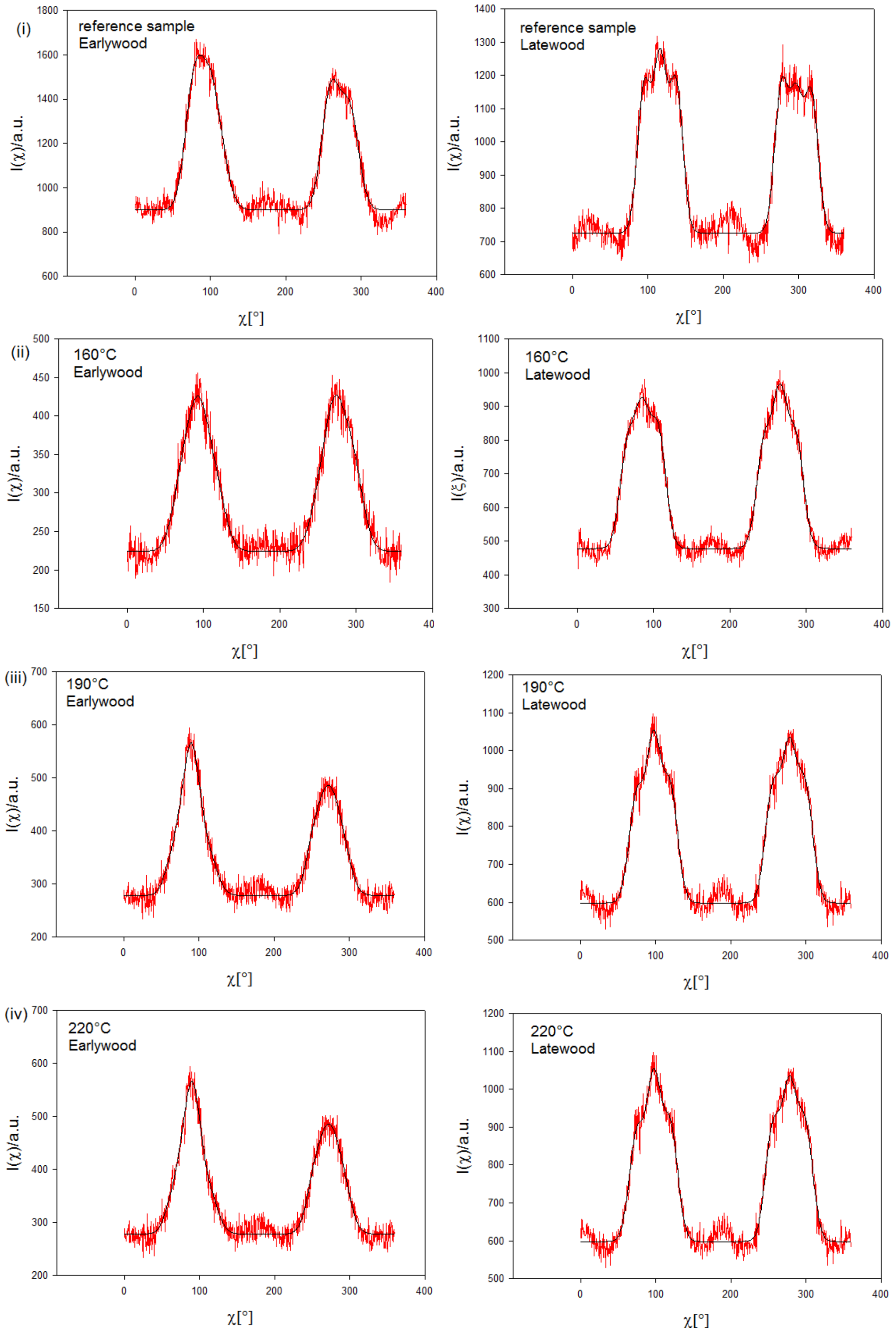

Figure 4.9.: WAXS scattering intensity distribution vs. the azimuthal angle for annual ring 17 and different treatment temperatures: (i) reference sample (ii)160°C (iii) 190°C (iv) 220°C; left column ... earlywood, right column ... latewood

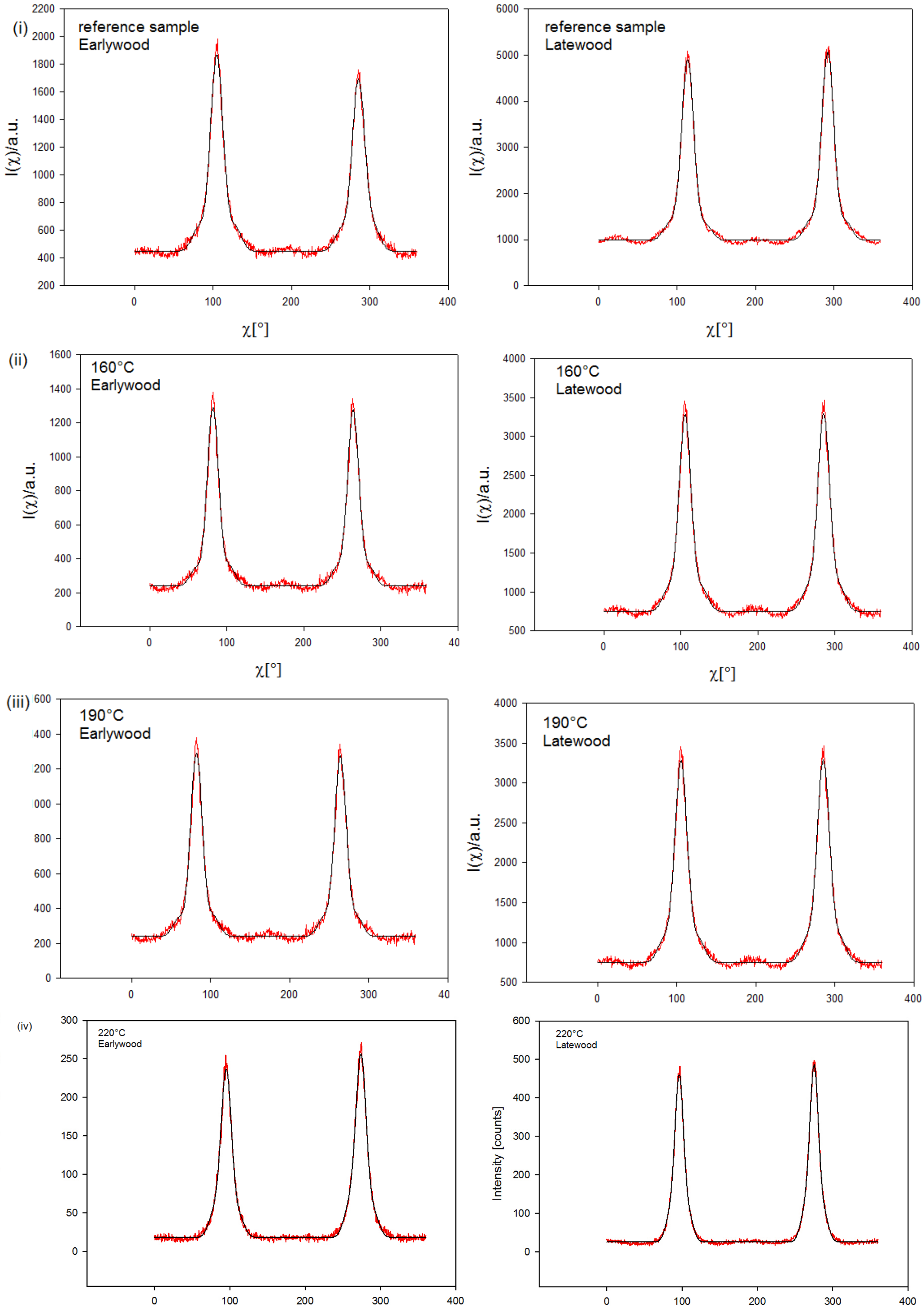

Figure 4.10.: WAXS scattering intensity distribution vs. the azimuthal angle for annual ring 49 and different treatment temperatures: (i) reference sample (ii)160°C (iii) 190°C (iv) 220°C; left column ... earlywood, right column ... latewood

4.3. The mean microfibril angle

The following intensity distributions are all obtained by SAXS.
To gain information on the microfibril angle from the scattering pattern, a three fold Gaussian curve, all three with equal widths, was used to fit the obtained data. The distance between the two outermost Gaussians yields the double mean microfibril angle.

The two selected growth rings of the former section were examples for large and small microfibril angle distributions. Both represent the two extreme cases, of the obtained data.
In the cross section of a stem are various intermediary stages of microfibril angle distributions. Their size is influenced by numerous outer and inner factors of a growing tree.
Therefore an overlook over these the collected data of one cross section is shown in the figures Fig. 4.11-4.18.
These eight figures show all measured scattering intensity distributions of the cross section of a stem of *Picea abies*. Fig. 4.11 (earlywood) and 4.12 (latewood) display those of the reference sample.

- Fig. 4.13 and 4.14 display the intensity distributions of wood treated at 160°C.
- Fig. 4.15 and 4.16 display the intensity distributions of wood treated at 190°C
- Fig. 4.17 and 4.18 display the intensity distributions of wood treated at 220°C.

To ensure clarity and comprehensibility, the growth rings where again split into early- and latewood. Therefore Fig. 4.11,4.13; 4.15 and 4.17 are the scattering patterns of the earlywood part of the cross section and Fig. 4.12; 4.14; 4.16 and 4.18 are those of the latewood part.

The χ [°] values of the maximum of the fit curves where aligned by an appropriate shift along the azimuthal angle (χ [°]-coordinate).

In the figures Fig. 4.11-4.18, the lowest of the two peaks represent the 3^{rd} annual ring. The two peaks at the upper end show the 75^{th} annual ring. The peaks of these outermost rings, near the bark, are highly orientated in latewood. In earlywood this difference is not visible. Their scattering patterns show a rather uniform appearance.

The scattering patterns of latewood show larger variety. Some are rather strong orientated and others show a good visible splitting.
The data gained from early- and latewood show strong spread and no systematic behaviour

can be observed in the diagrams. Therefore it is necessary to go from the qualitative level to a more quantitative one. The next task is to determine the mean microfibril angle and to consider its possible coherences with other quantities, for example the height of the maxima and their height ratios.

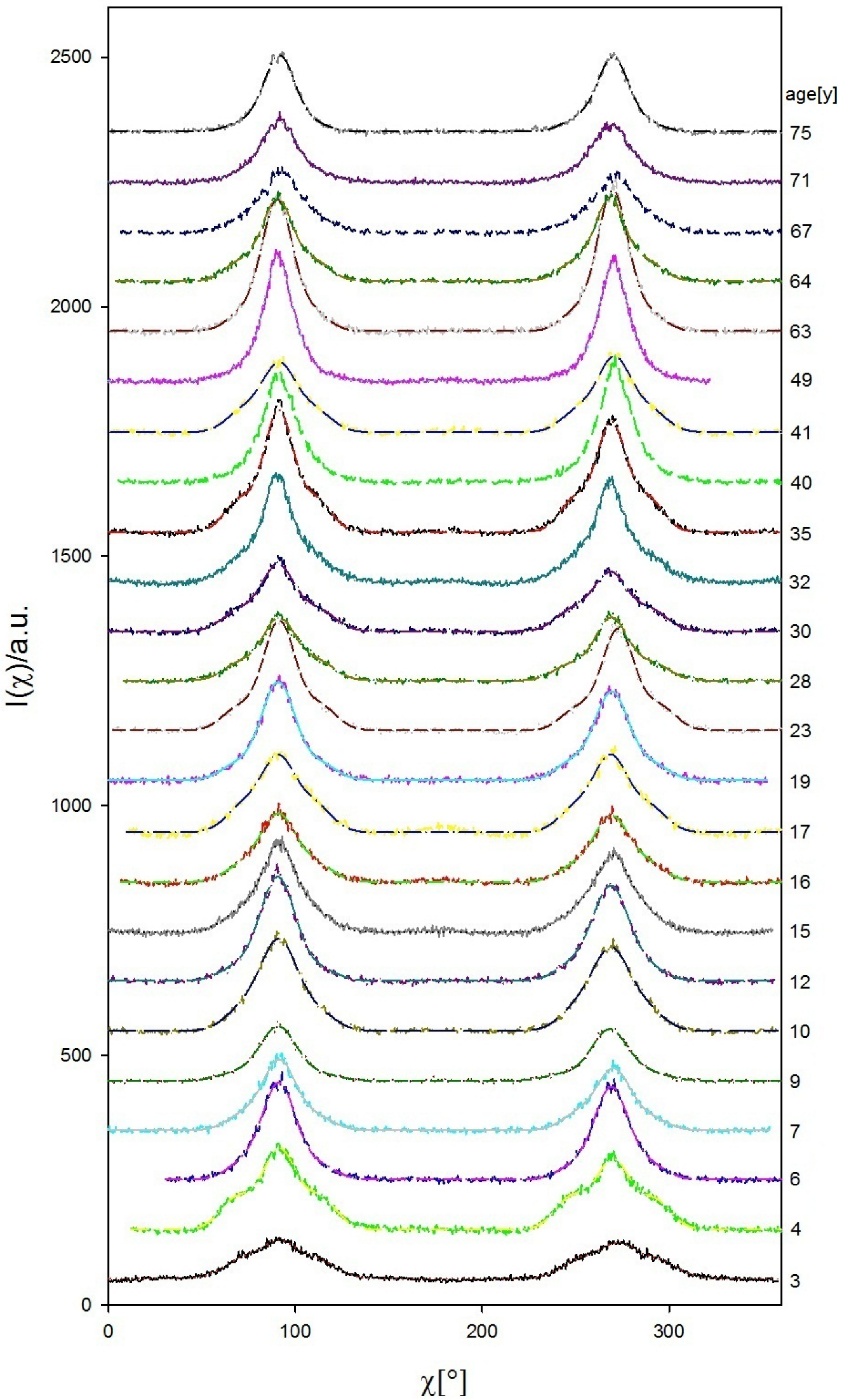

Figure 4.11.: Earlywood; untreated

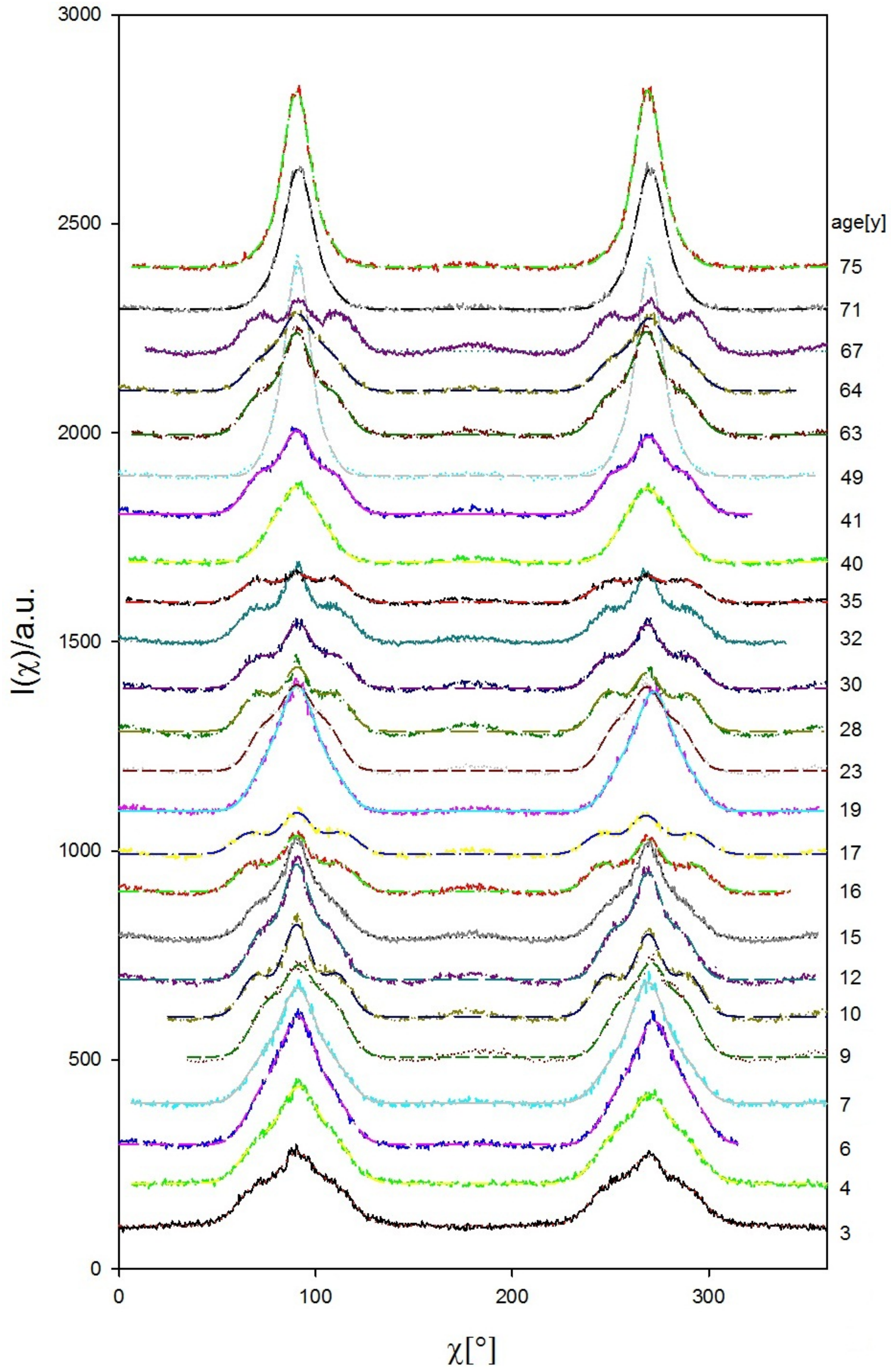

Figure 4.12.: Latewood; untreated

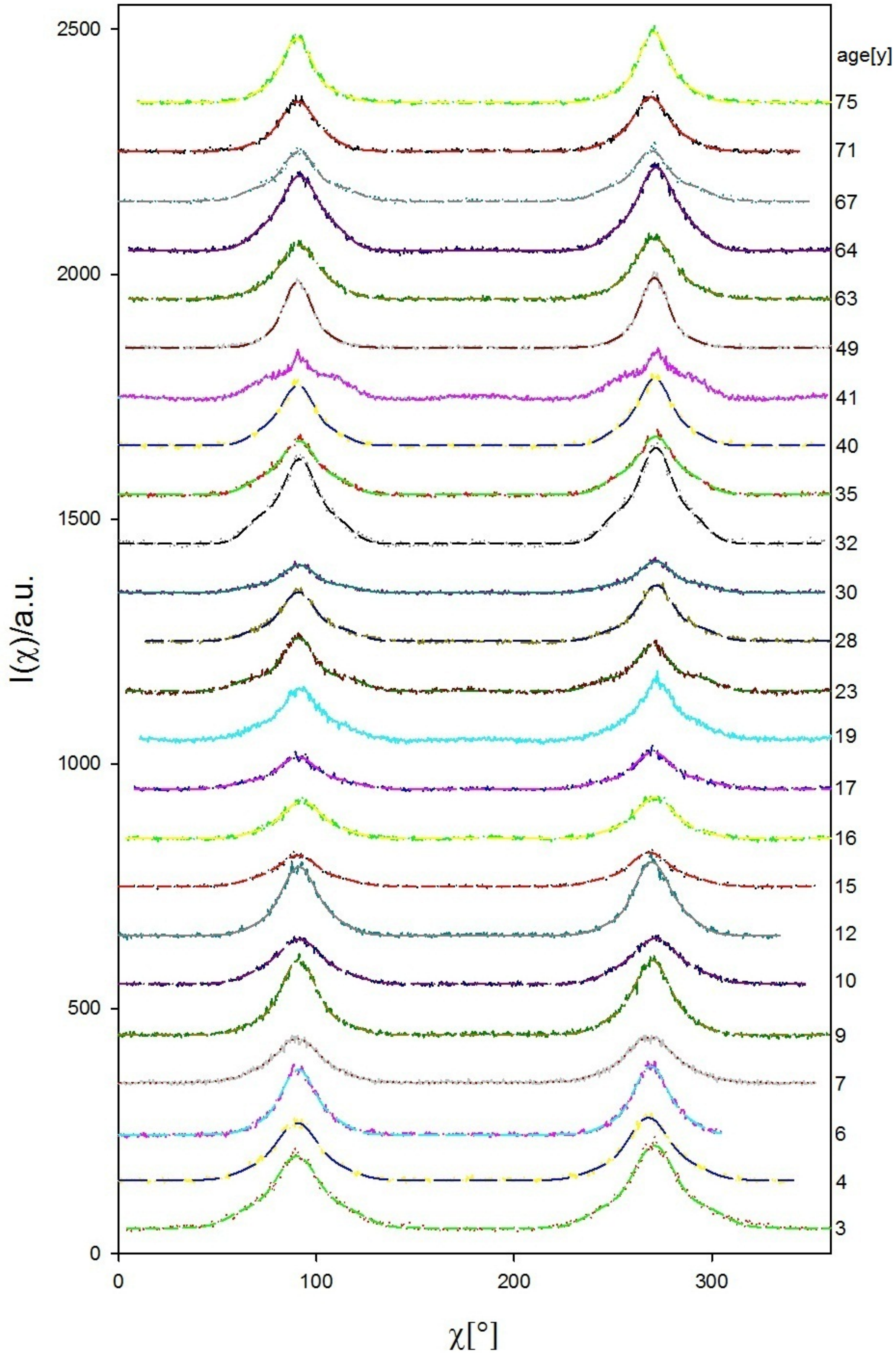

Figure 4.13.: Earlywood; 160°C

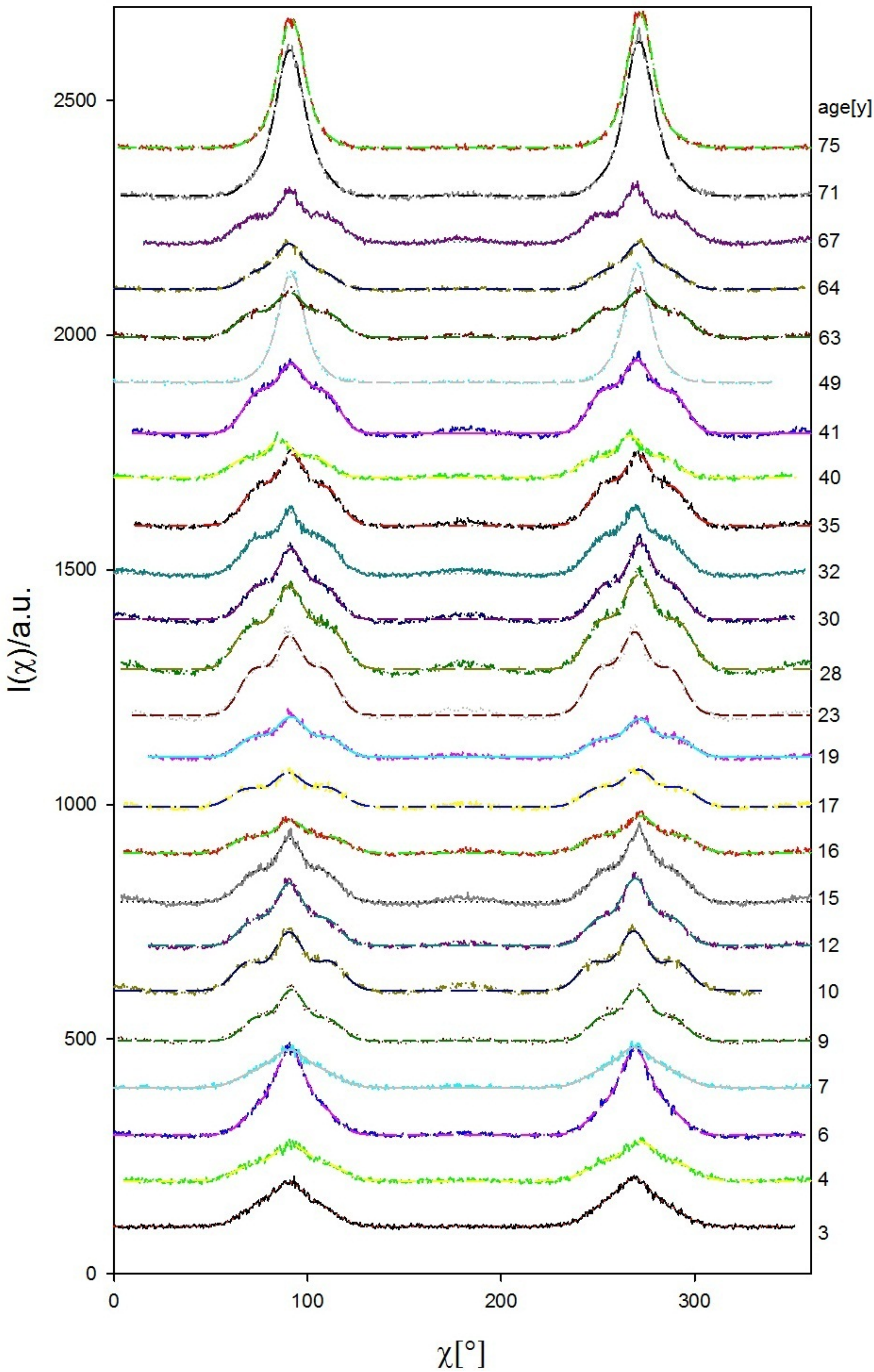

Figure 4.14.: Latewood; 160°C

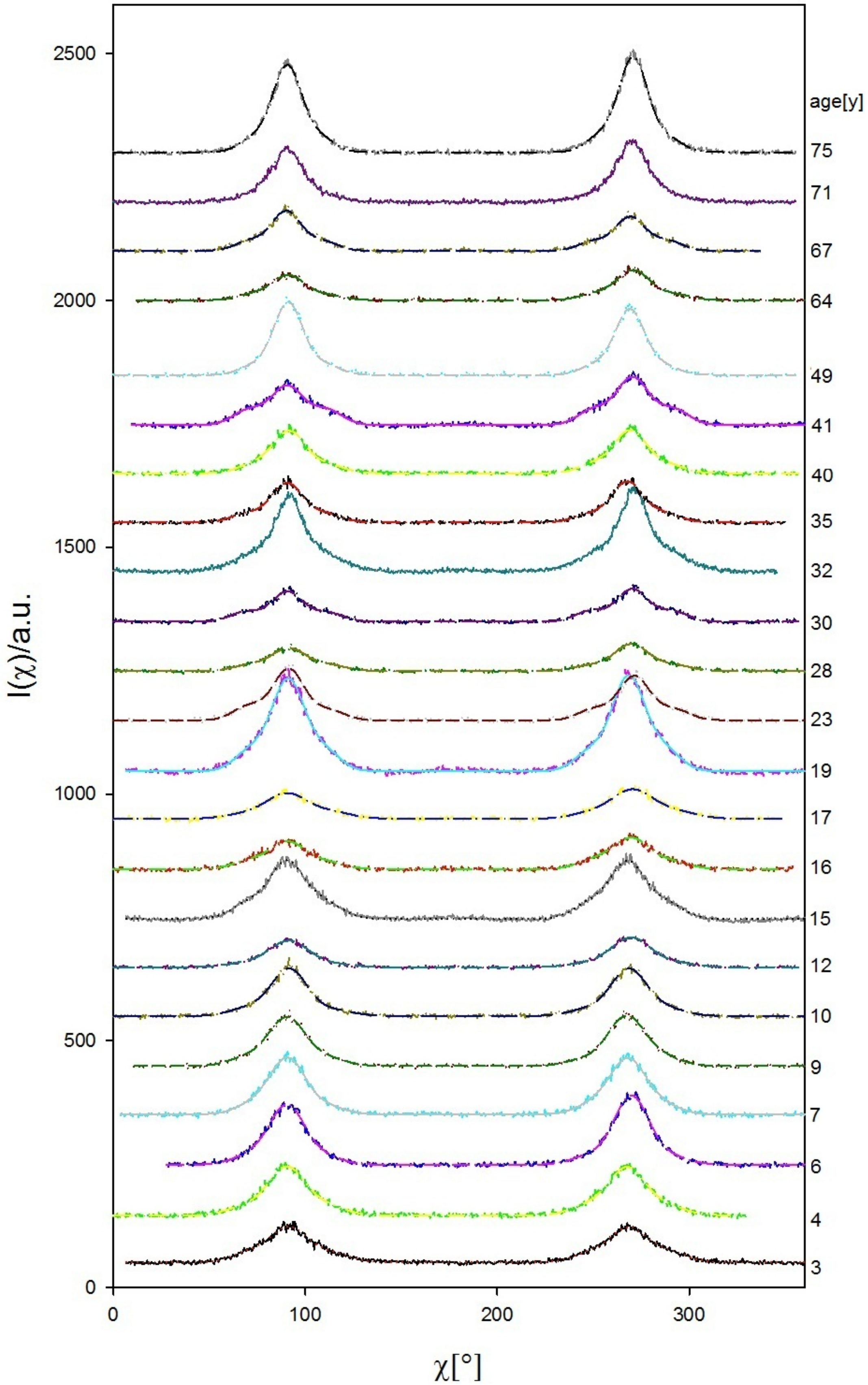

Figure 4.15.: Earlywood; 190°C

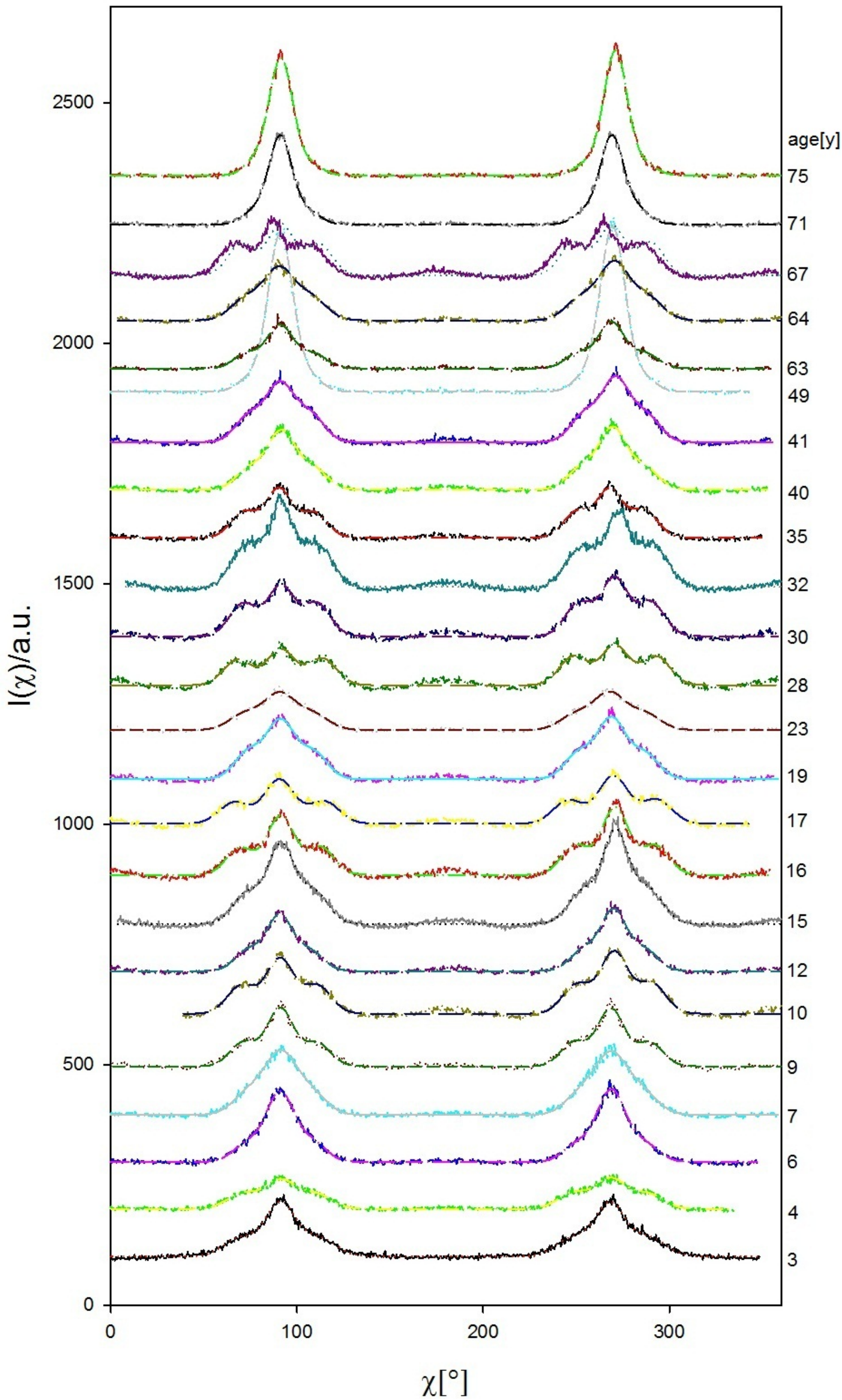

Figure 4.16.: Latewood; 190°C

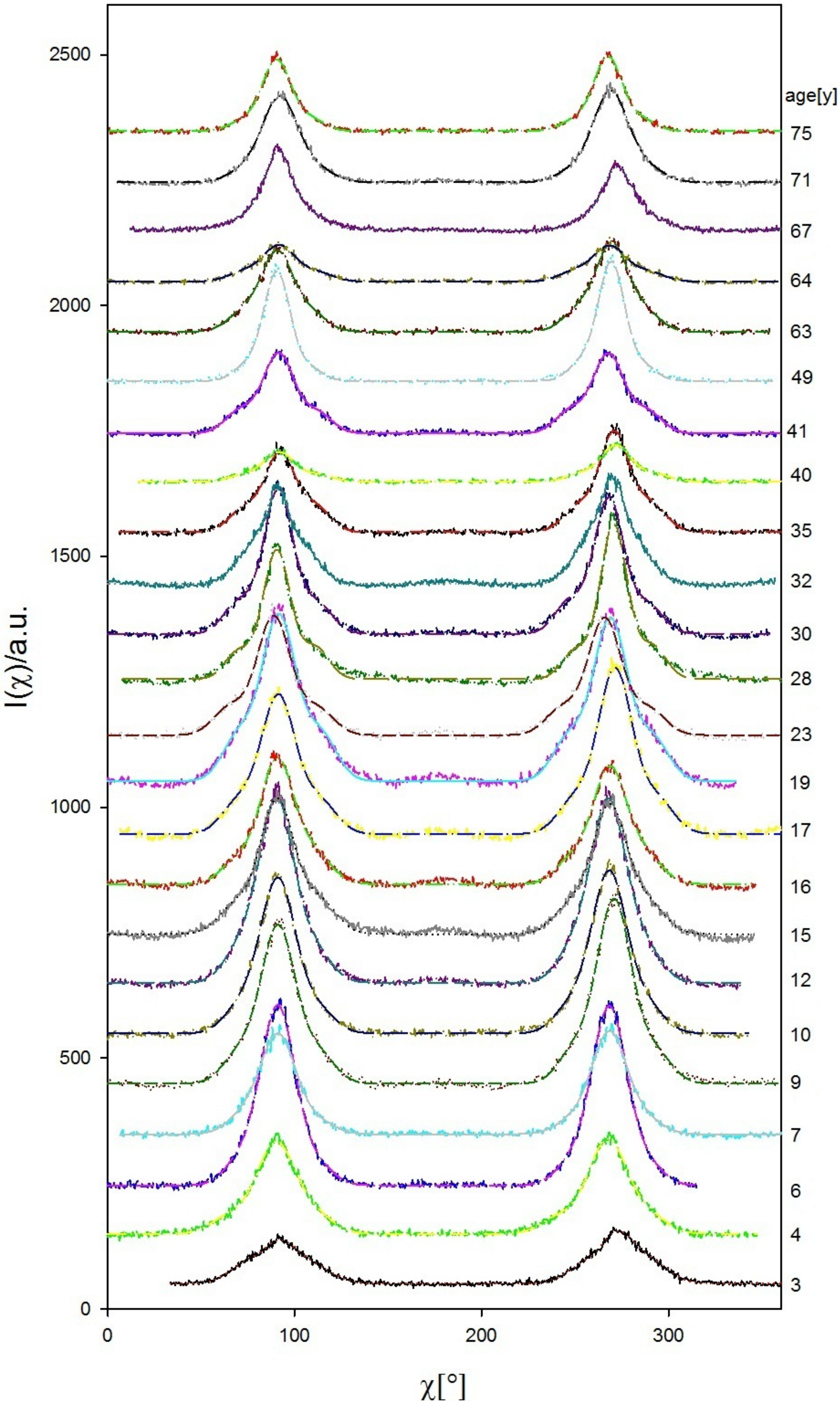

Figure 4.17.: Earlywood; 220°C

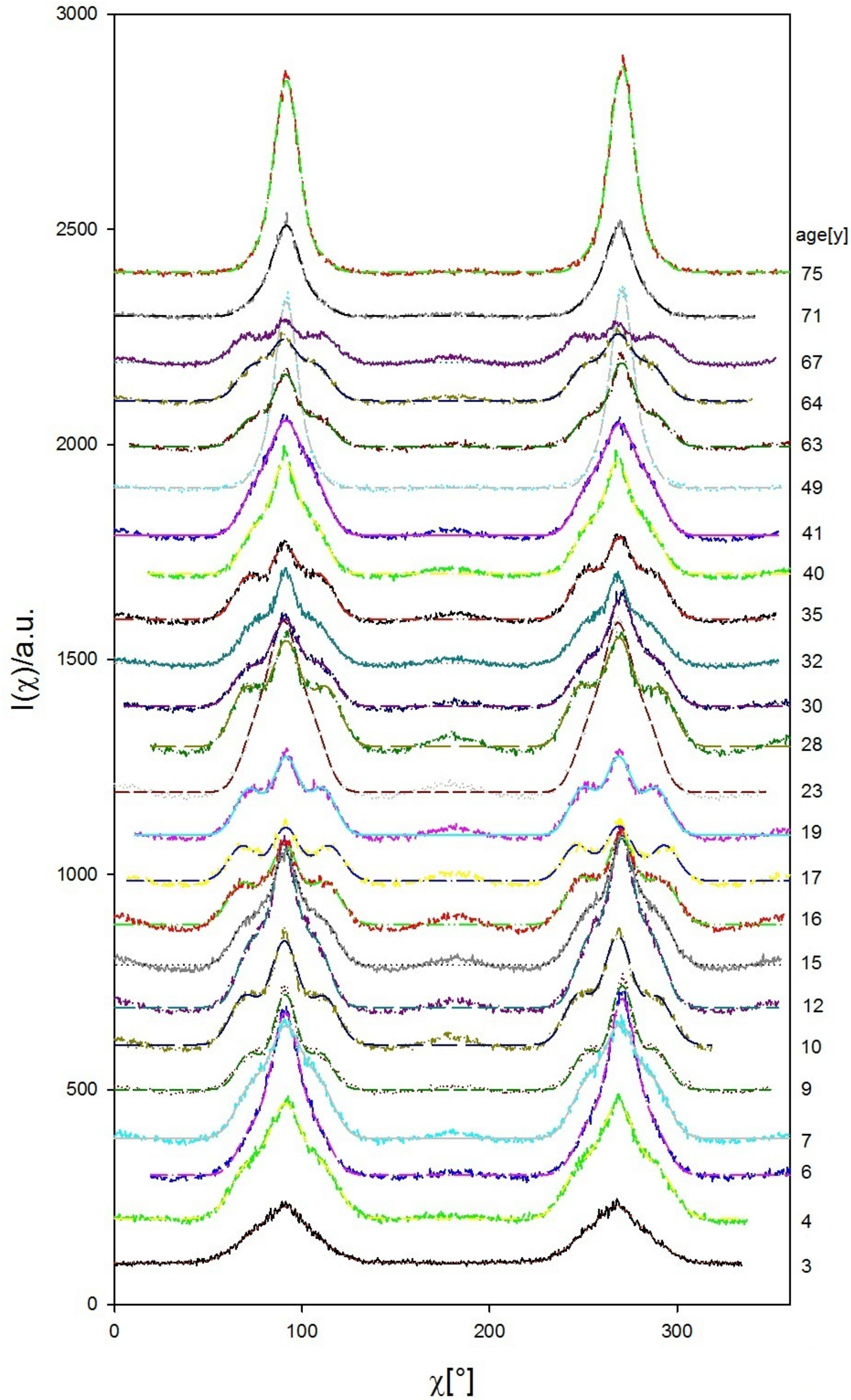

Figure 4.18.: Latewood; 220°C

5. Results

5.1. Three peak evaluation

In this section the evaluated data will be discussed. A value for the microfibril angle can be obtained in different ways. Due to the different scattering behaviour of early- and latewood, their microfibril angles will be viewed separately. Therefore one obtains a microfibril distribution of early- and latewood which shows slightly different behaviour in thermal treatment. Furthermore there are differences depending which scattering regime is taken into account. To obtain the microfibril angle, the distance between the first and the third maximum of a fit with three Gaussian functions is calculated. Three Gaussian functions were chosen because they describe sufficiently precise the scattering intensity distribution. The physical background is that the central Gaussian function arises from fibrils in a steep helical angle in the secondary cell wall of the rectangular shaped tracheids, the two side maxima from fibrils in a less steeper helical angle.

A summary of all values of the microfibril angles gained by SAXS is shown in table Tab. A in appendix A.
In the first column on the left side is the label of the samples in the following order: the first box indicates the annual ring and type of wood (earlywood (EW)/ latewood (LW)).
Below are located the related labels of the treated samples:

- TW2_Fu_0_001 - 0026 & TW2_Fu_1_001 - 022 ... untreated reference samples
- TW2_F160_0_001 - 0026 & TW2_F160_1_001 - 022 ... samples treated at 160°C
- TW2_F190_0_001 - 0026 & TW2_F190_1_001 - 022 ... samples treated at 190°C
- TW2_F220_0_001 - 0026 & TW2_F220_1_001 - 022 ... samples treated at 220°

The second column (coordinate 1^{st} max [°]) indicates the positions of the first maximum, the third (height 1^{st} max; Intensity/ a.u.) their height, the fourth the positions of the second maximum (coordinate 2^{nd} max [°]), the fifth their heights (height 2^{nd} max; I/a.u.), the sixth the positions of the third maximum (coordinate 3^{rd} max [°]), the sevenths their height (height 3^{rd} max; I/a.u.) and the eights column denotes the difference between the positions of the 1^{st} and the 3^{rd} maximum and therefore the double mean microfibril angle.

On page 8 of table Tab. A in appendix A the same specifications can be found for the second intensity distribution shifted about 180 °; therefore it is considered as:
The second column (coordinate 4^{th} max [°]) indicates the positions of the fourth maximum, the third (height 4^{th} max; Intensity /a.u.) their height, the fourth the positions of the fifth maximum (Coordinate 5. max [°]), the fifth their heights (Height 5. max; I/a.u.), the sixth the positions of the sixth maximum (coordinate 6^{th} max [°]), the seventh their height (height 6^{th} max; I/a.u.) and the eighth column denotes the difference between the positions of the 4^{th} and the 6^{th} maximum and therefore again the double mean microfibril angle.

In table Tab. B in appendix B can be found the corresponding values for the microfibril angle from the WAXS measurement. The structure of the data assembly is the same as for the SAXS regime. Using three Gaussian curves as evaluation method leads in the case of WAXS to some doubtful results.

Instead an evaluation method using one Gaussian curve is for some reason a better choice. This method will be discussed in section Sect. 5.2 in more detail.

Nonetheless, it is case-dependent, which method is appropriate. The values of the microfibril angle, used in Fig. 5.3 (b) and Figs. 5.4 (b), (c), are obtained case-dependent by use of the fitting method with one or three Gaussian curves.

As discussed in Sect. 5.2 it is necessary to take into account the heights of the three maxima of the Gaussian fit curves. The intensities contain information about the microfibril angle distribution in the specimen. In Fig. 4.11 - 4.18 as well as Fig.4.7 - Fig.4.8 the different ratios of the peak heights are easily visible. The ratios of the peak heights of earlywood are higher than those of latewood.

The numerical values given in appendix App. A and B for the mean microfibril angle are displayed in Fig. 5.1. In this illustration the double microfibril angle is plotted versus the age of the used sample in half-years [1]. In both early- and latewood are are shown together. From

[1]During the growth season (one year) early- and latewood is produced. The first half-year corresponds to the production of earlywood and the second half-year to the production of latewood

these graphical representations it is difficult to observe possible trends. But there are some noticeable qualitative differences between Fig. 5.1 (a) and (b).

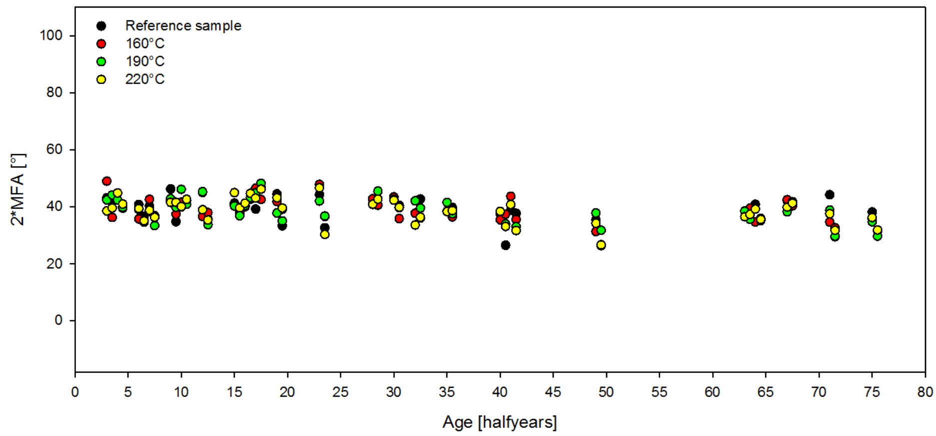

(a) Data obtained by SAXS

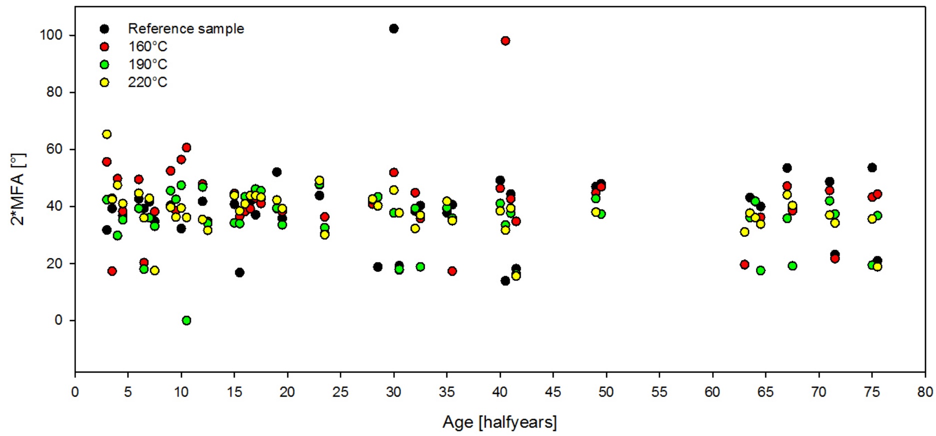

(b) Data obtained by WAXS

Figure 5.1.: Double microfibril angle vs age in half-years; in both illustrations early- and latewood are shown

The data gained via SAXS show less scatter than those by WAXS (note the different scaling in the diagrams). In both a tendency can be recognised: the microfibril angle shrinks with increasing age. This is i.a. published by Lindstrøm et al. [16]. Further in both (SAXS and WAXS) the double microfibril angle fluctuates about 40°.

According to Fig. 5.1 it is indeed feasible to say that thermal treatment does not cause an

immediately noticeable change of the microfibril angle. To put a finer point on the development of the microfibril angle it is reasonable to separate the data into early- and latewood and further to eliminate statistical outliers.
This is realized in Fig. 5.2; the figures (a) (SAXS) and (c) (WAXS) represent earlywood, (b) (SAXS) and (d) (WAXS) latewood.

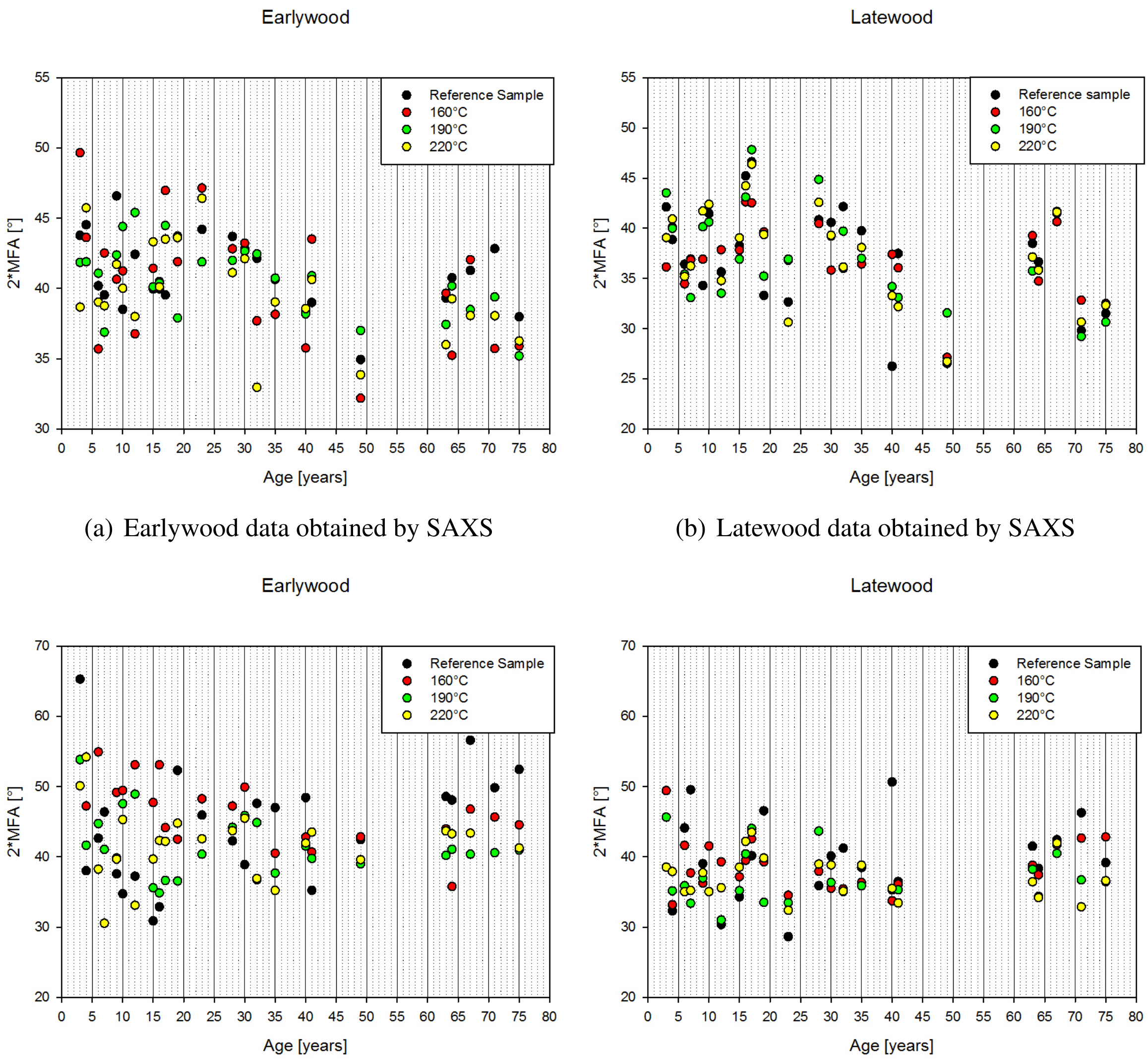

(a) Earlywood data obtained by SAXS

(b) Latewood data obtained by SAXS

(c) Earlywood data obtained by WAXS

(d) Latewood data obtained by WAXS

Figure 5.2.: Double microfibril angle vs age in half-years; in both illustrations early- and latewood are shown

In Fig. 5.2 one can again observe the tendency of the shrinking microfibril angle depending on the position in the cross section, which is corresponding to the tree age. To gain a quantitative prediction it is necessary to compare the data of each temperature range.

Therefore the numerical data for the microfibril angle are summarized in a bar chart for comparison of the effect of the heat treatment, shown in Fig. 5.3 (a) (SAXS) and (b) (WAXS). Again a strict separation into earlywood (light-grey columns) and latewood (black columns) was maintained.
Additionally, the data for the microfibril angle were normalized to its initial value before heat treatment. This serves to visualize the relative change of the microfibril angle with heat treatment temperature.

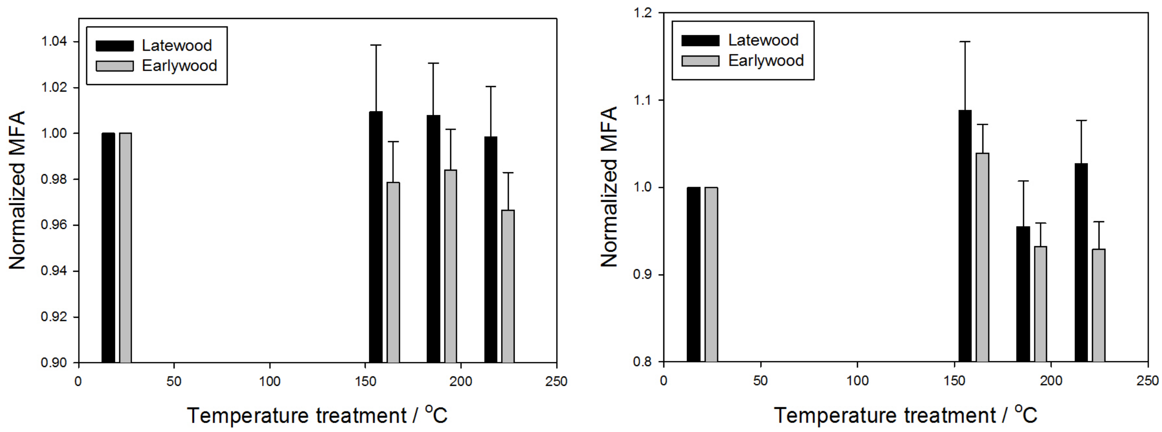

(a) Evaluated data obtained by SAXS

(b) Evaluated data obtained by WAXS

Figure 5.3.: Normalized microfibril angle, the untreated wood serves as reference sample to normalization; change of the microfibril angle depending on the temperature of treatment, the darker bars are related to latewood, the lighter to earlywood. The error bars are the standard deviation.

For the data obtained by SAXS the evaluation method with three Gaussian curves was chosen, for those of WAXS the evaluation method with one Gaussian curve was more suitable. Both diagrams (a) and (b) of Fig. 5.3 show tendencies of an decreasing microfibril angle for early and latewood, in the SAXS range as well as in the WAXS range.

It is noticeable that in both diagrams the mean microfibril angle of the samples treated at 160°C appears to be larger than the untreated sample, except the earlywood data in the SAXS regime. For these samples the mean microfibril angle shrinks from the first thermal treatment. The mean microfibril angle of the latewood samples treated at 160°C is slightly higher than the value of the reference sample. It has to be taken into account, that the error bars of the values exceeding the reference sample are quite high, and therefore one has to be very cautious with statements about a possible change of the microfibril angle with heat treatment temperature. For the heat treatment at 190°C and 220°C a decrease of the microfibril angle is observed, which is not as clearly pronounced in the core of the latewood samples at 220°C.

In Fig. 5.4 a more detailed analysis of the data is depicted. The data of the untreated samples serve as reference values for the mean microfibril angle and are normalized to one. In Fig. 5.4 (a), (b), (c) and (d) the relative change of the microfibril angle, depending on its initial value is plotted with a best-fit line for each temperature range.

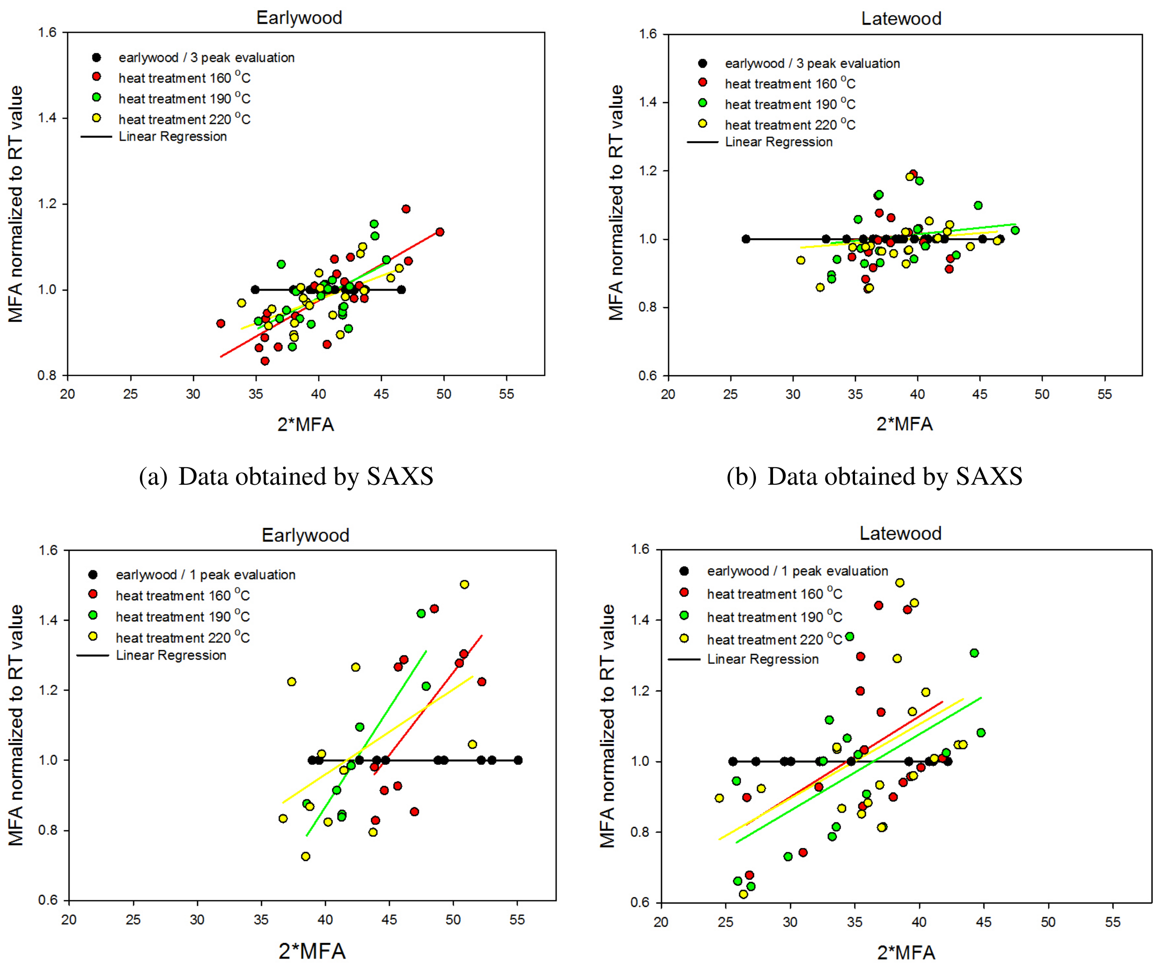

(a) Data obtained by SAXS

(b) Data obtained by SAXS

(c) Data obtained by WAXS

(d) Data obtained by WAXS

Figure 5.4.: Double microfibril angle vs age in half-years; in both illustrations early- and latewood are shown

The larger the initial value of the mean microfibril angle, the smaller is its possible decrease, due to a thermal treatment. To the contrary, the value of the mean microfibril angle increases, from a certain microfibril angle (around 40°). By way of comparison, a small mean microfibril angle tends to smaller values, caused by the treatment. This tendency is exemplified via the slope of the regression lines. All regression lines exhibit a positive slope even though the single data points show a large scatter.

Moreover it is noticeable that there is a different slope of the linear regressions between earlywood and latewood.

Therefore both are shown together in Fig. 5.5 (a) and (b).

In the direct comparison of early- and latewood, the slope of the regression lines of earlywood is higher than those of latewood. Especially in the small angle regime (Fig. 5.5 (a)), this is unambiguously visible, whereas in the wide angle regime (Fig. 5.5 (b)) it is less clear due to the larger scatter of the data points. Nevertheless, a general trend of a higher slope in earlywood seems to be visible.

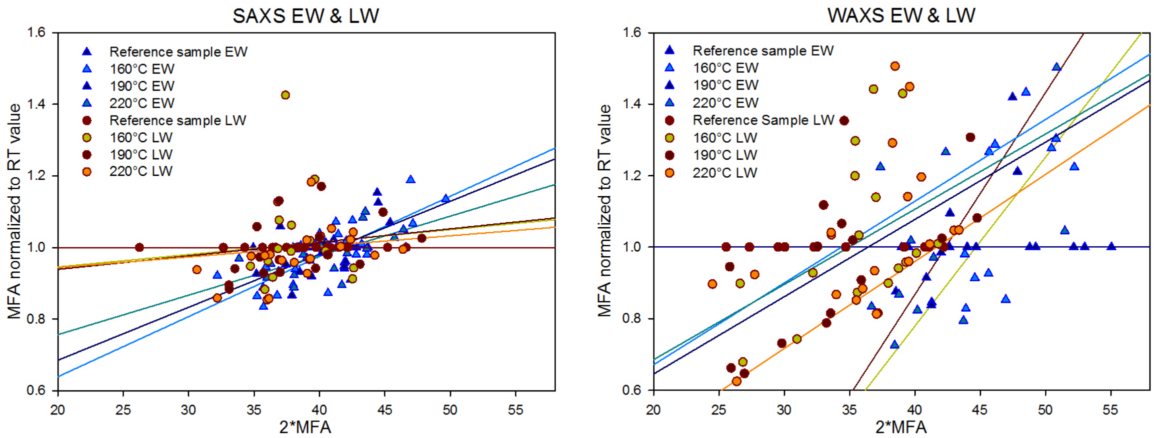

(a) Data obtained by SAXS

(b) Data obtained by WAXS

Figure 5.5.: Microfibril angle normalized to reference sample (RT=room temperature) value vs 2*microfibril angle. Comparison of earlywood and latewood for SAXS and WAXS.

In summary it can be said that despite the scatter of data, especially for latewood, it is possible to observe tendencies in form of regression lines and their different slope. From these results one can possibly deduce that at first a change of the microfibril angle occurs depending on the numerical value of the initial angle. If the initial microfibril angle is large, it shows a higher tendency to increase than to decrease, and vice versa for small initial microfibril angles. Therefore less orientated microfibrils tend to larger microfibril angles due to thermal treatment, orientated fibrils tend to a higher orientation.

How exactly the process of change in the helical angle takes place is a matter of speculation. As well it points to the fact that the functional interaction between the constituent parts in wood is of high complexity.

5.2. Evaluation of strongly orientated fibril bundles

As mentioned before the evaluation of strongly orientated microfibril bundles has to be adapted: It is more helpful to take the ratio of the peak heights into account. The heights of the side maxima have to be compared to the height of the central maximum of the central peak. The measured intensity is proportional to the number of microfibrils at a certain helical angle.

If the ratio of the peak heights (between the side maxima and the main maximum) is below the factor of two, the full width at half maximum of the central peak is considered to be the best approach to describe the mean microfibril angle.
In earlywood the majority of the microfibrils is coiled in a steep helical angle (earlywood is shown in Fig. 4.7 and 4.8 for SAXS and Fig. 4.9 and 4.10 for WAXS).

For latewood intensity distributions, as shown in Fig. 4.7 (for SAXS) and as well for those of Fig. 4.9 (for WAXS), the evaluation method with three peaks is applicable. Here definitely side maxima with sufficient intensity allow the determination of a distinct microfibril angle.

It has to be decided on a case-by case basis which method is fitting best.

5.2.1. Discussion of evaluation methods

In the cell wall the helical angle of the microfibrils is not strictly uniform. Therefore there is a distribution of various angles. The height of the side peaks represents the rate of microfbrils coiled at larger helical angles. The height decreases with decreasing amount of microfibrils coiled at those angles. As mentioned in Sect. 5.2, to chose the method of evaluation of the mean microfibril angle it is necessary to determine the value of the ratios of the peak heights. If the ratio of the peak heights is larger than the factor two, fibrils with minor slope cannot be neglected any more. In the latter case it is necessary to use a Gaussian fit with three peaks. In *Picea abies* this mostly is relevant for earlywood, because latewood is usually less orientated.

For the scattering patterns recorded with SAXS this classification was quite unambiguous. While using WAXS the decision was not that clear in all cases. Therefore the way of evaluation has to be decided from case to case, irrespectively whether the intensity distributions are originated from early- or latewood.

The intensity distribution of cylindrical scattering objects, measured on the detector is described by

$$I(\chi) = 4 \int_{\pi/2-\chi}^{\pi/2} \frac{f(\mu)\ sin(\mu)}{\sqrt{sin^2\chi - cos^2\mu}}\, d\mu, \tag{5.1}$$

as mentioned by Perret and Ruland [24]. Inverting this and expressing $f(\mu)$ leads to the distribution of the microfibril angle. The numerical integration can be avoided by functions with an analytical solution for $f(\mu)$, which was proposed in the paper of Fratzl et al. [8]

$$f(\mu) = \frac{k(m+l)\ u_m\ cos^m\chi + l(n+l)\ u_m\ cos^n\chi}{ku_m + lu_n} \tag{5.2}$$

where

$$u_m = \Gamma\left(\frac{m+2}{2}\right)/\Gamma\left(\frac{m+3}{2}\right) \tag{5.3}$$

with Γ indicating the Gamma-function and k, l, m, n being fit parameters. This formula is applicable for cells with non-rectangular, but as well as for cells with rectangular bases, such as wood cells from *Picea abies*. This is an alternative, which directly allows the determination of the microfibril angle in the real space from the scattering data in reciprocal space. In this, a fit in reciprocal space with Gaussian functions was chosen for simplicity. As the scatter in our data is high and we were mainly interested in relative differences arising from different thermal treatments. This is seen as an acceptable simplification.

The choice of the respective fit method – fit with one or three Gaussian functions certainly has an effect on the width of the distribution: For a fit with three Gaussian functions, the width of the central peak decreases in comparison to the fit of the scattering data with only one curve. Thus, to be precise, one should always compare samples, which were fitted with three functions, but not mix samples with different evaluation methods.

The diagrams shown in Fig. 5.6 and Fig. 5.7 serve as illustration for the two cases. Figure Fig. 5.6 displays the fitting with three Gaussian functions (solid black lines). Here the value of the ratio of the peak heights is 1.3.
In figure Fig. 5.7 (a) and (b) the ratio of the peak heights takes the value 5.5. The two side maxima of the three Gaussian functions, displayed in Fig. 5.7 (a) show low intensities (solid black lines in Fig. 5.7 (a)). Therefore, the microfibril angle is represented best by a fitting with a single Gaussian function (solid red line in Fig. 5.7 (b)).
The gained values for the microfibril angle show remarkable differences between between the two fitting methods.
The values for the mean microfibril angle given in Figs. 5.6 and 5.7 is the average value of the two peaks of each diagram.

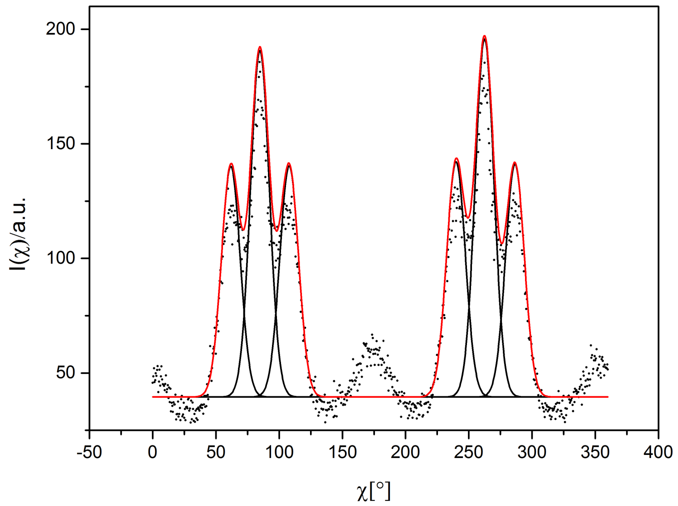

Figure 5.6.: SAXS pattern from *P. abies* latewood of the 17^{th} annual ring of heat treated wood ($220°C$). The black dots are the azimuthal intensity distribution, the black solid lines the three Gaussian curves and the solid red line the resulting fit curve. The microfibril angle was obtained from the value of the distance between the two side maxima. The mean microfibril angle is 23°.

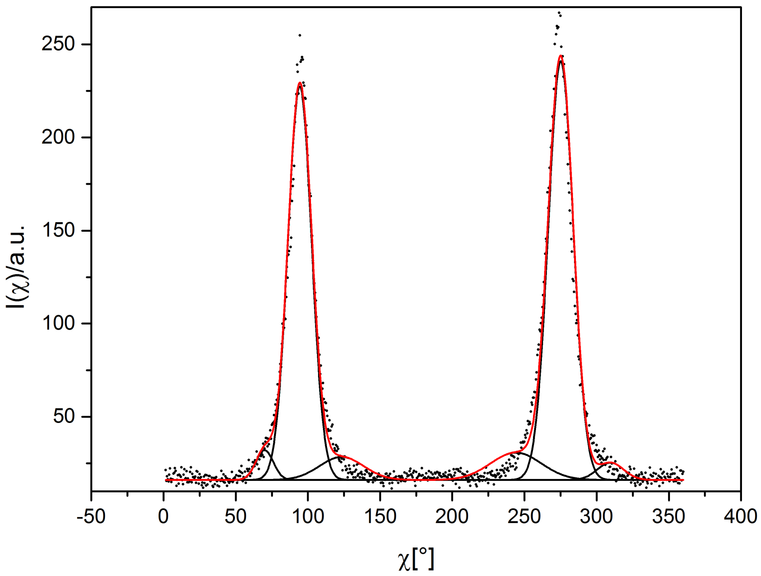

(a) SAXS pattern from *P. abies* latewood of the 49^{th} annual ring of heat treated wood ($220°C$)

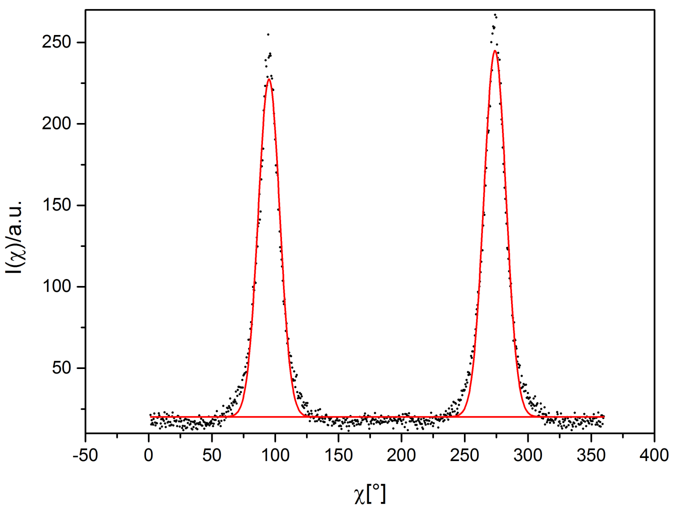

(b) SAXS pattern from *P. abies* latewood of the 49^{th} annual ring of heat treated wood ($220°C$)

Figure 5.7.: The black dots are the azimuthal intensity distribution, the black solid lines the three Gaussian curves (a) and the solid red lines the resulting fit curves ((a), (b)). For the evaluation method with three Gaussian curves (a) the microfibril angle was obtained from the value of the distance between the two side maxima and takes the mean value of 31°. (b) The azimuthal intensity distribution fitted with one Gaussian peak. The microfibril angle distribution is centred around zero and takes the mean value of 10°.

6. Conclusion

The aim of this thesis was to investigate if the thermal treatment of timber has an effect on the structure in the nanometre range. One of the parameters to describe the nanostructure of wood is the microfibril angle, which is inclined by the cellulose fibrils and the length axis of the stem. The microfibril angle was obtained by two approaches, either by measuring the orientated scattering intensity in the SAXS regime or by determination of the scattering intensity of the 200 reflections in dependence of the azimuthal angle in the WAXS regime.
It was evident that a change in the microfibril angle occurred, which was caused by the thermal treatment of timber. However, the effect was quite small and only became visible after measuring a high number of samples. In this thesis, 48 specimens were measured by SAXS and WAXS for each treatment temperature.

It was found that the change of the microfibril angle depends on its initial value. Though there is a large statistical scatter in the data, the same trend could be observed by a fit of regression lines to the respective data set:
For small microfibril angles (smaller than 22°, i.e. the distribution of microfibril angles broadens with increasing heat treatment temperature. This was the case for all samples, early– and latewood, and the effect was more pronounced visible in the SAXS than in the WAXS data. Differently, no clear influence of age or other parameters could be found on the level of significance.

The thermal treatment, which is intended to decrease the durability of wood, changes particular the structure of lignin. This increases the brittleness of wood, which led to the effect that it was much more difficult to prepare samples with a higher heat treatment temperature. This could be understood as an effect on the composite level, where the deterioration of the interface properties induce increasing brittleness. It is also very probable that the weaker linkage of the cellulose fibres and lignin matrix leads to the broadened distribution of microfibril angles. But the relation of structural and mechanical properties to the observed broadening of the distribution of the microfibril angle on the nanoscale is still unclear and needs further research.

Bibliography

[1] K. Abe and H. Yamamoto. Mechnical interaction between cellulose microfibril and matrix substance in wood cell wall determined by x–ray diffraction. *J Wood Sci*, 51:334–338, 2005.

[2] I. W. Bailey and Kerr T. The structural variability of the secondary wall as revealed by lignin residues. *Arnold Arboretum*, 18:264–272, 1937.

[3] R.K. Bamber. Heartwood, its function and formation. *Wood Science and Technology*, 10:1–8, 1976.

[4] J.R. Barnett and V. A. Bonham. Cellulose microfibril angle in the cell wall of wood fibres. *Biol Rev Camb Philos Soc.*, 79(2):461–72, 2004.

[5] J. H. Christensen, M. Baucher, A.P. O'Connell, M. Van Montagu, and W. Boerjan. Control of lignin biosynthesis. *Molecular biology of woody plants*, 1:227–237, 2000.

[6] Wikipedia contributors. Compton scattering. `http://en.wikipedia.org/wiki/File:Compton-scattering.svg`. Accessed: 2014-09-09.

[7] Wikipedia contributors. Lignin. `http://en.wikipedia.org/wiki/Lignin`. Accessed: 2014-09-09.

[8] P. Fratzl, O. Paris, and W.J. Landis. Bone mineralization in an osteogenesis imperfecta mouse model studied by small-angle x–ray scattering. *The American Society for Clinical Investigation, Inc.*, 97:396–402, 1996.

[9] A. Frey-Wyssling. Über die submikroskopische morphologie der zellwände. *Berichte der Deutschen Botanischen Gesellschaft*, 55:119–132, 1937.

[10] O. Glatter, O.and Kratky. *Small Angle X–ray Scattering*. Academic Press Inc., London, 1982.

[11] J. M. Hellgren, L. Puech, P. Barlow, S. Fink, E. J. Mellerowicz, and B. Sundberg. Auxin and cambial growth rate in poplar. *Cell and molecular Biology of Wood Formation*, pages 169–188, 2000.

[12] H. F. Jakob, S. Tschegg, and P. Fratzl. Hydration dependence of the wood cell wall structure in picea abies – a small-angle x-ray scattering study. *Macromolecules*, 29:8435–8440, 1996.

[13] V. J. James and N. Kirby. The connection between the presence of melanoma and changes in fibre diffraction patterns. *Cancers*, 2:1155–1165, 2010.

[14] H. Lichtenegger, M. Müller, and O. Paris. Imaging of the helical arrangement of cellulose fibrils in wood by synchrotron x–ray microdiffraction. *J. Appl. Cryst.*, 32:1127–1133, 1999.

[15] H. Lichtenegger, A. Reiterer, S. E. Stanzl-Tschegg, and P. Fratzl. Variation of cellulose microfibril angles in softwoods and hardwoods – a possible strategy of mechanical optimization. *Journal of Structural Biology*, 128:257–269, 1999.

[16] H. Lindstrøm, J. W. Ewans, and S.P. Verill. Influence of cambial age and growth condition on microfibril ange in young norway spruce (picea abies [l.] karst). *Holzforschung*, 52:573–581, 1998.

[17] U. Lüttge and M. Kluge. *Botanik*. VCH, Weinheim, 2012.

[18] J.D. MacLean. Rate of disintegration of wood under different heating conditions. *Proceedings, American Wood Preservers' Association*, 49:88–112, 1951.

[19] J. D. Mauseth. *Botany: An Introduction to Plant Biology*. Jones & Bartlett Publishers, Burlington, 2014.

[20] E.J. Mellerowicz, M. Baucher, B. Sundberg, and W. Boerjan. Unravelling cell wall formation in the woody dicot stem. *Plant Molecular Biology*, 47:239–274, 2001.

[21] H. Militz. Proceedings of conference: Enhancing the durability of lumber and engineered wood products. In *Heat Treatment Technologies in Europe: Scientific Background and Technological State–of–Art*, Göttingen, 2002.

[22] D. B. Mullick. The non-specific nature of defense in bark and wood during wounding, insect and pathogen attack. *Science*, 11:395–441, 1977.

[23] International Union of Pure and Applied Chemistry. *Compendium of Chemical Terminology Gold Book*. International Union of Pure and Applied Chemistry, 2.3.3 edition, 2014.

[24] R. Perret and Ruland W. Single and multiple x-ray small-angle scattering of carbon fibres. *J. Appl. Cryst.*, 2:209–218, 1969.

[25] C. Plomion, G. Leprovost1, and A. Stokes. Wood formation in trees. *Plant Physiology*, 127 (4):1513–1523, 2001.

[26] R. D. Preston. The organisation of the cell wall of the conifer tracheid. *Philosophical Transactions of the Royal Society of London. Series B, Biological Sciences*, 224(511):131–174, 1934.

[27] R. D. Preston. The fine structure of the walls of the conifer tracheids iii. *Biochim. et Biophys. Acta 2*, pages 370–383, 1948.

[28] R. D. Preston. *The physical biology of plant cell walls*. Chapman and Hall, London, 1974.

[29] R. D. Preston and A.B. Wardrop. The fine structure of the walls of the conifer tracheid iv. *Biochim. et Biophys. Acta 3*, pages 549–559, 1949.

[30] R. M. Rowell. *Handbook of Wood Chemistry and Wood Composites*. CRC Press Taylor & Francis Group, LLC, Boca Raton, 2013.

[31] P. Rudman. Studies in wood preservation. pt. iii. the penetration of the fine structure of wood by inorganic solutions, including wood preservatives. *Holzforschung*, 20(2):60–67, 1966.

[32] H. V Scheller and P. Ulvskov. Hemicelluloses. *Annual Review of Plant Biology*, 61:263–289, 2010.

[33] K. Sherif. Bacterial cellulose production and its industrial applications. *Bioprocessing & Biotechniques*, 2014.

[34] A.J. Stamm. Thermal degradation of wood and cellulose. *Industrial and Engineering Chemistry*, 48(3):413–417, 1956.

[35] C. M. Stewart. Excreation and heartwood formation in living trees. *Science*, 153:1068–1074, 1966.

[36] A. M. Taylor, B. L. Gartner, and J. J. Morrell. Heartwood formation and natural durability – a review. *Wood and Fiber Science*, 34 (4):587–611, 2002.

[37] J.-L. Wertz, O. Bédué, and J. P. Mercier. *Cellulose Science and Technology*. EPFL Press, Boca Raton, 2010.

[38] R. W. Whetten, J. J. Mackay, and R. R Sederoff. Recent advances in understanding lignin biosynthesis. *Annual Review of Plant Physiology and Plant Molecular Biology*, 49:585–609, 1998.

[39] A. Zaman, R. Alén, and R. Kotilainen. Thermal behavior of scots pine (pinus sylvestris) and silver birch (betula pendula) at 200-230¸ *Wood and Fiber Science*, 32(2):138–143, 2000.

[40] X. Zuo and A. Grishaev. Absorption edge. `https://ccrod.cancer.gov/confluence/download/attachments/41912958/PartOne_final.pdf?api=v2`. Accessed: 2014-09-09.

List of Figures

7. Curriculum vitae

Curriculum Vitae

Personal Information

Name	LUDACKA, Ursula
Nationality	AUT

Education

▹ Period	2010–2015
∘ Accquired qualifications	**Master study**
∘ Institute	University of Vienna
∘ Principal subjects	Solid State Physics
▹ Period	2007–2010
∘ Accquired qualifications	**Bachelor study**
∘ Institute	University of Vienna
∘ Principal subjects	Solid State Physics

Research

▹ Master thesis	"SAXS and WAXS investigations on cellulose of *Picea abies* – The influence of thermal treatment on the microfibril angle"' — Dynamics of Condensed Systems
▹ Bachelor thesis	"SAXS in-situ Zugversuche an Rattenschwanzsehnen – Möglichkeiten und Grenzen von Labor-SAXS-Anlagen" — Dynamics of Condensed Systems

Languages

First language	**German**
Other language	English

Appendices

A. Data of SAXS measurements

Sample	Coordinate 1. max.	Height 1.max	Coordinate 2.max	Height 2.max	Coordinate 3.max	Height 3.max	Difference x01-x03
3 Earlywood (EW)							
TW2_Fu_0_001	72,2821	34,9742	93,516	69,9342	115,4415	31,9992	43,1594
TW2_F160_0_001	61,7006	34,3868	86,1014	142,5255	110,6493	34,3204	48,9487
TW2_F190_0_001	64,823	20,427	85,0858	69,5238	107,1603	18,316	42,3373
TW2_F220_0_001	39,9236	35,3823	59,1441	78,6457	78,4014	30,5757	38,4778
3 Latewood (LW)							
TW2_Fu_0_002	69,2909	84,7889	90,9625	161,1747	111,3999	80,9729	42,109
TW2_F160_0_002	80,7207	34,9985	98,7667	86,599	116,9505	32,9386	36,2298
TW2_F190_0_002	80,5211	37,4147	102,9502	111,8094	124,6524	36,1022	44,1313
TW2_F220_0_002	96,9108	49,6729	116,8597	118,5245	136,4491	34,4986	39,5383
4 EW							
TW2_Fu_0_003	56,4119	62,384	79,2282	157,3687	101,1801	60,7131	44,7682
TW2_F160_0_003	87,6436	21,1125	109,0218	112,4487	130,0811	20,1107	42,4375
TW2_F190_0_003	98,4378	16,9136	120,141	96,0157	140,8157	18,7401	42,3779
TW2_F220_0_003	78,6864	34,8501	103,0406	177,521	123,4829	37,4389	44,7965
4 LW							
TW2_Fu_0_004	64,1796	89,3636	84,728	213,7858	103,6895	86,1424	39,5099
TW2_F160_0_004	65,5539	31,5487	85,9634	73,2626	105,6261	30,4587	40,0722
TW2_F190_0_004	96,2695	31,1726	116,7227	59,2257	136,0711	29,7669	39,8016
TW2_F220_0_004	93,4107	113,0511	114,0908	252,6081	134,3322	110,2133	40,9215
6 EW							
TW2_Fu_0_005	41,2861	30,5544	60,785	189,8282	82,051	27,395	40,7649
TW2_F160_0_005	127,6841	19,1809	145,9285	128,3658	163,3505	25,5449	35,6664
TW2_F190_0_005	43,1776	17,8777	62,7994	118,4976	82,2024	15,175	39,0248
TW2_F220_0_005	115,8312	51,4255	135,1024	351,1964	155,2012	42,1844	39,37
6 LW							
TW2_Fu_0_006	118,7255	112,7736	136,8118	282,6929	155,2895	95,0815	36,564
TW2_F160_0_006	77,0405	48,8708	94,2099	174,3155	111,6622	48,0288	34,6217
TW2_F190_0_006	86,1147	36,2641	104,0324	141,8426	121,2194	39,7935	35,1047
TW2_F220_0_006	54,0379	98,1973	71,7301	364,7632	89,0979	98,4187	35,06
7 EW							
TW2_Fu_0_007	77,7103	29,091	97,4271	138,0241	117,9698	25,299	40,2595
TW2_F160_0_007	76,383	15,8986	97,8139	84,8589	118,9637	15,4189	42,5807
TW2_F190_0_007	69,288	21,0474	87,1091	111,1178	107,4332	15,7376	38,1452
TW2_F220_0_007	66,5506	37,4291	84,6752	193,5329	105,2915	25,4558	38,7409

7 LW							
TW2_Fu_0_008	66,098	90,6029	84,4928	257,8561	102,9129	85,4368	36,8149
TW2_F160_0_008	72,3452	26,9302	90,7529	74,0337	109,0393	29,252	36,6941
TW2_F190_0_008	75,8226	44,3921	92,9845	121,9517	109,1861	43,7431	33,3635
TW2_F220_0_008	73,1828	111,8958	91,6742	242,2531	109,4502	118,833	36,2674
9 EW							
TW2_Fu_0_009	68,4634	15,2891	91,3225	107,5856	114,6665	11,9659	46,2031
TW2_F160_0_009	71,1482	21,7442	91,8138	148,0902	113,3228	20,9195	42,1746
TW2_F190_0_009	58,4321	16,7383	79,6807	97,0655	101,2059	14,759	42,7738
TW2_F220_0_009	72,6692	61,1237	93,0777	308,9114	114,1794	60,8547	41,5102
9 LW							
TW2_Fu_0_010	39,6951	111,963	56,9138	199,6313	74,4221	116,7519	34,727
TW2_F160_0_010	70,8279	46,9237	89,3293	106,0013	108,1627	44,207	37,3348
TW2_F190_0_010	70,2729	49,506	90,117	119,548	110,0234	47,1924	39,7505
TW2_F220_0_010	72,6692	61,1237	93,0777	308,9114	114,1794	60,8547	41,5102
10 EW							
TW2_Fu_0_011	73,6948	41,8829	93,1266	175,6725	113,6754	35,1841	39,9806
TW2_F160_0_011	84,8331	21,3881	104,6129	85,8465	126,3858	19,5891	41,5527
TW2_F190_0_011	70,2068	15,8169	92,143	94,7418	116,2927	10,7557	46,0859
TW2_F220_0_011	88,9829	54,651	108,4121	300,9598	129,02	49,1277	40,0371
10 LW							
TW2_Fu_0_012	44,7216	97,3364	65,4884	216,6404	86,1003	99,4247	41,3787
TW2_F160_0_012	94,8935	58,7294	116,1484	121,8349	137,1257	60,1835	42,2322
TW2_F190_0_012	31,1842	58,245	51,9138	113,6456	72,0157	57,9029	40,8315
TW2_F220_0_012	111,0957	111,3456	132,3797	237,7078	153,6694	108,7952	42,5737
12 EW							
TW2_Fu_0_013	71,6463	25,9262	93,8133	205,8549	116,6569	20,985	45,0106
TW2_F160_0_013	97,9857	19,5758	116,7144	135,008	134,5494	26,1805	36,5637
TW2_F190_0_013	72,2566	8,1095	94,7029	52,4372	117,482	5,9036	45,2254
TW2_F220_0_013	93,0422	70,3562	111,9568	356,7321	131,9714	65,2078	38,9292
12 LW							
TW2_Fu_0_014	78,3207	107,4064	96,3943	266,3915	114,0043	105,363	35,6836
TW2_F160_0_014	53,911	51,9251	72,7315	129,9193	91,8143	54,0071	37,9033
TW2_F190_0_014	74,1208	42,7577	91,232	114,1494	107,7883	39,1991	33,6675
TW2_F220_0_014	78,6309	143,5047	96,4837	356,7086	113,9413	142,681	35,3104

15 EW							
TW2_Fu_0_015	75,1357	38,5718	95,9111	169,9321	116,3881	34,9975	41,2524
TW2_F160_0_015	78,9395	15,7166	98,4677	60,1018	119,5525	12,9178	40,613
TW2_F190_0_015	63,6466	30,9347	83,9003	113,7998	103,9175	31,2567	40,2709
TW2_F220_0_015	82,9665	56,6775	105,1878	264,877	127,8874	65,9356	44,9209
15 LW							
TW2_Fu_0_016	75,7622	78,266	95,1704	219,5914	114,1073	76,9465	38,3451
TW2_F160_0_016	67,8514	58,7407	86,8757	130,899	105,7326	59,6963	37,8812
TW2_F190_0_016	69,0154	61,784	87,7027	163,4762	105,8374	64,572	36,822
TW2_F220_0_016	75,8076	105,0161	95,7805	252,8115	115,4263	103,0981	39,6187
16 EW							
TW2_Fu_0_017	64,5558	30,3588	84,1658	131,2535	104,6065	33,0725	40,0507
TW2_F160_0_017	68,9712	13,4422	88,8403	72,7484	108,9646	14,5662	39,9934
TW2_F190_0_017	76,9559	16,1049	96,9038	53,6157	117,3134	13,6299	40,3575
TW2_F220_0_017	82,7673	47,725	103,8231	245,8546	123,9526	59,3953	41,1853
16 LW							
TW2_Fu_0_018	86,419	65,9496	108,964	130,5073	131,0429	65,5928	44,6239
TW2_F160_0_018	64,1981	31,9649	85,6394	66,3455	106,8345	32,6053	42,6364
TW2_F190_0_018	75,4843	55,3258	97,3436	122,1651	118,651	57,2079	43,1667
TW2_F220_0_018	71,3719	95,4058	93,9617	181,6411	116,0517	97,5227	44,6798
17 EW							
TW2_Fu_0_019	62,1457	49,0613	81,4598	145,9132	101,3108	51,7112	39,1651
TW2_F160_0_019	58,4637	14,6792	82,2628	64,0315	104,9438	15,3261	46,4801
TW2_F190_0_019	80,2661	9,4104	102,0524	49,5955	125,1362	13,0681	44,8701
TW2_F220_0_019	63,6043	63,1471	84,7171	271,0337	106,64	64,8743	43,0357
17 LW							
TW2_Fu_0_020	66,9186	50,6357	90,7573	97,6787	113,6995	51,3772	46,7809
TW2_F160_0_020	63,185	37,1057	84,72	70,0421	105,7343	38,6734	42,5493
TW2_F190_0_020	83,6404	44,1388	107,8249	91,6871	131,8544	46,2381	48,214
TW2_F220_0_020	61,7086	81,5802	84,7317	122,6394	107,8402	81,7484	46,1316
19 EW							
TW2_Fu_0_021	76,2115	30,303	98,2471	193,8934	120,6809	31,748	44,4694
TW2_F160_0_021	59,8667	24,9379	80,7849	100,0943	101,6922	26,8904	41,8255
TW2_F190_0_021	65,2059	41,7948	84,4008	181,4897	102,9739	42,051	37,768
TW2_F220_0_021	94,7646	90,4546	115,8846	324,7961	137,8873	93,6418	43,1227

19 LW							
TW2_Fu_0_022	76,6283	96,5213	92,8427	276,5278	109,9092	82,8253	33,2809
TW2_F160_0_022	54,2231	41,5124	73,6523	83,5083	93,3153	40,0528	39,0922
TW2_F190_0_022	75,793	56,1447	93,1061	118,786	110,762	54,5728	34,969
TW2_F220_0_022	60,6103	106,0044	80,5866	178,7647	100,1508	106,661	39,5405
23 EW							
TW2_Fu_0_023	66,8494	43,3435	89,0262	216,4514	111,0462	46,9762	44,1968
TW2_F160_0_023	63,2463	24,3899	87,0676	107,5514	111,0414	27,5958	47,7951
TW2_F190_0_023	70,9445	28,8291	91,8166	103,3003	112,9168	20,1441	41,9723
TW2_F220_0_023	66,5069	55,8875	89,8736	235,1279	113,1348	52,6135	46,6279
23 EW							
TW2_Fu_0_024	71,1216	96,3475	87,7531	188,0579	103,6669	96,8145	32,5453
TW2_F160_0_024	62,7105	92,7681	81,1846	160,6191	99,2744	91,5306	36,5639
TW2_F190_0_024	72,3168	32,8224	91,0103	73,2274	109,0212	32,5154	36,7044
TW2_F220_0_024	88,4189	137,4191	103,4139	361,6496	118,6674	141,9879	30,2485
28 EW							
TW2_Fu_0_025	62,1106	33,4923	83,3595	122,6628	104,5872	36,04	42,4766
TW2_F160_0_025	56,3786	20,3056	77,3053	98,291	99,1246	22,1999	42,746
TW2_F190_0_025	70,1343	11,9144	90,3994	45,0388	110,9201	12,0826	40,7858
TW2_F220_0_025	62,2557	55,6737	82,5194	256,3197	103,1421	62,4756	40,8864
29 LW							
TW2_Fu_0_026	71,8766	91,1475	92,3555	149,3073	112,3948	87,6554	40,5182
TW2_F160_0_026	66,4036	88,5769	86,7652	169,9216	106,9806	90,704	40,577
TW2_F190_0_026	68,5885	52,9568	91,7315	74,1251	114,0302	55,2807	45,4417
TW2_F220_0_026	50,9601	135,2976	72,298	241,2297	93,5937	135,554	42,6336
30 EW							
TW2_Fu_1_001	69,6356	38,2298	91,1626	130,0201	113,0654	40,3091	43,4298
TW2_F160_1_001	72,8049	13,6341	94,4482	55,1301	116,1874	13,0247	43,3825
TW2_F190_1_001	72,2287	20,014	93,9012	60,3725	114,8274	18,0407	42,5987
TW2_F220_1_001	76,1254	62,9135	97,4207	285,4318	118,4181	58,9964	42,2927
30 LW							
TW2_Fu_1_002	67,8848	72,9637	88,5044	150,8885	108,3081	74,6601	40,4233
TW2_F160_1_002	82,1376	66,4171	100,2046	145,3137	117,9556	67,9191	35,818
TW2_F190_1_002	72,8754	67,4681	93,1945	103,984	112,4953	67,5149	39,6199
TW2_F220_1_002	65,6101	85,5222	85,6169	197,2967	105,4075	92,0381	39,7974

32 EW							
TW2_Fu_1_003	68,353	46,0116	89,3326	204,1661	110,364	52,163	42,011
TW2_F160_1_003	75,578	51,3723	94,7188	167,1154	113,2519	44,226	37,6739
TW2_F190_1_003	85,0364	32,8868	106,1521	146,2067	127,0873	31,6542	42,0509
TW2_F220_1_003	77,4722	61,0884	94,2412	180,5421	111,0488	58,7338	33,5766
32 LW							
TW2_Fu_1_004	89,4145	77,4411	110,9434	167,1151	132,1256	78,1708	42,7111
TW2_F160_1_004	75,8873	71,188	94,1142	124,657	111,8774	68,974	35,9901
TW2_F190_1_004	64,0695	84,751	83,6373	168,4353	103,5853	85,8538	39,5158
TW2_F220_1_004	79,0923	88,5813	97,3884	197,4825	115,4194	84,9632	36,3271
35 EW							
TW2_Fu_1_005	71,196	62,2344	92,3337	239,9515	112,6913	62,2752	41,4953
TW2_F160_1_005	72,3925	29,3774	91,5025	105,8539	110,7513	28,492	38,3588
TW2_F190_1_005	79,5773	17,7193	100,7048	78,9843	121,0562	16,8428	41,4789
TW2_F220_1_005	66,5946	45,4341	86,0076	155,2581	104,8818	49,6426	38,2872
35 LW							
TW2_Fu_1_006	65,9606	49,6376	86,2694	62,3592	105,6851	53,4249	39,7245
TW2_F160_1_006	62,8736	76,9714	81,1042	143,0647	99,2704	74,0354	36,3968
TW2_F190_1_006	81,8847	53,1717	100,6112	100,4715	119,402	51,4185	37,5173
TW2_F220_1_006	78,5469	95,4815	98,2255	166,0719	117,1864	97,9324	38,6395
40 EW							
TW2_Fu_1_007	67,1378	29,2149	86,1237	205,6563	104,7273	35,8279	37,5895
TW2_F160_1_007	76,9515	28,5832	94,1207	118,6591	112,3642	22,8026	35,4127
TW2_F190_1_007	76,7293	18,0078	94,9597	83,3839	114,8963	16,2896	38,167
TW2_F220_1_007	57,0549	14,0862	75,3119	57,5511	95,4034	13,73	38,3485
40 LW							
TW2_Fu_1_008	72,3586	60,5324	85,5564	153,0489	98,8176	64,0008	26,459
TW2_F160_1_008	74,7642	36,8307	93,4139	76,2286	112,1276	39,9217	37,3634
TW2_F190_1_008	82,0991	42,0596	99,0524	118,2076	116,0418	43,7628	33,9427
TW2_F220_1_008	56,2099	96,3277	72,8514	252,2142	89,2639	104,2812	33,054
41 EW							
TW2_Fu_1_009	70,9714	41,2877	90,3124	132,5235	109,7414	40,4193	38,77
TW2_F160_1_009	67,0923	19,6678	88,8938	61,5148	110,7432	21,6137	43,6509
TW2_F190_1_009	61,0276	30,1828	81,1495	78,0599	101,6866	30,7716	40,659
TW2_F220_0_009	71,5118	45,6143	91,8624	157,3652	112,2391	41,3566	40,7273

41 LW							
TW2_Fu_1_0010	109,8235	90,3089	128,7157	189,5474	147,5275	89,1584	37,704
TW2_F160_1_010	64,3835	81,8356	82,133	139,5979	99,8768	81,3933	35,4933
TW2_F190_1_010	78,966	53,9614	95,6713	117,6877	111,9436	55,9482	32,9776
TW2_F220_1_010	81,0398	98,0508	97,0307	241,2093	112,6677	113,958	31,6279
49 EW							
TW2_Fu_1_011	110,23	32,2395	128,9658	242,1096	145,5896	35,6711	35,3596
TW2_F160_1_011	71,154	16,7229	86,7465	131,603	102,4201	17,8002	31,2661
TW2_F190_1_011	77,3971	17,6291	95,8143	145,1659	115,1762	19,9603	37,7791
TW2_F220_1_011	78,5183	28,9248	95,2365	216,0774	112,6976	24,1279	34,1793
49 LW							
TW2_Fu_1_012	84,1429	81,922	96,9409	500,2027	110,4368	68,3511	26,2939
TW2_F160_1_012	98,2534	29,4527	111,5364	225,8894	124,8744	30,046	26,621
TW2_F190_1_012	92,1016	27,3287	108,3987	326,9034	123,8023	31,6448	31,7007
TW2_F220_1_012	83,1179	58,0879	96,2011	426,1686	109,6771	58,7765	26,5592
63 EW							
TW2_Fu_1_013	70,2619	34,8436	89,3336	259,9258	108,7182	36,8237	38,4563
TW2_F160_1_013	66,3373	17,6119	85,8935	104,7104	104,7648	18,1479	38,4275
TW2_F190_1_013	61,2538	17,8658	80,1554	111,2835	99,675	17,5549	38,4212
TW2_F220_1_013	78,2937	37,2297	96,7161	155,6735	114,7569	35,8095	36,4632
63 LW							
TW2_Fu_1_014	64,2507	90,7657	83,6425	237,7529	102,5308	93,1987	38,2801
TW2_F160_1_014	71,3199	49,6215	91,1346	91,4752	110,7828	48,508	39,4629
TW2_F190_1_014	77,8183	30,977	95,6432	88,6995	113,394	30,137	35,5757
TW2_F220_1_014	64,7934	63,1439	83,1762	165,5014	102,0528	64,3941	37,2594
64 EW							
TW2_Fu_1_015	66,124	36,0803	86,6313	161,5495	106,9622	37,0484	40,8382
TW2_F160_1_015	68,4691	38,7637	86,1769	143,0935	103,0855	41,9817	34,6164
TW2_F190_1_015	60,0196	11,2218	78,9006	49,6678	99,2938	9,7587	39,2742
TW2_F220_1_015	73,138	19,1547	92,2046	70,3758	112,3172	17,6486	39,1792
64 LW							
TW2_Fu_1_016	87,8265	67,6726	106,2976	171,3621	123,6764	75,5214	35,8499
TW2_F160_1_016	76,3257	33,9251	93,7034	93,4826	111,4371	33,2016	35,1114
TW2_F190_1_016	68,6321	44,0222	86,607	104,4402	104,0784	45,3156	35,4463
TW2_F220_1_016	92,8211	73,6729	110,481	133,6659	128,3469	75,4601	35,5258

67 EW							
TW2_Fu_1_017	65,3402	26,8715	86,2355	115,254	107,4316	21,8608	42,0914
TW2_F160_1_017	79,4174	23,9702	100,0592	99,3053	121,8944	24,6328	42,477
TW2_F190_1_017	93,9146	19,8852	113,002	79,2607	132,1216	18,7123	38,207
TW2_F220_1_017	59,3893	23,1661	79,0601	154,7751	99,2243	27,3255	39,835
64 LW							
TW2_Fu_1_018	57,0893	85,0055	77,8546	112,8585	98,6417	88,8843	41,5524
TW2_F160_1_018	54,9082	51,1388	75,15	102,8546	95,2047	53,6888	40,2965
TW2_F190_1_018	67,8234	66,194	89,0467	105,1236	109,5469	64,161	41,7235
TW2_F220_1_018	77,3545	59,9426	98,167	90,0283	118,5875	61,2062	41,233
71 EW							
TW2_Fu_1_019	70,9438	16,3816	91,8594	118,9577	115,1219	14,6031	44,1781
TW2_F160_1_019	87,6804	15,1068	106,2156	97,1243	122,2627	18,6623	34,5823
TW2_F190_1_019	77,071	16,3513	95,3812	102,936	115,8303	13,7518	38,7593
TW2_F220_1_019	68,5612	25,2189	87,0309	165,7766	106,0563	26,6712	37,4951
71 LW							
TW2_Fu_1_020	75,4348	48,7453	90,3076	326,1904	104,8748	45,5829	29,44
TW2_F160_1_020	70,0518	41,24	86,9928	304,7773	102,6395	47,9814	32,5877
TW2_F190_1_020	77,013	25,7181	91,5248	182,7159	106,6664	26,6718	29,6534
TW2_F220_1_020	95,0209	40,2304	110,3385	206,0927	126,7166	33,9496	31,6957
75 EW							
TW2_Fu_1_0021	70,4452	17,6022	90,4484	150,7297	108,6108	15,1633	38,1656
TW2_F160_1_0021	64,0661	20,8192	80,9877	127,7131	99,6149	18,5576	35,5488
TW2_F190_1_0021	77,6017	27,0742	95,2109	173,0254	112,2906	28,3725	34,6889
TW2_F220_1_0021	71,1434	19,1802	89,3641	139,9929	107,3226	23,3959	36,1792
75 LW							
TW2_Fu_0_022	67,4699	46,8212	83,6741	413,1546	98,9642	54,6962	31,4943
TW2_F160_1_022	73,2008	24,2481	89,1604	271,695	104,7336	25,5478	31,5328
TW2_F190_1_022	78,0355	28,476	91,9234	241,338	107,7215	22,3352	29,686
TW2_F220_1_022	76,8359	43,2778	92,1391	442,2852	108,6405	38,0014	31,8046

	Coordinate 4. max.	Height 4.max	Coordinate 5.max	Height 5.max	Coordinate 6.max	Height 6.max	Difference x04-x06
3 Earlywood (EW)							
TW2_Fu_0_001	253,1845	35,3431	275,0193	67,145	297,5589	**32,1721**	44,3744
TW2_F160_0_001	242,0225	36,1084	266,6601	164,3598	292,3792	**37,1314**	50,3567
TW2_F190_0_001	241,6179	18,127	261,7814	67,9039	282,9763	**20,2532**	41,3584
TW2_F220_0_001	219,9265	31,4876	239,5798	96,4397	258,7893	**36,0513**	38,8628
3 Latewood (LW)							
TW2_Fu_0_002	248,2999	85,4289	269,5401	153,0861	290,4084	**76,851**	42,1085
TW2_F160_0_002	259,5457	35,2935	277,0963	94,1617	295,5716	**35,2356**	36,0259
TW2_F190_0_002	258,5802	36,2036	279,8718	110,6761	301,475	**37,2605**	42,8948
TW2_F220_0_002	273,9873	43,7532	293,1132	118,8334	312,5721	**41,3044**	38,5848
4 EW							
TW2_Fu_0_003	235,621	64,1512	257,8254	136,1931	279,9009	**57,4061**	44,2799
TW2_F160_0_003	263,3922	21,083	286,4458	123,3901	308,2093	**25,5138**	44,8171
TW2_F190_0_003	277,141	19,1527	297,5711	94,7837	318,5529	**17,2388**	41,4119
TW2_F220_0_003	255,0958	34,0313	280,308	184,177	301,7616	**36,7105**	46,6658
4 LW							
TW2_Fu_0_004	243,8782	93,7403	263,1882	190,9589	282,0919	**88,3441**	38,2137
TW2_F160_0_004	246,4785	34,8282	266,4471	78,7339	286,5679	**32,8439**	40,0894
TW2_F190_0_004	273,863	32,3989	294,1141	61,4638	314,0196	**30,3343**	40,1566
TW2_F220_0_004	271,2848	111,7947	291,5387	252,0381	312,206	**107,154**	40,9212
6 EW							
TW2_Fu_0_005	218,9712	26,425	238,6123	181,0127	258,5703	**29,2089**	39,5991
TW2_F160_0_005	306,0107	20,2791	324,2711	135,0122	341,7315	**25,6445**	35,7208
TW2_F190_0_005	220,1103	17,4384	242,1926	137,9607	263,2417	**14,6902**	43,1314
TW2_F220_0_005	292,8186	47,4751	312,2473	348,8088	331,4858	**45,1521**	38,6672
6 LW							
TW2_Fu_0_006	299,4851	107,0695	317,6329	271,0621	335,7396	**100,718**	36,2545
TW2_F160_0_006	255,4199	48,9228	272,5087	172,9934	289,7016	**51,5861**	34,2817
TW2_F190_0_006	263,731	36,7361	281,837	147,0626	299,4835	**37,197**	35,7525
TW2_F220_0_006	233,3548	106,805	251,392	398,198	268,6578	**98,0826**	35,303
7 EW							
TW2_Fu_0_007	257,2457	31,9748	276,3494	119,3595	296,0415	**23,7487**	38,7958
TW2_F160_0_007	253,8654	15,5454	275,5238	88,1999	296,3268	**19,7527**	42,4614
TW2_F190_0_007	246,403	20,755	264,1349	108,7061	282,011	**19,2203**	35,608
TW2_F220_0_007	241,9594	27,0983	261,6087	199,9447	280,7363	**30,0452**	38,7769

7 LW							
TW2_Fu_0_008	244,4024	80,5263	262,6648	272,9135	281,4662	**89,1255**	37,0638
TW2_F160_0_008	251,3147	29,3443	269,5663	78,7669	288,2585	**30,0815**	36,9438
TW2_F190_0_008	254,3782	43,6173	270,555	119,0182	287,1616	**45,4244**	32,7834
TW2_F220_0_008	251,907	118,0176	269,8609	243,9895	288,0835	**118,0096**	36,1765
9 EW							
TW2_Fu_0_009	243,6367	12,8579	268,5143	102,0711	290,6116	**14,6197**	46,9749
TW2_F160_0_009	250,1848	26,313	270,3305	147,2184	289,311	**22,5689**	39,1262
TW2_F190_0_009	234,0313	12,8196	256,399	99,3884	275,998	**16,8131**	41,9667
TW2_F220_0_009	252,1674	68,9045	272,7186	359,7779	294,074	**64,0102**	41,9066
9 LW							
TW2_Fu_0_010	219,5262	108,2587	236,1472	202,0729	253,3801	**115,9255**	33,8539
TW2_F160_0_010	250,0044	48,4161	267,9032	106,2574	286,4935	**46,7718**	36,4891
TW2_F190_0_010	247,8349	50,4047	267,6343	118,8716	288,356	**49,2982**	40,5211
TW2_F220_0_010	252,1674	68,9045	272,7186	359,7779	294,074	**64,0102**	41,9066
10 EW							
TW2_Fu_0_011	252,4336	41,3525	270,7672	154,4336	289,4605	**40,4275**	37,0269
TW2_F160_0_011	265,4779	22,9264	284,9346	87,7821	306,4252	**20,4044**	40,9473
TW2_F190_0_011	246,7139	13,0703	268,9018	93,9885	289,4336	**13,3772**	42,7197
TW2_F220_0_011	265,4558	54,7533	285,4834	314,972	305,4353	**54,7294**	39,9795
10 LW							
TW2_Fu_0_012	223,08	97,6068	244,3295	193,7881	264,6152	**99,1011**	41,5352
TW2_F160_0_012	273,2822	58,8692	294,229	124,3405	315,8171	**61,0537**	42,5349
TW2_F190_0_012	211,1877	60,1154	231,3714	127,512	251,5699	**63,3021**	40,3822
TW2_F220_0_012	289,2348	114,7888	310,221	249,8412	331,3759	**108,4377**	42,1411
12 EW							
TW2_Fu_0_013	251,7946	31,2433	272,0217	184,8888	291,6294	**25,3659**	39,8348
TW2_F160_0_013	274,9261	19,1146	294,8685	144,1778	311,8869	**32,2329**	36,9608
TW2_F190_0_013	249,9859	7,9428	272,7996	58,6753	295,5441	**8,278**	45,5582
TW2_F220_0_013	271,2868	69,7673	289,3508	351,1092	308,3494	**70,3413**	37,0626
12 LW							
TW2_Fu_0_014	257,1305	110,4324	275,0571	246,2355	292,7199	**103,6335**	35,5894
TW2_F160_0_014	232,8058	54,052	251,446	140,2371	270,6213	**55,758**	37,8155
TW2_F190_0_014	253,8698	42,2653	270,4726	124,7831	287,2491	**42,7657**	33,3793
TW2_F220_0_014	258,8792	150,7277	276,2574	378,7194	293,1232	**148,8635**	34,244

15 EW							
TW2_Fu_0_015	254,7666	40,494	274,5423	146,0829	293,4321	**33,1691**	38,6655
TW2_F160_0_015	254,2218	14,2603	275,6034	66,4699	296,4615	**15,9955**	42,2397
TW2_F190_0_015	241,5534	30,1012	261,2563	112,9762	281,5021	**30,8701**	39,9487
TW2_F220_0_015	261,9635	56,3303	283,0467	251,7982	303,6777	**58,0495**	41,7142
15 LW							
TW2_Fu_0_016	254,7216	80,7799	273,8257	211,6435	292,8332	**74,5105**	38,1116
TW2_F160_0_016	248,2233	61,3128	267,2432	143,4382	285,9858	**62,2678**	37,7625
TW2_F190_0_016	248,8274	63,9677	267,3572	191,7324	285,8318	**67,252**	37,0044
TW2_F220_0_016	255,9606	117,4232	275,3869	282,7258	294,3909	**110,8114**	38,4303
16 EW							
TW2_Fu_0_017	242,696	29,2857	262,5557	126,6457	282,5792	**33,3485**	39,8832
TW2_F160_0_017	247,0643	15,184	267,4873	81,3543	288,0388	**13,575**	40,9745
TW2_F190_0_017	256,6064	18,3146	275,9781	61,0378	297,0364	**14,7379**	40,43
TW2_F220_0_017	261,876	50,4602	281,702	226,1951	300,9099	**55,7004**	39,0339
16 LW							
TW2_Fu_0_018	265,0422	65,7574	287,8853	121,9904	310,8212	**63,4408**	45,779
TW2_F160_0_018	245,0856	34,6197	266,4778	76,8377	287,689	**33,9691**	42,6034
TW2_F190_0_018	255,399	61,3065	276,9375	138,998	298,4168	**60,6146**	43,0178
TW2_F220_0_018	251,4578	106,9938	273,4251	200,6691	295,2117	**104,1377**	43,7539
17 EW							
TW2_Fu_0_019	240,151	45,0897	259,3926	147,9211	280,0499	**48,806**	39,8989
TW2_F160_0_019	238,4127	14,9893	262,1486	73,5446	285,8591	**17,6992**	47,4464
TW2_F190_0_019	260,9951	12,1745	282,2654	56,9813	305,0858	**13,9877**	44,0907
TW2_F220_0_019	243,1132	66,6313	264,7893	324,4808	287,0771	**68,5415**	43,9639
17 LW							
TW2_Fu_0_020	245,5031	48,7712	268,4142	91,4264	291,9622	**48,9555**	46,4591
TW2_F160_0_020	244,7863	38,8778	265,6933	77,18	287,2931	**38,9914**	42,5068
TW2_F190_0_020	262,9843	48,221	287,1366	98,2202	310,4084	**49,7845**	47,4241
TW2_F220_0_020	239,8457	83,1915	262,4309	126,6294	286,4559	**82,402**	46,6102
19 EW							
TW2_Fu_0_021	255,4699	34,6172	276,7862	174,0575	298,4301	**30,5157**	42,9602
TW2_F160_0_021	241,1677	25,1604	261,5851	112,6056	283,1396	**28,6446**	41,9719
TW2_F190_0_021	242,2704	39,8111	261,7592	188,1517	280,2896	**43,7514**	38,0192
TW2_F220_0_021	271,3559	87,8653	293,1627	318,8136	315,4542	**85,473**	44,0983

19 LW							
TW2_Fu_0_022	257,3645	95,5671	273,9235	262,8441	290,6681	**82,0859**	33,3036
TW2_F160_0_022	233,2412	36,8749	253,4029	79,6771	273,4237	**39,4568**	40,1825
TW2_F190_0_022	253,1392	53,9906	270,6917	123,5365	288,6039	**52,4725**	35,4647
TW2_F220_0_022	238,7641	108,5144	258,0894	178,9236	277,9582	**107,6496**	39,1941
23 EW							
TW2_Fu_0_023	248,3469	42,2771	270,3649	200,5975	46,4915	**292,5396**	44,1927
TW2_F160_0_023	243,3983	23,9877	266,3903	92,3467	289,8858	**27,4416**	46,4875
TW2_F190_0_023	250,7973	23,199	271,8049	88,7338	292,59	**21,5249**	41,7927
TW2_F220_0_023	244,0379	53,0697	266,7979	231,1976	290,2312	**51,8071**	46,1933
23 EW							
TW2_Fu_0_024	250,1555	98,839	266,2947	183,6957	282,905	**95,7611**	32,7495
TW2_F160_0_024	241,2809	95,17	259,618	169,7797	278,3239	**93,7623**	37,043
TW2_F190_0_024	250,0183	32,1505	268,22	74,7534	287,1279	**33,6917**	37,1096
TW2_F220_0_024	266,1559	137,2699	281,4975	361,8821	297,1597	**144,8273**	31,0038
28 EW							
TW2_Fu_0_025	238,7165	30,5177	261,1568	124,4009	283,618	**32,3974**	44,9015
TW2_F160_0_025	236,9159	21,1178	258,1783	112,0941	279,7906	**24,7843**	42,8747
TW2_F190_0_025	247,0009	11,148	268,8389	53,6329	290,2016	**12,3646**	43,2007
TW2_F220_0_025	242,2047	56,6819	262,6852	307,2568	283,5462	**64,4895**	41,3415
29 LW							
TW2_Fu_0_026	250,2694	91,7156	270,6342	137,3027	291,4054	**87,6989**	41,136
TW2_F160_0_026	247,2816	95,6395	267,3443	194,1684	287,6267	**95,4005**	40,3451
TW2_F190_0_026	249,0492	60,252	271,0961	82,0941	293,3142	**59,4685**	44,265
TW2_F220_0_026	229,1744	137,1748	249,8378	247,6408	271,6832	**134,2197**	42,5088
30 EW							
TW2_Fu_1_001	248,5311	40,7122	269,0922	113,9525	290,725	**40,7018**	42,1939
TW2_F160_1_001	253,5658	15,3426	274,7126	62,6181	296,6241	**16,0178**	43,0583
TW2_F190_1_001	251,9293	21,9521	273,6242	65,5007	294,6513	**20,2927**	42,722
TW2_F220_1_001	253,2646	65,0995	274,1821	268,5477	295,2002	**56,4265**	41,9356
30 LW							
TW2_Fu_1_002	246,3722	72,3219	266,417	148,1628	287,086	**73,8219**	40,7138
TW2_F160_1_002	262,1258	69,3051	280,5212	157,8403	297,9463	**67,7033**	35,8205
TW2_F190_1_002	253,1663	69,0189	272,4312	119,9103	291,9833	**69,9376**	38,817
TW2_F220_1_002	245,7916	95,4357	265,0678	244,014	284,5731	**99,4571**	38,7815

32 EW							
TW2_Fu_1_003	247,1982	47,0225	267,5911	191,7978	289,4489	**51,5942**	42,2507
TW2_F160_1_003	255,6531	57,2238	274,8028	188,9039	293,3479	**49,7195**	37,6948
TW2_F190_1_003	264,1799	36,118	285,6354	159,6753	307,0257	**35,28**	42,8458
TW2_F220_1_003	257,3006	71,0171	273,286	200,4899	289,6323	**60,4995**	32,3317
32 LW							
TW2_Fu_1_004	268,9394	73,8314	289,4675	156,0465	310,5351	**77,1137**	41,5957
TW2_F160_1_004	254,5934	72,4515	272,401	131,966	290,5923	**67,6403**	35,9989
TW2_F190_1_004	243,9621	82,1141	264,3431	150,7058	283,8485	**84,7599**	39,8864
TW2_F220_1_004	256,2991	88,6742	274,1511	189,6614	292,2234	**85,7216**	35,9243
35 EW							
TW2_Fu_1_005	250,5688	63,0356	270,467	215,1052	290,3417	**64,0658**	39,7729
TW2_F160_1_005	252,9845	32,1404	271,9957	114,1257	290,9191	**30,9047**	37,9346
TW2_F190_1_005	257,9526	15,7571	278,0035	81,7516	297,9277	**16,9034**	39,9751
TW2_F220_1_005	244,8198	48,5812	264,7115	197,6529	284,6103	**54,143**	39,7905
35 LW							
TW2_Fu_1_006	244,9888	49,6369	264,644	58,1013	284,7341	**51,0745**	39,7453
TW2_F160_1_006	241,9568	82,4271	260,1337	142,633	278,4048	**74,2088**	36,448
TW2_F190_1_006	260,3725	53,0816	278,2372	99,4548	296,8304	**56,9004**	36,4579
TW2_F220_1_006	257,9595	106,7197	276,7683	182,146	295,4569	**103,319**	37,4974
40 EW							
TW2_Fu_1_007	246,046	31,8243	265,8591	222,451	285,1766	**31,595**	39,1306
TW2_F160_1_007	256,6269	30,0768	274,493	132,1917	292,7286	**24,7307**	36,1017
TW2_F190_1_007	254,0276	18,5713	272,6827	84,9443	292,2215	**16,3059**	38,1939
TW2_F220_1_007	236,8642	15,3932	255,4996	71,1461	275,6419	**15,0645**	38,7777
40 LW							
TW2_Fu_1_008	250,6109	55,6122	263,1116	145,8197	276,621	**72,8191**	26,0101
TW2_F160_1_008	255,0379	40,4198	274,1515	85,3846	292,4609	**38,6424**	37,423
TW2_F190_1_008	259,8405	43,3683	277,0001	125,2732	294,2509	**43,3666**	34,4104
TW2_F220_1_008	233,7402	100,5088	250,3501	249,7987	267,2012	**103,8491**	33,461
41 EW							
TW2_Fu_1_009	250,0054	40,4808	269,7508	144,9344	289,2366	**39,9991**	39,2312
TW2_F160_1_009	248,2648	21,9901	269,5095	68,715	291,6373	**22,7256**	43,3725
TW2_F190_1_009	240,9073	31,6621	261,0407	95,0037	282,0515	**32,3012**	41,1442
TW2_F220_0_009	247,9903	45,8702	268,1189	156,0052	288,5111	**44,7026**	40,5208

41 LW							
TW2_Fu_1_0010	289,3755	89,089	307,972	175,0743	326,617	**88,1232**	37,2415
TW2_F160_1_010	242,7059	85,2558	260,9029	148,7798	279,3169	**81,6626**	36,611
TW2_F190_1_010	258,9878	57,1458	275,7595	128,2179	292,2141	**53,9896**	33,2263
TW2_F220_1_010	258,6755	102,5806	275,0661	237,3242	291,4067	**108,0259**	32,7312
49 EW							
TW2_Fu_1_011	290,6383	32,2027	308,5466	231,4045	325,1457	**34,2059**	34,5074
TW2_F160_1_011	250,9802	18,1301	267,1712	140,69	284,0871	**15,5277**	33,1069
TW2_F190_1_011	255,267	19,0185	273,6786	131,581	291,4996	**17,5056**	36,2326
TW2_F220_1_011	257,7664	35,4059	274,0585	234,7695	291,2824	**28,6079**	33,516
49 LW							
TW2_Fu_1_012	262,4371	82,2117	275,797	494,7639	289,19	**71,9529**	26,7529
TW2_F160_1_012	277,5638	35,5384	290,7714	237,5966	305,2233	**25,3014**	27,6595
TW2_F190_1_012	271,6449	29,7094	286,8349	341,334	303,0486	**29,7446**	31,4037
TW2_F220_1_012	262,1368	67,4416	275,2898	451,3666	289,0086	**62,5482**	26,8718
63 EW							
TW2_Fu_1_013	248,8017	36,9277	268,9237	279,4009	288,9512	**33,5575**	40,1495
TW2_F160_1_013	245,3708	16,8284	265,5654	120,6048	286,2571	**19,9882**	40,8863
TW2_F190_1_013	243,1627	21,2173	260,619	123,2285	279,5937	**17,8004**	36,431
TW2_F220_1_013	257,6042	41,8612	275,7077	169,4223	293,1139	**38,2817**	35,5097
63 LW							
TW2_Fu_1_014	242,4834	88,4592	261,6868	240,3255	281,1877	**92,59**	38,7043
TW2_F160_1_014	252,2447	52,2399	271,89	95,2594	291,2997	**49,2632**	39,055
TW2_F190_1_014	255,738	31,349	273,5539	94,6569	291,6237	**30,509**	35,8857
TW2_F220_1_014	244,1418	67,2975	262,5055	191,516	281,1092	**68,519**	36,9674
64 EW							
TW2_Fu_1_015	244,3783	33,0469	264,5585	161,154	285,058	**36,2735**	40,6797
TW2_F160_1_015	248,0045	38,2624	266,3602	160,8513	283,8506	**44,2088**	35,8461
TW2_F190_1_015	238,7763	12,7858	258,5499	60,0949	279,8397	**11,7536**	41,0634
TW2_F220_1_015	250,0077	19,8648	268,9178	69,3517	289,3423	**19,0003**	39,3346
64 LW							
TW2_Fu_1_016	266,3934	69,706	285,3941	163,5043	303,8266	**70,4986**	37,4332
TW2_F160_1_016	257,0575	35,8147	274,4045	93,2138	291,3852	**34,5244**	34,3277
TW2_F190_1_016	248,5053	45,1964	266,6517	116,4479	284,8406	**45,3073**	36,3353
TW2_F220_1_016	270,5567	77,4191	288,7679	147,1648	306,654	**76,3476**	36,0973

67 EW							
TW2_Fu_1_017	244,1246	25,8541	264,6484	106,1176	284,5821	**23,6828**	40,4575
TW2_F160_1_017	258,1026	25,6261	278,3961	99,9863	299,7076	**26,4407**	41,605
TW2_F190_1_017	272,7147	19,0603	292,1199	67,8823	311,4721	**20,0522**	38,7574
TW2_F220_1_017	242,6615	20,9236	260,5317	122,3744	278,9558	**24,833**	36,2943
64 LW							
TW2_Fu_1_018	235,6051	85,8039	256,1112	111,4401	277,0359	**88,0542**	41,4308
TW2_F160_1_018	233,6683	55,0912	253,9172	110,6511	274,6566	**54,8058**	40,9883
TW2_F190_1_018	246,0295	67,3753	266,639	102,5837	287,5963	**67,4677**	41,5668
TW2_F220_1_018	254,6314	61,649	275,4313	84,382	296,6211	**59,9633**	41,9897
71 EW							
TW2_Fu_1_019	248,7735	17,9831	269,3285	110,3973	290,2461	**18,074**	41,4726
TW2_F160_1_019	266,3096	19,4991	284,926	106,7055	303,1556	**20,7576**	36,846
TW2_F190_1_019	254,7343	17,8255	274,6957	118,8521	294,7491	**16,3769**	40,0148
TW2_F220_1_019	244,4329	24,5075	263,8063	176,6507	283,0437	**28,0353**	38,6108
71 LW							
TW2_Fu_1_020	253,7191	49,8533	269,2056	325,3089	283,8715	**44,8709**	30,1524
TW2_F160_1_020	250,4789	41,2922	267,5001	323,448	283,5467	**48,4519**	33,0678
TW2_F190_1_020	255,0708	25,6688	269,5243	182,4172	283,8335	**30,4359**	28,7627
TW2_F220_1_020	273,2123	42,548	287,8632	200,697	302,7852	**38,8179**	29,5729
75 EW							
TW2_Fu_1_0021	249,3723	22,7247	268,9411	146,852	287,1525	**16,5462**	37,7802
TW2_F160_1_0021	242,4565	18,043	260,93	140,0056	278,6982	**23,9223**	36,2417
TW2_F190_1_0021	257,9316	30,9777	275,4691	189,6517	293,6049	**26,5738**	35,6733
TW2_F220_1_0021	248,155	20,1317	266,5155	146,6779	284,5058	**21,9188**	36,3508
75 LW							
TW2_Fu_0_022	245,7165	46,4308	262,2694	415,3114	277,218	**56,6623**	31,5015
TW2_F160_1_022	253,1428	25,8959	269,4968	283,9273	286,5709	**26,1222**	33,4281
TW2_F190_1_022	255,7028	23,4555	271,4911	258,5952	287,2953	**22,8602**	31,5925
TW2_F220_1_022	254,9587	45,1726	270,9772	476,2804	287,8014	**43,3933**	32,8427

B. Data of WAXS measurements

Sample	Coordinate 1. max.	Height 1.max	Coordinate 2.max	Height 2.max	Coordinate 3.max	Height 3.max	Difference x01-x03
3 Earlywood (EW)							
TW2_Fu_0_001	60.3862	135.3641	60.3851	217.4673	92.1103	285.0384	31.7241
TW2_F160_0_001	54.2260	33.3587	83.8108	449.9026	109.8626	161.8043	55.6366
TW2_F190_0_001	59.9227	54.6944	80.4070	298.4640	102.2588	197.1312	42.3361
TW2_F220_0_001	87.2299	119.0377	109.5481	121.4025	152.5603	5.3482	65.3304
3 Latewood (LW)							
TW2_Fu_0_002	65.2538	648.2906	86.0840	1093.8654	104.5411	794.8393	39.2873
TW2_F160_0_002	69.9630	501.1232	33.4803	15.7814	87.2601	400.6273	17.2971
TW2_F190_0_002	61.0697	210.5924	82.3315	371.7001	103.9445	167.2516	42.8748
TW2_F220_0_002	63.1540	19.3209	86.1823	311.4400	105.6160	270.0457	42.4620
4 EW							
TW2_Fu_0_003	68.1280	394.0101	68.1281	343.7278	97.8211	789.5905	29.6931
TW2_F160_0_003	58.0524	49.8254	87.3567	491.7582	107.8238	68.9065	49.7714
TW2_F190_0_003	82.6740	143.9866	96.9649	218.5605	112.4754	143.6526	29.8014
TW2_F220_0_003	53.6897	16.8294	80.9989	243.5382	101.1830	71.3137	47.4933
4 LW							
TW2_Fu_0_004	67.0367	823.3128	85.8133	1410.4715	103.8750	890.2200	36.8383
TW2_F160_0_004	79.6106	289.8194	98.4495	518.1963	117.8785	282.3540	38.2679
TW2_F190_0_004	77.7224	275.9731	95.2015	536.3438	113.0539	316.6851	35.3315
TW2_F220_0_004	71.9219	262.1132	92.5228	493.7556	112.9389	256.6344	41.0170
6 EW							
TW2_Fu_0_005	67.8882	145.2078	89.1314	1027.2808	110.5552	168.7788	42.6670
TW2_F160_0_005	60.6587	85.7741	85.0620	718.8880	110.1292	99.3313	49.4705
TW2_F190_0_005	86.4587	102.1791	106.0041	606.1435	125.7424	119.3797	39.2837
TW2_F220_0_005	69.7331	101.5050	91.4211	693.3792	114.3545	82.0616	44.6214
6 LW							
TW2_Fu_0_006	75.7024	536.5700	96.2206	2181.2038	114.9992	643.0625	39.2968
TW2_F160_0_006	81.2140	320.6744	121.6280	307.7261	101.5396	1487.5185	20.3256
TW2_F190_0_006	92.7543	1088.7963	74.6294	220.8831	110.7947	218.5772	18.0404
TW2_F220_0_006	66.5801	206.9818	84.3033	808.3546	102.5849	208.4359	36.0048
7 EW							
TW2_Fu_0_007	83.2913	229.4498	102.0964	432.6732	124.9358	75.5075	41.6445
TW2_F160_0_007	56.4785	24.3026	86.9559	461.9051	110.7611	49.2529	54.2826
TW2_F190_0_007	79.8191	138.0208	97.2647	535.3591	115.8497	95.4736	36.0306
TW2_F220_0_007	71.8307	75.3475	93.1947	421.0861	114.6580	64.0621	42.8273

7 LW							
TW2_Fu_0_008	84.5282	629.5598	104.1097	1319.2271	65.2538	525.7029	34.8522
TW2_F160_0_008	63.2036	173.6614	82.4229	575.0256	101.4168	211.5271	38.2132
TW2_F190_0_008	74.7614	297.8063	91.1292	811.1313	107.8395	253.6243	33.0781
TW2_F220_0_008	84.2622	342.2432	119.1964	373.0433	101.7775	777.7952	17.5153
9 EW							
TW2_Fu_0_009	65.9444	111.8505	84.9451	425.1413	106.3257	115.7675	40.3813
TW2_F160_0_009	74.4552	100.3326	101.8562	663.7689	126.9167	107.1776	52.4615
TW2_F190_0_009	62.4967	72.0411	85.8750	350.8203	108.0415	71.0381	45.5448
TW2_F220_0_009	62.9928	114.2464	82.6166	414.0414	102.7049	117.3067	39.7121
9 LW							
TW2_Fu_0_010	74.4214	114.5335	101.1696	1624.6994	217.3023	1625.1378	142.8809
TW2_F160_0_010	79.6617	380.2987	98.9439	807.4133	118.1503	364.0029	38.4886
TW2_F190_0_010	71.0181	146.7933	92.2360	308.7363	113.5257	156.4869	42.5076
TW2_F220_0_010	73.1795	212.3541	91.7222	465.7471	109.4343	189.8669	36.2548
10 EW							
TW2_Fu_0_011	69.0604	454.2066	85.0957	679.9395	101.2821	144.8957	32.2217
TW2_F160_0_011	74.6249	278.3469	96.4653	330.5515	131.0824	26.0299	56.4575
TW2_F190_0_011	70.1892	51.7736	93.4444	311.2047	117.5897	52.1498	47.4005
TW2_F220_0_011	81.9659	99.9906	98.5132	323.6886	121.3782	47.1102	39.4123
10 LW							
TW2_Fu_0_012	109.7031	-181.7656	109.7031	1425.6055	172.3588	2842.3746	62.6557
TW2_F160_0_012	33.4467	2580.4965	73.9220	201.9012	94.0784	-69.3831	60.6317
TW2_F190_0_012	89.6229	1783.0543	67.3382	126.8586	89.6229	315.4994	0.0000
TW2_F220_0_012	68.6918	185.8762	86.4049	1899.8029	104.8172	185.8179	36.1254
12 EW							
TW2_Fu_0_013	52.4261	168.8425	72.4160	935.0389	94.1843	154.0025	41.7582
TW2_F160_0_013	61.7843	110.5654	84.6344	696.4262	109.6159	100.7012	47.8316
TW2_F190_0_013	85.8237	75.5091	107.5803	423.7088	132.6112	73.3349	46.7875
TW2_F220_0_013	77.3922	133.7581	95.0343	516.2719	112.7945	123.0911	35.4023
12 LW							
TW2_Fu_0_014	66.1023	789.0792	83.5078	1531.6742	100.7203	779.3819	34.6180
TW2_F160_0_014	64.7491	442.9505	81.8942	712.5996	99.5059	492.1282	34.7568
TW2_F190_0_014	92.6585	194.5847	109.6506	629.7596	126.7439	207.8875	34.0854
TW2_F220_0_014	70.1470	322.1221	86.2592	541.8022	101.7801	260.0811	31.6331

15 EW							
TW2_Fu_0_015	87.6381	351.9944	109.8994	412.7631	128.4377	50.4083	40.7996
TW2_F160_0_015	55.6973	62.4435	77.2542	243.5269	100.2395	77.9312	44.5422
TW2_F190_0_015	72.6789	189.4989	90.8093	383.4033	106.8957	125.9579	34.2168
TW2_F220_0_015	81.5691	77.7233	104.3983	315.3352	125.3859	94.4712	43.8168
15 LW							
TW2_Fu_0_016	88.0296	612.0462	70.4989	680.6457	104.8415	1204.4025	16.8119
TW2_F160_0_016	88.0835	457.9341	106.0983	723.2060	124.5925	462.4960	36.5090
TW2_F190_0_016	84.3219	275.5266	101.4124	603.8257	118.3178	263.6942	33.9959
TW2_F220_0_016	70.0912	293.8780	89.1448	541.8305	108.5142	268.8226	38.4230
16 EW							
TW2_Fu_0_017	79.8804	175.6536	98.3401	486.3553	119.1514	173.6038	39.2710
TW2_F160_0_017	68.1528	20.5492	88.0572	229.4757	106.4291	97.8656	38.2763
TW2_F190_0_017	88.4808	58.8789	109.4349	224.9620	131.9307	61.0525	43.4499
TW2_F220_0_017	83.1334	101.4785	104.0966	208.0026	124.0255	66.5723	40.8921
16 LW							
TW2_Fu_0_018	81.2193	481.3027	102.3479	747.2112	123.0184	465.6489	41.7991
TW2_F160_0_018	88.6677	305.9842	107.7133	414.7361	127.8261	314.9223	39.1584
TW2_F190_0_018	69.0302	302.4813	91.0241	561.6079	112.7707	281.8033	43.7405
TW2_F220_0_018	59.9171	309.4501	82.1107	460.2771	103.7283	292.6784	43.8112
17 EW							
TW2_Fu_0_019	78.2482	555.6360	99.5186	472.1639	115.3287	148.4151	37.0805
TW2_F160_0_019	72.6792	84.8215	93.4449	158.9330	115.5893	74.9855	42.9101
TW2_F190_0_019	67.8908	77.9490	90.0950	268.7669	114.0063	64.3846	46.1155
TW2_F220_0_019							
17 LW							
TW2_Fu_0_020	94.7854	430.4275	115.9809	508.2603	137.4321	442.0362	42.6467
TW2_F160_0_020	65.4094	284.3232	85.2722	378.9410	106.4153	330.3984	41.0059
TW2_F190_0_020	74.2616	271.6905	97.3507	416.5926	119.7678	288.7424	45.5062
TW2_F220_0_020	61.9157	197.8742	83.4199	236.1242	105.1821	198.9329	43.2664
19 EW							
TW2_Fu_0_021	86.7446	152.9953	107.6540	446.1765	138.7720	56.3623	52.0274
TW2_F160_0_021	83.7717	167.3499	102.8939	294.4036	122.9814	169.9425	39.2097
TW2_F190_0_021	67.0343	201.0831	86.3724	688.5785	106.4733	176.0774	39.4390
TW2_F220_0_021	94.0643	122.8449	115.3112	305.9417	136.3229	146.7911	42.2586

19 LW							
TW2_Fu_0_022	75.3760	350.4698	93.2677	1588.7533	111.1824	365.6665	35.8064
TW2_F160_0_022	83.7734	348.4892	102.4561	456.3265	121.9598	357.9429	38.1864
TW2_F190_0_022	74.5739	334.3769	91.6419	768.9565	108.1584	309.0841	33.5845
TW2_F220_0_022	59.0546	211.2367	78.2914	283.9060	98.3006	218.7817	39.2460
23 EW							
TW2_Fu_0_023	67.0891	163.5269	89.1333	614.5252	110.9063	213.7078	43.8172
TW2_F160_0_023	91.4256	184.1851	114.3103	296.6290	138.9903	133.3599	47.5647
TW2_F190_0_023	65.2529	94.7664	88.5817	254.0794	113.0602	80.3087	47.8073
TW2_F220_0_023	62.2271	63.6902	86.4900	207.7886	111.3467	67.5363	49.1196
23 EW							
TW2_Fu_0_024	121.8286	714.8504	106.0908	1539.8749	91.3922	852.3682	-30.4364
TW2_F160_0_024	77.2907	762.9748	95.6865	1102.0700	113.6118	716.7976	36.3211
TW2_F190_0_024	72.5615	124.8403	88.6474	342.1941	105.1386	181.6711	32.5771
TW2_F220_0_024	91.9342	205.8818	106.8126	665.7386	121.9893	214.8234	30.0551
28 EW							
TW2_Fu_0_025	74.8054	268.0735	95.0931	374.6698	116.3471	160.6894	41.5417
TW2_F160_0_025	87.9283	164.7353	107.2725	358.2389	128.7304	123.7351	40.8021
TW2_F190_0_025	74.9495	108.7629	94.9523	202.9711	117.3458	74.5775	42.3963
TW2_F220_0_025	81.0654	121.9807	101.4950	314.4788	123.6409	101.7937	42.5755
29 LW							
TW2_Fu_0_026	116.2959	729.5173	97.1919	648.6437	135.0692	622.0716	18.7733
TW2_F160_0_026	86.7954	702.0169	106.6181	965.8637	126.9820	696.9604	40.1866
TW2_F190_0_026	64.2285	319.8917	86.5673	278.9326	107.5921	298.3485	43.3636
TW2_F220_0_026	61.2740	361.0022	81.3507	462.2476	101.5318	337.3356	40.2578
30 EW							
TW2_Fu_1_001	90.5270	279.7820	125.5991	287.1957	192.8941	12.8443	102.3671
TW2_F160_1_001	55.9280	51.0460	82.0241	184.3308	107.8022	54.5556	51.8742
TW2_F190_1_001	92.9539	104.1246	113.6398	103.2144	130.6800	73.4254	37.7261
TW2_F220_1_001	75.1638	152.3541	98.2833	422.0840	120.8730	151.5312	45.7092
30 LW							
TW2_Fu_1_002	108.7291	631.0436	90.5078	591.8125	127.9126	637.4559	19.1835
TW2_F160_1_002	100.6545	559.9310	134.8898	481.0577	118.3872	796.1861	17.7327
TW2_F190_1_002	80.0007	367.4953	116.1314	367.5979	97.9822	478.7829	17.9815
TW2_F220_1_002	69.3288	316.1562	88.2151	465.5914	107.0575	313.5872	37.7287

32 EW							
TW2_Fu_1_003	66.9598	293.9386	85.2528	436.4978	105.3466	292.8410	38.3868
TW2_F160_1_003	82.9959	217.8523	105.5255	724.1134	127.7912	183.7154	44.7953
TW2_F190_1_003	74.6899	110.2008	93.3831	239.6643	113.9930	154.8433	39.3031
TW2_F220_1_003	80.0564	192.2094	96.0426	485.3335	112.3391	192.7841	32.2827
32 LW							
TW2_Fu_1_004	58.6879	456.9711	78.5923	635.6158	98.9641	466.9769	40.2762
TW2_F160_1_004	75.0110	434.0074	92.9604	701.1112	110.7837	435.4647	35.7727
TW2_F190_1_004	65.9200	401.1795	103.7491	404.9338	84.7623	730.8807	18.8423
TW2_F220_1_004	77.2219	315.8329	95.6826	735.1735	114.1372	286.0681	36.9153
35 EW							
TW2_Fu_1_005	80.8427	368.2623	99.9743	597.0958	118.5996	362.5761	37.7569
TW2_F160_1_005	88.9627	182.0498	108.7354	597.3082	128.1643	242.4891	39.2016
TW2_F190_1_005	69.0456	50.4959	89.0057	166.0820	108.5616	55.6852	39.5160
TW2_F220_1_005	85.4119	118.8241	105.6019	386.2285	127.2350	132.8500	41.8231
35 LW							
TW2_Fu_1_006	57.8539	390.7253	78.1143	386.8789	98.4716	403.9946	40.6177
TW2_F160_1_006	76.8132	504.0755	111.7952	533.8791	94.1296	812.0543	17.3164
TW2_F190_1_006	63.8378	255.0349	81.5019	446.9970	99.7662	287.9848	35.9284
TW2_F220_1_006	95.4130	379.8561	113.1074	460.2780	130.4256	359.2420	35.0126
40 EW							
TW2_Fu_1_007	61.2474	104.8110	86.7265	773.8172	110.4064	110.3845	49.1590
TW2_F160_1_007	87.6445	142.9705	110.4973	799.3600	134.0155	131.9277	46.3710
TW2_F190_1_007	73.0980	65.4055	94.3948	292.5117	114.1456	80.5847	41.0476
TW2_F220_1_007	72.7532	46.5981	90.4988	148.5162	111.1806	37.0721	38.4274
40 LW							
TW2_Fu_1_008	87.4687	684.9200	64.1787	46.8124	101.3850	1099.0311	13.9163
TW2_F160_1_008	71.0656	318.7071	91.7797	324.1565	169.1584	21.1149	98.0928
TW2_F190_1_008	74.4708	257.2155	91.2073	694.5944	107.9864	247.2295	33.5156
TW2_F220_1_008	70.1212	353.3099	86.0231	844.2246	101.7908	389.6660	31.6696
41 EW							
TW2_Fu_1_009	66.6190	213.0834	89.3448	684.4914	110.9443	223.1346	44.3253
TW2_F160_1_009	96.4409	124.9017	117.2889	295.8269	139.0686	126.4714	42.6277
TW2_F190_1_009	83.6527	197.1600	102.0875	315.1065	121.2641	120.1213	37.6114
TW2_F220_0_009	56.2102	158.5421	76.4053	370.2697	95.5465	147.8557	39.3363

41 LW							
38.5833	38.5833	564.5444	20.8822	541.5470	56.7784	1046.8187	18.1951
TW2_F160_1_010	73.6630	635.6975	91.3008	697.7030	108.4450	607.8844	34.7820
TW2_F190_1_010	86.8973	612.0452	69.9262	328.3917	103.2515	313.2440	16.3542
TW2_F220_1_010	89.7165	317.4225	121.0883	346.1223	105.2868	923.2220	15.5703
49 EW							
TW2_Fu_1_011	81.3493	165.6975	104.6705	1416.8719	128.2820	168.9274	46.9327
TW2_F160_1_011	59.3897	97.8486	81.9843	1052.5001	104.2020	107.7973	44.8123
TW2_F190_1_011	82.1848	91.0526	104.4143	678.2957	124.9438	98.7366	42.7590
TW2_F220_1_011	78.4909	90.1097	96.9216	767.5731	116.4617	81.1555	37.9708
49 LW							
TW2_Fu_1_012	87.9985	350.7223	130.2223	403.2179	108.9963	3950.9572	20.9978
TW2_F160_1_012	83.8977	208.4709	105.9812	2416.0037	128.6538	215.1947	44.7561
TW2_F190_1_012	83.9243	173.0004	102.8554	2050.4191	120.9453	163.9451	37.0210
TW2_F220_1_012	89.0591	141.0319	128.0879	157.1299	107.8840	1881.0237	18.8846
63 EW							
TW2_Fu_1_013	67.8645	145.3483	91.5513	939.2040	115.8151	133.6190	47.9506
TW2_F160_1_013	65.2207	114.8859	88.7325	805.4526	112.1032	112.6846	46.8825
TW2_F190_1_013	55.1966	91.0954	73.8626	466.0503	92.5100	93.8879	37.3134
TW2_F220_1_013	98.8349	174.2890	113.9809	389.9507	129.8809	141.5658	31.0460
63 LW							
TW2_Fu_1_014	118.6955	612.7540	80.1197	575.8992	99.1549	1326.3829	-19.5406
TW2_F160_1_014	78.9113	372.8083	118.5362	377.1400	98.5547	728.5657	19.6434
TW2_F190_1_014	70.7261	166.9230	88.6469	414.3448	106.8318	192.9232	36.1057
TW2_F220_1_014	80.6215	242.4178	99.2499	577.3737	118.3015	222.5536	37.6800
64 EW							
TW2_Fu_1_015	79.8253	135.7025	100.3166	420.4468	122.9497	133.7112	43.1244
TW2_F160_1_015	74.9490	239.8888	95.5844	1060.3134	116.6491	271.3309	41.7001
TW2_F190_1_015	66.5866	51.6721	85.7737	173.6504	108.4073	45.0175	41.8207
TW2_F220_1_015	80.2991	85.8510	97.9511	191.9237	116.3771	86.7640	36.0780
64 LW							
TW2_Fu_1_016	78.8295	452.8766	99.0878	1118.3924	118.8407	492.1031	40.0112
TW2_F160_1_016	94.4851	270.0534	112.7150	840.4462	130.6856	242.8867	36.2005
TW2_F190_1_016	103.3484	705.2525	85.9443	234.2646	120.8409	233.2633	17.4925
TW2_F220_1_016	80.9581	282.7831	97.9455	551.2730	114.7397	273.2713	33.7816

67 EW							
TW2_Fu_1_017	75.0559	84.5896	98.5329	461.1778	128.5468	63.4197	53.4909
TW2_F160_1_017	74.0031	66.9595	98.0634	318.6132	121.1291	90.9007	47.1260
TW2_F190_1_017	77.5342	134.0867	94.7995	216.4614	113.3325	91.6609	35.7983
TW2_F220_1_017	83.3406	52.7867	104.3998	310.5098	127.4087	56.0398	44.0681
64 LW							
TW2_Fu_1_018	79.1807	571.3246	99.1284	506.5288	118.3492	548.9791	39.1685
TW2_F160_1_018	65.6643	439.1899	84.6613	626.4326	104.1598	436.1172	38.4955
TW2_F190_1_018	85.1669	474.7633	66.0864	389.8395	104.3058	371.7466	19.1389
TW2_F220_1_018	84.0531	205.4474	103.9177	258.1910	124.3716	216.6046	40.3185
71 EW							
TW2_Fu_1_019	46.6583	105.3029	69.4342	607.7652	95.3206	98.1681	48.6623
TW2_F160_1_019	58.0853	99.6802	81.1810	744.8687	103.6995	113.5427	45.6142
TW2_F190_1_019	93.3315	68.3315	113.2878	374.1524	135.2843	66.0789	41.9528
TW2_F220_1_019	56.4444	109.7344	73.0595	512.0446	93.4035	50.8645	36.9591
71 LW							
TW2_Fu_1_020	113.3332	3906.7070	136.9056	319.4343	90.1998	358.6281	-23.1334
TW2_F160_1_020	105.3881	2519.6683	127.7877	283.2724	83.6485	278.7581	-21.7396
TW2_F190_1_020	62.7093	185.0962	81.6779	1687.7332	100.0380	174.3512	37.3287
TW2_F220_1_020	75.3817	156.3186	92.5027	1175.3177	109.5710	156.0526	34.1893
75 EW							
TW2_Fu_1_0021	50.2149	146.6311	76.9062	1169.6447	103.7845	127.9096	53.5696
TW2_F160_1_0021	69.0427	102.0932	90.0195	859.1225	112.3003	104.8270	43.2576
TW2_F190_1_0021	92.7511	739.6876	75.4739	125.0316	112.1182	98.3266	19.3671
TW2_F220_1_0021	68.1741	56.5305	85.5427	382.7259	103.8123	56.3771	35.6382
75 LW							
TW2_Fu_1_022	88.3263	349.6987	129.7086	402.9360	109.2437	3951.1109	20.9174
TW2_F160_1_022	84.1188	209.3690	106.1189	2415.7744	128.4325	215.2856	44.3137
TW2_F190_1_022	84.2720	172.9897	102.3423	2051.3068	121.0187	164.0327	36.7467
TW2_F220_1_022	89.1843	140.3464	126.7932	156.6171	108.0689	1880.7054	18.8846

	Coordinate 4. max.	Height 4.max	Coordinate 5.max	Height 5.max	Coordinate 6.max	Height 6.max	Difference x04-x06
3 Earlywood (EW)							
TW2_Fu_0_001	209.6516	37.4960	244.1530	409.0084	274.9408	268.3400	65.2892
TW2_F160_0_001	255.1379	308.5797	282.0364	182.7639	282.0356	116.4844	26.8977
TW2_F190_0_001	225.5243	14.0647	255.7926	283.3444	279.3482	242.6647	53.8239
TW2_F220_0_001	239.7821	17.4951	266.1736	124.4614	289.8889	104.5634	50.1068
3 Latewood (LW)							
TW2_Fu_0_002	250.7094	1072.0537	279.1369	407.7707	279.1387	683.4655	28.4293
TW2_F160_0_002	219.2889	27.0232	250.8129	522.5958	268.7036	378.0519	49.4147
TW2_F190_0_002	238.4372	159.6451	261.5607	420.4795	284.0719	200.9828	45.6347
TW2_F220_0_002	260.2008	232.8800	280.2397	331.9084	298.7357	37.4038	38.5349
4 EW							
TW2_Fu_0_003	251.8406	524.0885	273.3309	632.3167	289.8544	289.7706	38.0138
TW2_F160_0_003	242.6287	59.2960	268.3470	493.6529	289.8627	67.6922	47.2340
TW2_F190_0_003	256.9410	95.9387	277.9074	383.2015	298.5669	87.9121	41.6259
TW2_F220_0_003	245.1279	90.7814	264.6087	234.0565	299.3353	16.0012	54.2074
4 LW							
TW2_Fu_0_004	250.6953	821.5254	266.5287	974.4988	282.9989	890.6196	32.3036
TW2_F160_0_004	262.7378	387.3147	280.4779	335.3985	295.9063	321.8133	33.1685
TW2_F190_0_004	258.4876	320.7497	276.3118	517.2075	293.6431	299.1716	35.1555
TW2_F220_0_004	254.3225	321.8703	274.3285	398.9910	292.2089	250.9332	37.8864
6 EW							
TW2_Fu_0_005	247.5576	107.6652	269.5044	971.0164	290.2029	134.2161	42.6453
TW2_F160_0_005	236.4903	85.4570	265.4463	792.9235	291.4236	102.4568	54.9333
TW2_F190_0_005	264.2988	99.2525	286.8698	701.0689	309.0279	101.8103	44.7291
TW2_F220_0_005	253.8398	140.3752	272.5291	606.8462	292.0884	87.4906	38.2486
6 LW							
TW2_Fu_0_006	256.4467	891.9709	278.5188	2147.9788	300.5494	366.6324	44.1027
TW2_F160_0_006	260.4424	325.7210	281.5219	1526.4185	302.0657	326.2955	41.6233
TW2_F190_0_006	253.9320	237.3025	272.0760	1082.0095	289.8060	225.7822	35.8740
TW2_F220_0_006	248.9909	212.0264	266.7730	783.5294	284.0160	224.6761	35.0251
7 EW							
TW2_Fu_0_007	255.7323	98.2877	279.6783	578.4350	302.1016	75.2912	46.3693
TW2_F160_0_007	258.4910	210.2923	268.5938	781.3705	2515.8577	-86991898.2113	2257.3667
TW2_F190_0_007	257.1273	123.8634	277.5041	605.5195	298.1782	89.9348	41.0509
TW2_F220_0_007	258.4014	125.9184	273.8602	287.7952	288.9420	89.7619	30.5406

7 LW							
TW2_Fu_0_008	259.2822	494.9029	285.6316	1847.6607	308.8446	430.3776	49.5624
TW2_F160_0_008	243.4933	185.7363	262.5480	588.3195	281.2042	217.5857	37.7109
TW2_F190_0_008	254.8150	325.1363	271.3355	789.8534	288.2063	269.9661	33.3913
TW2_F220_0_008	264.3110	354.7641	282.1609	785.4509	299.5110	362.0862	35.2000
9 EW							
TW2_Fu_0_009	248.1966	82.8096	267.8126	369.3351	285.7759	99.1897	37.5793
TW2_F160_0_009	257.6043	110.9300	282.5120	604.0903	306.7636	106.8306	49.1593
TW2_F190_0_009	244.8589	74.8532	265.5099	266.1861	284.6756	88.0486	39.8167
TW2_F220_0_009	244.3936	113.8939	264.1218	424.7067	284.0661	112.6727	39.6725
9 LW							
TW2_Fu_0_010	248.7766	1077.3677	268.1077	1679.4620	287.8014	1040.2798	39.0248
TW2_F160_0_010	261.3713	420.9715	279.6190	723.5798	297.6211	382.4593	36.2498
TW2_F190_0_010	254.1751	181.9501	272.8578	202.5493	291.1353	170.8793	36.9602
TW2_F220_0_010	252.1343	208.4907	270.8950	522.2618	289.8691	191.0022	37.7348
10 EW							
TW2_Fu_0_011	246.1568	200.1456	263.0144	824.3382	280.8639	183.4161	34.7071
TW2_F160_0_011	248.3423	79.0891	272.5439	508.5374	297.7824	82.6661	49.4401
TW2_F190_0_011	250.7605	56.9876	275.4610	313.4272	298.3202	55.0106	47.5597
TW2_F220_0_011	255.2032	64.5960	277.2132	372.5292	300.5063	59.8797	45.3031
10 LW							
TW2_Fu_0_012	289.7296	-722.4517	289.7295	6720.0345	289.7300	-1819.8229	4.0000e-4
TW2_F160_0_012	253.5860	212.6350	273.9300	2556.8147	295.1303	186.8682	41.5443
TW2_F190_0_012	140.8965	-91.9709	270.2090	2081.4276	250.3567	160.4847	109.4602
TW2_F220_0_012	249.4378	199.9334	266.6523	1932.4484	284.4711	192.2406	35.0333
12 EW							
TW2_Fu_0_013	235.7348	126.4299	255.0086	816.0960	272.9777	140.3282	37.2429
TW2_F160_0_013	237.3986	106.8507	264.9441	796.8668	290.4783	104.1236	53.0797
TW2_F190_0_013	271.3978	59.9537	295.9736	452.9959	320.3249	80.1595	48.9271
TW2_F220_0_013	258.1396	179.8355	274.9227	429.6669	291.2384	127.9441	33.0988
12 LW							
TW2_Fu_0_014	250.1689	751.7119	265.5414	1132.5397	280.5256	787.4446	30.3567
TW2_F160_0_014	243.8889	397.5991	263.6920	963.1756	283.1675	413.4627	39.2786
TW2_F190_0_014	274.9853	222.0533	290.3399	575.9520	305.9877	218.8606	31.0024
TW2_F220_0_014	248.2742	268.2585	266.2175	682.3389	283.8651	250.9670	35.5909

15 EW							
TW2_Fu_0_015	271.2220	351.7523	290.2667	350.5063	302.0745	64.2443	30.8525
TW2_F160_0_015	231.2050	65.7863	255.2191	293.9426	278.9120	68.5922	47.7070
TW2_F190_0_015	252.0277	157.9067	270.4565	399.7651	287.5887	164.7728	35.5610
TW2_F220_0_015	262.8655	71.2248	282.2825	267.7811	302.5498	131.1200	39.6843
15 LW							0.0000
TW2_Fu_0_016	252.3278	544.1221	269.6668	1145.8703	286.6139	590.2944	34.2861
TW2_F160_0_016	267.4790	434.2333	285.8725	746.0777	304.6382	485.6991	37.1592
TW2_F190_0_016	265.3289	256.5594	283.1252	655.2665	300.5127	282.3973	35.1838
TW2_F220_0_016	251.8100	276.2331	270.9863	553.3438	290.3520	277.7687	38.5420
16 EW							
TW2_Fu_0_017	262.1689	187.3279	278.6562	355.7797	295.0398	185.9455	32.8709
TW2_F160_0_017	247.1521	36.8599	271.7311	316.0995	300.2372	24.1701	53.0851
TW2_F190_0_017	275.2128	78.1326	292.0394	161.1154	310.0773	82.9557	34.8645
TW2_F220_0_017	262.2226	75.2421	283.7477	226.8820	304.5354	82.4514	42.3128
16 LW							
TW2_Fu_0_018	264.3922	426.1713	284.8240	615.6033	304.7228	446.4801	40.3306
TW2_F160_0_018	269.6732	294.1439	288.8661	426.5500	309.1686	312.2540	39.4954
TW2_F190_0_018	250.9298	326.8977	271.2140	460.0745	291.3408	325.7446	40.4110
TW2_F220_0_018	242.7509	293.4746	263.6502	417.1010	284.9421	308.7988	42.1912
17 EW							
TW2_Fu_0_019	260.0107	408.5970	260.0099	128.1749	285.3054	433.7706	25.2947
TW2_F160_0_019	252.2583	56.3731	272.6376	164.8074	296.3936	104.9191	44.1353
TW2_F190_0_019	254.6971	106.8076	273.5006	155.6605	291.3118	82.8004	36.6147
TW2_F220_0_019	242.7509	293.4746	263.6502	417.1010	284.9421	308.7988	42.1912
17 LW							
TW2_Fu_0_020	277.1096	430.8665	296.9160	388.2723	317.2578	404.8409	40.1482
TW2_F160_0_020	244.6748	293.9821	265.8500	431.4036	287.2268	305.1030	42.5520
TW2_F190_0_020	255.7790	287.8892	278.0795	389.8549	299.8108	290.1530	44.0318
TW2_F220_0_020	241.5189	204.7160	263.4475	230.5051	285.0072	211.9410	43.4883
19 EW							
TW2_Fu_0_021	265.6176	86.0794	288.1627	472.7713	317.9081	22.7067	52.2905
TW2_F160_0_021	262.5462	139.7032	283.5095	347.9600	305.0543	169.6949	42.5081
TW2_F190_0_021	248.0197	208.8706	266.8876	598.3932	284.5764	250.3958	36.5567
TW2_F220_0_021	274.6335	114.9153	296.5711	336.1251	319.4266	136.3418	44.7931

19 LW							
TW2_Fu_0_022	252.1075	441.9060	274.9468	1798.3040	298.6540	225.2280	46.5465
TW2_F160_0_022	263.8240	350.6812	283.5237	503.5317	303.1146	336.8703	39.2906
TW2_F190_0_022	254.0427	333.3686	271.1110	744.3117	287.5597	338.1027	33.5170
TW2_F220_0_022	239.1218	219.0638	258.9049	277.3403	278.9457	220.2254	39.8239
23 EW							
TW2_Fu_0_023	248.9858	267.0108	273.1053	584.2894	294.9143	159.6372	45.9285
TW2_F160_0_023	269.3695	138.5228	293.5114	343.1046	317.6250	169.0436	48.2555
TW2_F190_0_023	250.4740	96.4269	268.6178	136.6817	290.8406	123.7457	40.3666
TW2_F220_0_023	245.2140	70.8312	265.9162	146.9072	287.7685	89.5589	42.5545
23 EW							
TW2_Fu_0_024	274.1614	772.3389	288.2884	1397.1315	302.7926	687.3910	28.6312
TW2_F160_0_024	258.0408	812.0073	275.5894	970.1868	292.5564	780.7874	34.5156
TW2_F190_0_024	248.8744	166.3430	265.7842	345.0652	282.3281	148.2402	33.4537
TW2_F220_0_024	269.4503	173.1014	285.7671	687.2359	301.8352	240.4917	32.3849
28 EW							
TW2_Fu_0_025	257.2375	157.0054	278.2129	420.6458	299.4838	187.5955	42.2463
TW2_F160_0_025	263.2483	117.2952	287.3958	466.7067	310.4850	134.2797	47.2367
TW2_F190_0_025	255.7874	83.2904	277.4576	251.1901	299.9767	91.7273	44.1893
TW2_F220_0_025	260.3364	92.2629	283.5442	315.8766	304.0579	130.1221	43.7215
29 LW							
TW2_Fu_0_026	280.5979	616.1686	298.4137	587.9774	316.4831	572.1662	35.8852
TW2_F160_0_026	268.7380	725.7008	287.5062	763.5720	306.6870	739.8245	37.9490
TW2_F190_0_026	244.7067	308.3025	266.8284	301.0614	288.3493	307.8769	43.6426
TW2_F220_0_026	241.4298	328.3175	260.8136	394.2091	280.3716	357.9955	38.9418
30 EW							
TW2_Fu_1_001	272.5476	220.7954	291.3240	210.5597	311.4249	213.2473	38.8773
TW2_F160_1_001	243.6952	106.0664	269.5236	131.5224	293.6106	25.3576	49.9154
TW2_F190_1_001	267.4203	60.0805	290.5208	190.6461	313.2816	78.0570	45.8613
TW2_F220_1_001	256.4242	158.5494	279.6118	397.0652	301.9179	142.9431	45.4937
30 LW							
TW2_Fu_1_002	269.0002	586.3469	289.0416	787.4990	309.1042	586.9640	40.1040
TW2_F160_1_002	280.5259	521.2901	298.6243	860.9770	316.0401	519.8455	35.5142
TW2_F190_1_002	261.0059	370.4243	279.2244	496.4912	297.3418	352.0195	36.3359
TW2_F220_1_002	248.9103	304.3289	267.9914	517.4899	287.7483	328.7517	38.8380

32 EW							
TW2_Fu_1_003	242.8466	227.6773	266.6978	707.5237	290.4469	240.1951	47.6003
TW2_F160_1_003	267.7863	308.6101	287.6860	492.2446	304.5260	227.4734	36.7397
TW2_F190_1_003	253.8715	112.7426	275.7812	321.1431	298.7429	114.6264	44.8714
TW2_F220_1_003	259.8893	196.4416	277.8762	616.9392	296.8018	171.4495	36.9125
32 LW							
TW2_Fu_1_004	238.5493	433.5210	258.8955	677.0638	279.7838	463.3725	41.2345
TW2_F160_1_004	255.2591	482.0340	273.4477	690.0208	290.6842	435.4007	35.4251
TW2_F190_1_004	249.0522	469.1230	266.9816	604.0162	284.1038	413.0257	35.0516
TW2_F220_1_004	258.0459	327.1061	276.1063	649.0929	293.1380	314.8167	35.0921
35 EW							
TW2_Fu_1_005	256.7915	286.2701	280.6271	939.7975	303.7847	289.3169	46.9932
TW2_F160_1_005	268.8907	201.9729	288.8020	651.0191	309.3818	226.2786	40.4911
TW2_F190_1_005	250.5434	61.2880	269.6499	159.3683	288.2122	53.0415	37.6688
TW2_F220_1_005	269.8597	164.4414	287.3563	281.2491	305.0660	138.9090	35.2063
35 LW							
TW2_Fu_1_006	239.3808	401.1864	257.7361	309.5442	277.8470	444.6428	38.4662
TW2_F160_1_006	257.1200	525.5958	275.3755	891.4599	293.4563	501.8209	36.3363
TW2_F190_1_006	244.7092	274.2316	262.4021	424.0282	280.5744	288.6865	35.8652
TW2_F220_1_006	273.6660	341.4494	293.0836	608.9679	312.4896	346.3569	38.8236
40 EW							
TW2_Fu_1_007	240.3962	113.6198	265.3722	774.8841	288.8267	124.7984	48.4305
TW2_F160_1_007	270.0091	165.7271	291.4777	744.1993	312.8228	137.9354	42.8137
TW2_F190_1_007	253.0754	78.0043	273.5248	299.3055	294.5987	67.6088	41.5233
TW2_F220_1_007	251.6548	33.8587	272.7869	165.0127	293.6183	41.6420	41.9635
40 LW							
TW2_Fu_1_008	245.0717	149.1518	271.7791	1680.6577	295.7098	185.5631	50.6381
TW2_F160_1_008	244.3996	138.5327	261.2015	366.3104	278.1415	153.7144	33.7419
TW2_F190_1_008	253.8952	264.0699	271.7109	725.8405	289.1807	243.0383	35.2855
TW2_F220_1_008	246.6943	346.4441	264.4311	991.2000	282.2005	375.4015	35.5062
41 EW							0.0000
TW2_Fu_1_009	251.2194	274.0905	268.6432	431.1610	286.4409	349.0928	35.2215
TW2_F160_1_009	278.1701	128.2520	297.9280	275.4593	318.8432	130.8620	40.6731
TW2_F190_1_009	261.4743	133.5752	281.2021	359.5718	301.2427	153.5334	39.7684
TW2_F220_1_009	234.7842	148.8189	256.1892	419.6788	278.3073	143.3363	43.5231

41 LW							
TW2_Fu_1_0010	200.4260	565.5143	218.4577	1084.4878	236.8910	533.8210	36.4650
TW2_F160_1_010	253.2605	610.9619	271.5965	800.4978	289.3657	593.0947	36.1052
TW2_F190_1_010	248.7922	296.0656	266.6092	695.8622	284.0897	299.3356	35.2975
TW2_F220_1_010	268.1264	316.5638	284.8958	998.3085	301.5523	351.7774	33.4259
49 EW							
TW2_Fu_1_011	263.0379	144.1197	285.5469	1237.3940	305.4796	163.0146	42.4417
TW2_F160_1_011	242.6183	101.4905	264.2919	1034.0422	285.4455	107.5380	42.8272
TW2_F190_1_011	263.2061	83.3478	283.2715	593.2199	302.1975	103.3292	38.9914
TW2_F220_1_011	259.1550	99.4935	277.8720	833.3341	298.7465	86.1155	39.5915
49 LW							
TW2_Fu_1_012	268.3239	344.2178	289.5442	3846.7783	308.3704	390.9228	40.0465
TW2_F160_1_012	267.2693	218.8333	287.6579	2429.4389	310.2822	216.1597	43.0129
TW2_F190_1_012	266.8684	188.4691	285.5620	2115.6162	302.2158	161.9987	35.3474
TW2_F220_1_012	273.1782	155.4919	290.0221	1916.6923	308.9175	150.4105	35.0975
63 EW							
TW2_Fu_1_013	246.9632	143.4592	271.5859	970.2023	295.5332	138.6935	48.5700
TW2_F160_1_013	246.7772	119.9142	268.3925	765.7274	290.7494	126.3589	43.9722
TW2_F190_1_013	232.4227	75.5306	254.1657	501.5590	272.6232	101.2407	40.2005
TW2_F220_1_013	272.1026	101.9308	294.3386	635.3800	315.7705	114.5031	43.6679
63 LW							
TW2_Fu_1_014	258.7258	558.0779	279.5386	1489.5668	300.2190	588.5087	41.4932
TW2_F160_1_014	260.3044	388.7648	279.5567	701.9602	299.0936	387.6592	38.7892
TW2_F190_1_014	248.7173	171.6217	267.5156	467.5545	286.9504	174.9428	38.2331
TW2_F220_1_014	262.3748	247.5026	280.7171	540.6509	298.8129	255.3036	36.4381
64 EW							
TW2_Fu_1_015	258.0318	113.8407	281.7175	492.8519	306.0896	126.2463	48.0578
TW2_F160_1_015	259.1230	255.5120	277.0893	880.2898	294.8787	351.1024	35.7557
TW2_F190_1_015	246.1209	47.9444	267.4644	167.8787	287.1944	49.4550	41.0735
TW2_F220_1_015	256.3437	80.2714	278.1524	272.3802	299.6033	66.2987	43.2596
64 LW							
TW2_Fu_1_016	260.4439	466.8886	280.2407	1019.6436	298.7877	517.2888	38.3438
TW2_F160_1_016	274.6299	248.5152	293.7292	899.0111	312.0611	244.2715	37.4312
TW2_F190_1_016	268.0018	224.5975	285.1320	709.3605	302.3611	244.4454	34.3593
TW2_F220_1_016	261.8791	279.4211	279.2245	578.6795	296.0522	262.9870	34.1731

67 EW							
TW2_Fu_1_017	246.4590	53.5006	278.6457	465.6185	303.0569	86.3336	56.5979
TW2_F160_1_017	254.5385	67.5008	278.3985	314.5163	301.3221	99.8927	46.7836
TW2_F190_1_017	253.0154	82.9492	273.0533	269.3656	293.3739	105.0938	40.3585
TW2_F220_1_017	262.2914	42.9582	284.4110	300.0431	305.6631	56.8473	43.3717
64 LW							
TW2_Fu_1_018	257.5290	549.5493	278.7310	641.6443	299.9605	544.1259	42.4315
TW2_F160_1_018	244.0402	407.2314	264.8829	773.3727	285.7621	436.1774	41.7219
TW2_F190_1_018	244.6583	362.9997	264.9377	581.9500	285.1492	385.1126	40.4909
TW2_F220_1_018	262.4070	195.8442	282.7362	312.5856	304.3771	210.7705	41.9701
71 EW							
TW2_Fu_1_019	224.8886	99.7781	250.4906	621.3755	274.7325	97.7104	49.8439
TW2_F160_1_019	237.0119	105.1466	260.1781	740.8033	282.6648	118.6600	45.6529
TW2_F190_1_019	275.4356	73.4354	295.9234	368.1981	316.0134	66.2181	40.5778
TW2_F220_1_019	227.1032	73.0344	253.7554	676.2363	161.1060	19.9821	-65.9972
71 LW							
TW2_Fu_1_020	269.4746	395.5230	292.2615	4082.5480	315.7484	375.9331	46.2738
TW2_F160_1_020	264.2668	271.2326	285.5897	2531.6335	306.9283	291.5513	42.6615
TW2_F190_1_020	242.7898	208.6199	260.7812	1662.7166	279.4984	201.3250	36.7086
TW2_F220_1_020	257.5138	180.8908	273.7613	1133.6572	290.3936	161.6530	32.8798
75 EW							
TW2_Fu_1_021	231.7679	147.2610	258.7686	1121.1146	284.2026	132.9121	52.4347
TW2_F160_1_021	250.4390	98.8028	274.0716	893.0271	294.9877	116.0934	44.5487
TW2_F190_1_021	253.3318	110.0446	274.0002	891.8219	294.2892	114.6761	40.9574
TW2_F220_1_021	245.5536	67.7802	266.1133	476.5270	286.8149	67.9163	41.2613
75 LW							
TW2_Fu_1_022	269.2149	343.1969	289.5442	3844.5945	308.3704	391.8117	39.1555
TW2_F160_1_022	266.3581	217.9224	287.6579	2428.5778	309.1730	215.0606	42.8149
TW2_F190_1_022	267.0495	187.9580	284.4431	2115.6162	303.5124	162.1381	36.4629
TW2_F220_1_022	272.2702	155.4919	289.9403	1917.5901	308.8583	150.3913	36.5881